의학박사 학위논문

Regulation of Energy Metabolism by Hypothalamic POMC Neuron-Adipose Tissue Interorgan Mitohormesis Response

시상하부 POMC 뉴론-지방조직 간 미토콘드리아 호르메시스 반응에 의한 에너지 대사 조절 연구

2021년 8월

서울대학교 대학원

의학과 중개의학 전공

민 세 희

A thesis of the Degree of Doctor of Philosophy

시상하부 POMC 뉴론-지방조직 간 미토콘드리아 호르메시스 반응에 의한 에너지 대사 조절 연구

Regulation of Energy Metabolism by Hypothalamic POMC Neuron-Adipose Tissue Interorgan Mitohormesis Response

August 2021

Translational Medicine Major

Seoul National University Graduate School

College of Medicine

Se Hee Min

Regulation of Energy Metabolism by Hypothalamic POMC Neuron-Adipose Tissue Interorgan Mitohormesis Response

지도 교수 조 영 민

이 논문을 의학박사 학위논문으로 제출함
2021년 7월

서울대학교 대학원

의학과 중개의학 전공

민 세 희

민세희의 의학박사 학위논문을 인준함
2021년 7월

위 원 장 _____
부위원장 _____
위 원 _____
위 원 _____
위 원 _____

Abstract

Regulation of Energy Metabolism by Hypothalamic POMC Neuron-Adipose Tissue Interorgan Mitohormesis Response

Se Hee Min

Translational Medicine Major

Seoul National University Graduate School

College of Medicine

A low-grade mitochondrial stress can benefit health and survival, a phenomenon termed mitohormesis. In this study, I demonstrate the opposing effects low-level and high-level mitochondrial ribosomal (mitoribosomal) stress in hypothalamic proopiomelanocortin (POMC) neurons on systemic energy metabolism. POMC neuron-specific severe mitoribosomal stress due to *Crif1* homodeficiency which is a pivotal mitochondrial ribosomal protein, causes obesity with POMC neuronal loss in mice. By contrast, mild mitoribosomal stress caused by *Crif1* heterodeficiency in POMC neurons leads to high-turnover metabolism and resistance to diet-induced obesity: high level of energy expenditure despite the increase in food intake. *Crif1* heterodeficient mice show inguinal white adipose tissue (iWAT) browning and smaller fat droplets in the brown adipose tissue (BAT). These metabolic benefits are mediated by enhanced thermogenic program and mitochondrial unfolded protein responses (UPR^{mt}) in distal adipose tissues. In POMC neurons, partial *Crif1* deficiency increases the expression of β-endorphin (β

-END) and mitochondrial DNA-encoded peptide MOTS-c. Central administration of MOTS-c or β-END recapitulates the adipose phenotype of *Crif1* heterodeficient mice, suggesting these factors as potential mediators. Consistently, regular running exercise at moderate intensity stimulates hypothalamic MOTS-c/β-END expression and induces adipose tissue UPR^{mt} and thermogenesis. These findings indicate that POMC neuronal mitohormesis may underlie exercise-induced high-turnover metabolism.

Keywords: mitoribosomal stress, hypothalamus, thermogenesis, exercise, proopiomelanocortin, obesity, MOTS-c, mitohormesis

Student Number : 2016-30009

CONTENTS

LIST OF TABLE AND FIGURES

1. Introduction

Mitochondria is a highly dynamic organelle, the primary function of which is to generate ATP during oxidative phosphorylation (OXPHOS) through the metabolization of nutrients, resulting in regulating energy homeostasis. Recent advances in mitochondrial research have revealed that the mitochondria also play a critical role as signaling organelles (Friedman and Nunnari, 2014). The mitochondria constantly communicate with the nucleus and cytoplasm, in response to cellular needs and their own dysfunction under both physiological and stressor conditions. In this communication, multiple mechanisms such as respiratory chain dysfunction, mitochondrial protein unfolding, changes in mitochondrial membrane potential, and mitochondrial fission/fusion are involved (Chandel, 2015). They promote a wide range of adaptive defense mechanisms including increased mitochondrial biogenesis and antioxidant defenses, augmented cytoprotective responses, and enhanced metabolism, which can contribute to the extension of a healthy life. The most critical molecules involved in the communication between the mitochondria and other parts of the cell are mild reactive oxygen species (ROS) such as the superoxide anion and hydrogen peroxide (Murphy 2009). Within healthy cells, the primary production source of signaling mild ROS is mitochondrial OXPHOS. Therefore, the continuous production and scavenging of mild ROS during OXPHOS is crucial to maintain homeostasis under physiological condition. However, mitochondrial dysfunction leads to excessive ROS which can lead to oxidative stress damage and cell injury, potentially resulting in metabolic disorders and aging-related diseases (Murphy 2009).

However, recent evidence from research suggests that low-levels of mitochondrial stress may be rather cytoprotective than harmful in the long run (Yun and Finkel, 2014) (Ristow and Zarse, 2010; Yun and Finkel, 2014). Repeated exposure to low-levels of mitochondrial stress induces various cytosolic and nuclear responses which make cells less susceptible to subsequent higher level of stresses. This adaptive response, largely known as mitochondrial hormesis (mitohormesis), has been shown to increase stress resilience, leading to lowering disease susceptibility, and extend lifespan in several model organisms .

The mitochondrial unfolded protein response (UPR^{mt}) is a transcriptional responses that is activated by various mitochondrial insults to maintain mitochondrial homeostasis (Shpilka and Haynes, 2018; Yi et al., 2018). It is an adaptive stress response that promotes survival and recovery (Mottis et al., 2019; Shpilka and Haynes, 2018). When unfolded or misfolded proteins are accumulated inside the mitochondria beyond the capacity of chaperone proteins to handle them, they are degraded by mitochondrial proteases and exported to the cytosol via the ring finger ubiquitin ligase HAF1-dependent mechanism (Haynes et al., 2010; Yun and Finkel, 2014). These mitochondria-derived signals are transferred to the nucleus through retrograde signaling pathways to communicate mitochondrial proteotoxic stress to the nucleus to induce an adaptive response to resolve the insult by promoting mitochondrial chaperon and protease production (Haynes et al., 2010). Indeed, UPR^{mt} is activated by a variety of mitochondrial stress including dysfunction of electron transport, mitochondrial ribosomes, misfolded proteins, and xenobiotics or toxins, and recognized as mitochondrial adaptive response to promote a recovery from mitochondrial stress and to maintain cellular function

(Shpilka and Haynes, 2018). Although UPR^{mt} has been most well studied in *Caenorhabditis elegans* (*C. elegans)*, its mechanisms are increasingly being identified in vertebrates, especially in the context of the integrated stress response (ISR) that regulates an adaptive translational program (Anderson and Haynes, 2020; Costa-Mattioli and Walter, 2020; Mottis et al., 2019).

Mitochondria have their own ribosomes, or mitoribosomes, which are required to synthesize the 13 mitochondrial DNA (mtDNA)-encoded electron transport chain (ETC) proteins (Sharma et al., 2003). Four mitochondrial ETC complexes, except for complex-II, are composed of proteins encoded by nuclear DNA (nDNA) and mtDNA. Hence, appropriate stoichiometric ratios between nDNA- and mtDNA-encoded ETC proteins are critical for mitochondrial respiration (Houtkooper et al., 2013). Deficiencies in nuclear-encoded mitoribosomal proteins triggers the imbalance between nDNA- and mtDNA-encoded proteins and causes mitonuclear protein imbalance, which in turn activates the UPR^{mt} in *C. elegans* (Houtkooper et al., 2013) and yeast (Suhm et al., 2018). Notably, UPR^{mt} was firstly thought to occur within cells with mitochondrial stress (cell-autonomous fashion). However, mitochondrial perturbation in one tissue can lead to UPR^{mt} activation in a neighbouring or distal tissue by the cell-non-autonomous nature (Durieux et al., 2011). For example, knockdown of ETC components in the nervous system of *C. elegans* can increase UPR^{mt} responses in the intestine and extend life span through this cell-non-autonomous UPR^{mt} (Durieux et al., 2011).

Mitochondrial communication is key to adaptive stress response following mitochondrial perturbation. Interestingly, a short open reading frame within the

mtDNA encodes small signaling functional peptide called mitochondria-derived peptide (MDP). Recently, several MDPs have been identified (Reynolds et al., 2020). The firstly-identified MDP humanin, encoded from the mitochondrial 16S ribosomal RNA gene, has multiple beneficial effects on age-related human diseases (Lee et al., 2013; Zuccato et al., 2019). The small humanin-like peptides (SHLPs) have insulin-sensitizing effect (Cobb et al., 2016). These MDPs represent a unique class of mitochondrial-encoded signaling factors that respond to mitochondrial stress and promote health (Galluzzi et al., 2018; Mottis et al., 2019; Quiros et al., 2016; Tan and Finkel, 2020). Notably, The mitochondrial open reading frame of the 12S ribosomal RNA-c, MOTS-c, directly mediates mitonuclear communication by translocating to the nucleus upon metabolic stress and regulating adaptive nuclear gene expression to promote cellular homeostasis (Kim et al., 2018). In mice, MOTS-c improves insulin resistance and glucose intolerance induced by consumption of a high fat diet (HFD), aging, and ovariectomy and restores physical capacity in aged mice (Lee et al., 2015; Lu et al., 2019b) (Reynolds et al., 2019). Therefore, MDPs represent a unique mitochondria-derived signaling molecule to cope with mitochondrial stress and promote heath. (Reynolds et al., 2019)

The hypothalamus is one of the most important brain regions involved in the central control of feeding and energy expenditure. In particular, the arcuate nucleus (ARH) within the hypothalamus is critical for the regulation of feeding and metabolism in the body (Waterson and Horvath, 2015). The ARH is sensitive to circulating signals related to energy status through its proximity to third ventricle and blood-brain barrier which is permeable by capillary endothelial cells and tanycytes. There are two distinct, functionally antagonistic types of neurons in the

ARH: one is the orexigenic (appetite-stimulating) neuropeptide Y (NPY) and agouti-related peptide (AgRP)-expressing AgRP/NPY neurons, and the other is the anorexigenic (appetite-suppressing) pro-opiomelanocortin (POMC)-expressing POMC neurons. Especially, POMC neurons project mainly to second-order neurons in the paraventricular hypothalamic nucleus (PVN), but also to the dorsomedial hypothalamus (DMH), the lateral hypothalamus (LH) and the ventromedial hypothalamus (VMH). These second-order neurons further process the received information and project to multiple neurocircuits outside of the hypothalamus, leading to an integrated response on energy intake and expenditure. (Morton et al., 2006; Schwartz et al., 2000). There are substantial evidence that POMC neuronal activity is strongly tied to mitochondria. In mice, POMC neuronal activity can be upregulated by mitochondrial-derived ROS (Diano et al., 2011). Moreover, normal mitochondrial dynamics (*i.e.* fusion and fission) in POMC neurons are essential for maintaining whole-body energy and glucose homeostasis under the altered metabolic conditions (Ramirez et al., 2017; Santoro et al., 2017). These findings substantiate the importance of mitochondria or mitochondria-derived signaling in the normal functions of POMC neurons. Although the evident importance of mitochondria-originated signals in POMC neurons had been suggested (Mishra et al., 2014), detailed signaling mechanisms and molecules are largely unknown.

In current study, I investigated the metabolic impacts of mitoribosomal stress in hypothalamic POMC neurons by depleting mitoribosomal protein CR6-interacting factor 1 (*Crif1*). This study shows that mitoribosomal stress in POMC neurons can either beneficial or harmful in terms of body metabolism depending on

the magnitude of mitochondrial stress in a dose-dependent manner; homozygous deletion of *Crif1* was detrimental (*i.e.* severe stress), whereas heterozygous disruption was beneficial (*i.e.* mild stress). I further revealed that the low-level mitoribosomal stress in POMC neurons induces high metabolic turnover and obesity resistance through cell-non-autonomous mitochondrial stress responses between the hypothalamus and the distal adipose tissues by enhancing inducible thermogenesis. In addition, I found that mild mitoribosomal stress increases β-END and MOTS-c expression in POMC neurons, which coordinates mitoribosomal stress response. Finally, in aspect of physiologic regulator or condition related to POMC neuronal mitoribosomal stress, I found that regular exercise and the myokine interleukin-6 stimulate hypothalamic MOTS-c and β-END production.

2. Materials and Methods

2.1. Animals

To generate POMC neuron-specific *Crif1* deficient mice, *Crif1* floxed mice (K won et al., 2008) were cross mated with Pomc-Cre mice (Jackson Laboratory) or Pomc-ERT2-Cre mice (MGI Mouse). Tamoxifen (75 mg/kg dissolved in DMSO) was then injected into the peritoneum of the Pomc-ERT2-Cre; $Crif1^{f/+}$ mice at 7 weeks of age. To isolate POMC neurons or POMC neuron-specific transcripts, the mice were mated with Rosa26; eGFP-loxP mice or RiboTag ($Rpl22^{HA}$) mice (both from Jackson Laboratory). C57BL/6J male mice at 7 – 8 weeks of age were purchased from Orient Bio. All mice had free access to a standard chow diet (Cargill Agri Purina) and water unless indicated. To induce diet-induced obesity, mice were fed a high-fat diet (60% fat, Research Diet). Animals were housed under controlled temperature conditions (22 ± 1°C) and subjected to a 12-h light-dark cycle, with light from 08:00 to 20:00 hours. All animal procedures were approved by the Institutional Animal Care and Use Committee of the Asan Institute for Life Sciences (Seoul, Korea).

2.2. Cell lines

N1 (Cedarlane) and AtT20 (Obtained from Dr. Byung Ju Lee, University of Ulsan) cells were maintained in Dulbecco's modified Eagle's medium containing 10% fetal bovine serum (FBS) and 1% penicillin/streptomycin.

2.3. FACS sorting of POMC cells

The medial basal hypothalamus of mice with eGFP-labeled POMC neurons were dissected, mechanically chopped into small pieces in lysis buffer (HBSS containing 0.002% Dnase 1) on ice using a scalpel. Chopped tissues were incubated in lysis buffer containing 0.01% trypsin in a 37 °C water bath for 30 min during which time the sample tubes were gently inverted every 5 min. After centrifugation (1000 rpm for 5 min), pellets were gently resuspended in 10% FBS-containing Neurobasal Media (Thermo Fisher Scientific) and dissociated into single cells by pipetting with 1 ml, 200 μl, and 10 μl tips (at least 10 times each). Pomc-eGFP^{+} cells and Pomc-eGFP^{-} cells were gated and sorted by fluorescence-activated cell sorting (FACS) with the BD FACS Aria II Cell Sorter. Non-fluorescent hypothalamic cells were obtained from C57 mice to set the threshold of eGFP fluorescence. Successful FACS of eGFP cells and *Crif1* depletion was confirmed by *Pomc* and *Crif1* qRT-PCR analysis in eGFP^{+} cells and eGFP^{-} cells. For this, the hypothalami from two animals were pooled into one sample and total RNA was extracted using an RNeasy Plus mini kit (Qiagen).

2.4. Metabolic phenotyping

Food intake levels and body weights were monitored weekly after weaning until sacrifice. Body composition (lean mass and fat mass) was measured using dual x-ray absorptiometry (iNSiGHT VET DXA, OsteoSys) during the late light phase at the indicated ages. Energy expenditure (EE) and locomotor activity were

determined using a comprehensive lab monitoring system (CLAMS) (Columbus Instruments). Mice were placed in the CLAMS chambers for 48 h to acclimatize to these conditions before measurement. During this period, day-night cycles were the same as those during the initial housing of the animals and food was provided as pellets on the floor of the CLAMS cages. For the glucose tolerance test, D-glucose (1 g/kg, Sigma) was orally administrated to overnight-fasted mice. For the insulin tolerance test, insulin (Humulin-R® 0.25 U/kg, Eli Lilly) were injected into the peritoneum following a 5 h-fasting. Blood samples were obtained from the tail vein for glucose measurement immediately before and at the indicated times after injections. Glucose levels were measured using a glucometer (ACCU-CHEK Aviva Plus System, Aviva).

2.5. Body temperature measurements

Skin temperature of mice was determined with thermal camera (FLIR T650SC, FLIR Systems). Rectal temperatures were measured with thermometers (BAT-12 Microprobe Thermometer, Physitemp Instruments) before and during 4°C cold exposure.

2.6. Immunostaining of the hypothalamus

Mice were anesthetized with an intraperitoneal injection of 40 mg/kg Zoletil® and 5 mg/kg Rompun®, and then perfused with 50 ml saline followed by 50 ml 1% paraformaldehyde (PFA) via the left ventricle of the heart. Whole brains were collected, fixed with 1% PFA for 2 h, and dehydrated in 30% sucrose solution until

the tissues sank to the bottom of the container. Coronal brains including the hypothalamus were sectioned at a 30 μm thickness using a cryostat (Leica). One of every five slices (about 10 brain slices per animal) was collected. For β-END staining, hypothalamic slices were blocked with 3% bovine serum albumin (BSA) in 0.5% PBST and then incubated with anti-β-END antibody (1:1500, rabbit, Phoenix Pharmaceuticals) at 4˚C for 48 h and then at room temperature (RT) for 1 h. For α-MSH staining, hypothalamic slices were pretreated with 1% NaOH/1% H_2O_2 for 20 min followed by 0.3% glycine for 10 min, blocked for 1 h with 5% normal donkey serum in 0.5% PBST and incubated with anti-α-MSH antibody (1:1000, sheep, MerckMillipore) in blocking solution for 48 h at 4˚C. For MOTS-c staining, hypothalamic slices were blocked with 3% BSA in 0.1% PBST and subjected to treatment with anti-MOTS-c antibody (1:200, rabbit, produced by Dr. Changhan Lee) for 48 h at 4˚C. For c-Fos staining, hypothalamic slices were blocked with 3% BSA in 0.5% PBST and incubated with anti-c-Fos antibody (1:1000, rabbit, Synaptic Systems) for 24 h at 4˚C. After washing, slides were incubated with the appropriate Alexa-Flour 488- or 555-conjugated secondary antibodies (1:1000) at RT for 2 h. For nuclear staining, slides were treated with DAPI (1:10000) for 10 min before mounting. Immunofluorescence images were obtained using a confocal microscopy (Carl Zeiss 710, Germany). Quantification of the average fluorescence intensity of approximately 100 cells and the numbers of POMC neurons were analyzed on 5−7 hypothalamic slices or 3 brainstem and pituitary slices per mouse using ImageJ (NIH) or Photoshop version CS6 (Adobe Systems).

To determine β-END- and α-MSH-immunoreactive axonal projections, mice were cardiac-perfused with 4% PFA dissolved in borate buffer (38 g/L, pH 9.5) and post-fixed in 20% sucrose – 4% PFA – borate solution at 4 °C for 5 h. Hypothalamic slices were blocked with 3% BSA in 0.5% PBST buffer for 1 h at RT, incubated with anti-β-END antibody (1:1000, rabbit, Phoenix Pharmaceuticals) or anti-α-MSH antibody (1:1000, sheep, MerckMillipore) in blocking solution at 4°C for 72 h and then with Alexa-Fluor-conjugated secondary antibodies (1:1000) at RT for 1 h. Quantitative analysis of the β-END$^+$ or α-MSH$^+$ axonal projection density was conducted in the entire area of PVH and DMH (3 brain sections per mouse) as previously described (Bouret et al., 2004) and the average values were presented. After adjustment of the brightness and contrast and elimination of background, I measured the density of immunoreactivity in these areas.

2.7. Pomc in situ hybridization

Mice were cardiac-perfused with 4% PFA dissolved in DEPC water. Whole brains were collected, post-fixed overnight, dehydrated in 30% sucrose solution for 48 h, and sectioned into 14 μm-thick slices. Fluorescence in situ hybridization (FISH) was performed using RNAscope® fluorescent multiplex reagents (Advanced Cell Diagnostics) according to the manufacturer's instructions. RNA probes for mouse *Pomc* (Advanced Cell Diagnostics) was incubated with the brain

slices and signal amplification was achieved using the multiplex reagents. For POMC and MOTS-c double staining, brain slices were subjected to *Pomc* in situ hybridization and then to MOTS-c immunostaining as described in the immunostaining section.

2.8. mRNA expression measurement

Total RNA was isolated from tissues or cells using Trizol reagent (Thermo Fisher), and cDNA was prepared from total RNA using M-MLV reverse transcriptase and oligo-dT primers (Invitrogen). The produced cDNA was then amplified on a 7500 Fast Real-Time PCR System (Applied Biosystems). Real-time PCR was performed in triplicate using SYBR Green premix (Enzynomics). All quantitative calculations were performed using the $^{\Delta\Delta}$CT method. All mouse primer sequences are listed in Table S1. To assay *Crif1* and UPR^{mt} gene expression specifically in POMC neurons, immunoprecipitation (IP) of POMC neuronal polyribosomes was conducted as described previously (Sanz et al., 2009). Hypothalamic samples from RiboTag mice were homogenized with a Dounce homogenizer on ice in 500 μl ice-cold homogenization buffer (50 mM Tris, pH 7.4, 100 mM KCl, 12 mM $MgCl_2$, 1% NP-40, 1 mM dithiothreitol (DTT), 1:100 protease inhibitor, 200 units/ml Rnasin®, 0.1 mg/ml cycloheximide in 10% w/v Rnase-free DW). After centrifugation (4°C at 11.9 × g for 10 min), 50 μl of supernatant was immediately frozen and stored as an input sample. The remaining supernatant was split into 2 samples and subjected to IP using a hemagglutinin antibody (Covance) or mouse monoclonal IgG1 (Merck) and protein A/G magnetic

beads (Promega) on a rotator at 4°C overnight. The following day, RiboTag-IP fractions were placed on a DynaMag-2 magnet (Life Technologies) on ice, and the bead pellet was washed with high salt buffer (HSB: 50 mM Tris, 300 mM KCl, 12 mM $MgCl_2$, 1% NP-40, 1 mM DTT, and 100 μg/ml cyclohexamide). The beads were re-suspended in 400 μl of supplemented RLT buffer (10 μl beta-mercaptoethanol/10 ml of RLT Buffer) from the RNeasy plus micro kit (Qiagen) and vortexed vigorously. RLT buffer containing the immunoprecipitated RNA was removed from the magnetic beads prior to RNA purification using an RNeasy kit (Qiagen) in accordance with the manufacturer's protocol. Likewise, 350 μl of RLT was added to the input fractions prior to RNA isolation. Both input and RiboTag-IP samples were eluted in 14 μl of water and subjected to real time PCR.

2.9. Immunoblotting

Fifty micrograms of tissue lysates were separated using 8% SDS-PAGE and transferred to PVDF membranes (GE Healthcare). After incubation in blocking buffer, the membranes were incubated overnight at 4 °C with antibodies against ATP5A1 (1:1000), MTCO1 (1:1000) and β-ACTIN (1:5000). Blots were developed using horseradish peroxidase (HRP)-linked secondary antibody and a chemiluminescent detection system (PerkinElmer). The band intensities of ATP5A1 and MTCO1 were normalized to that of β-ACTIN. The expression ratios of ATP5A1 versus MTCO1 were determined.

2.10. Adipose tissue histology and sympathetic innervation

The BAT, iWAT and gWAT were dissected, fixed in 4% PFA overnight and embedded in paraffin. Paraffin tissue sections were stained with hematoxylin and eosin (H&E) and observed by microscopy (BX53, Olympus). Sympathetic nerve terminals were stained as described previously (Vargovic et al., 2011). Paraffin sections of mouse adipose tissue were deparaffinized and rehydrated by washing twice for 10 min with xylene, followed by washes in 100%, 95% and 70% ethanol (2 min twice each). Sections were rinsed in distilled water, placed into a warmed citrate buffer (0.01 M, pH 6.0) for 5 min, followed by immersion in a hot citrate buffer (58 °C) and cooled at RT, washed with Tris-buffered saline (TBS) for 5 min three times, transferred into methanol solutions containing 0.5% H_2O_2 and washed again in TBS. Pre-blocking procedure with a 20 μg/ml solution of anti-rabbit IgG (Santa Cruz) for 1 h at RT was followed by blocking with 2% of normal horse serum for 1 h at RT. Slides were incubated with rabbit anti-tyrosine hydroxylase antibody (1:250, rabbit, MerckMillipore) overnight at 4 °C and then with Alexa-Flour 488-conjugated anti-rabbit secondary antibody (1:500) for 1 h at RT.

Chemical sympathetic denervation in the iWAT was performed as described previously (Harris, 2012). Briefly, under anesthesia, I exposed one side of the iWAT from a Pomc-Cre; $Crif1^{f/+}$ male mouse (6–8 weeks of age) and microinjected 6-hydroxydopamine (6-OHDA) using a microsyringe [20 injections of 1 μl of 6-OHDA solution (9 mg dissolved in 1 ml of 0.15 M NaCl containing 1% (w/v) ascorbic acid)] as described previously (Chao et al., 2011). I microinjected the same volume of vehicle (20 injections) to the other side of the iWAT in the Pomc-Cre; $Crif1^{f/+}$ mice or to both sides of iWAT of $Crif1^{f/f}$ controls. Two weeks after the

6-OHDA injections, both sides of the iWAT were collected, divided into two pieces, and subjected to histological and gene expression analysis.

2.11. Mitochondrial mass and morphology examinations

The mitochondrial morphology and network complexity in the POMC neurons were assessed by immunogold electron microscopy and analysis as described previously by Dietrich, M.O. et al (Dietrich et al., 2013). Briefly, mice were transcardially perfused with 0.9% saline with heparin followed by fixative solution (4% PFA, 0.1% glutaraldehyde, 15% picric acid in 0.1 M phosphate buffer, pH 7.4). The brains were then removed and fixed overnight with the same fixative without glutaraldehyde. The brain were sliced at a 50 μm thickness using a vibrotome and subjected to POMC immunostaining using a primary antibody to β-END (1:1000, rabbit, Phoenix Pharmaceuticals, 48 h at 4 °C with gentle shaking) prior to the EM analysis. For mitochondria mass and morphology analysis in the BAT, mice were transcardially perfused as above. The BAT was cut into 1 mm^3 fragments, washed in fresh 0.1 M phosphate buffer (pH 7.4) and fixed in the same buffer containing 2.5% glutaraldehyde at RT for 4 h. Tissues were then washed three times in fresh 0.1 M phosphate buffer (pH 7.4) for 10 min each. Subsequently, the tissues were fixed in 1% OsO_4 for 1 h at RT and washed three times in 0.1 M phosphate buffer for 10 min each. Finally, the tissues were embedded in Epon using standard techniques following dehydration with ethyl alcohol and propylene oxide. Ultrathin sections (60 nm) were cut from the blocks using a Reichert–Jung Ultracut E ultramicrotome and a diamond knife. The sections were collected and stained with uranyl acetate, followed by lead citrate, and then observed using a JEM 1400 transmission electron microscope (JEOL Ltd.). To assess mitochondria biogenesis,

DNA was extracted from the BAT and iWAT using DNA extraction kit (Qiagen) and the mtDNA content in the BAT and iWAT was quantitated using real time PCR analysis and normalized by the nDNA content as previously described (Weimer et al., 2014).

2.12. ELISA and radioimmunoassay

Mediobasal hypothalamic blocks were collected, weighed and quickly frozen in liquid nitrogen and stored at −80°C until use. Hypothalamic MOTS-c protein contents were measured using a MOTS-c commercial ELISA kit (MyBioSource) in accordance with the manufacturer's protocol. Briefly, 50 μl of protein lysate from the mouse hypothalamus or N1 cells was added to the reaction and the absorbance of the sample was measured at 450 nm within 30 min. The hypothalamic α-MSH and β-END contents were measured using commercial RIA (Phoenix Pharmaceutical) and ELISA (MyBioSource) kits, respectively, according to the respective protocols provided by the manufacturer. Total protein amounts of samples were assayed using a BCA protein assay kit (Thermo Fisher) and hypothalamic peptide content was normalized by total protein content.

2.13. Intracerebroventricular cannulation and peptide administration

Stainless steel cannulae (26 gauge; Plastics One) were implanted into the third cerebral ventricle or intra-ARH of the mice as previously described (Kim et al., 2006). Peptides were dissolved in 0.9% saline solution just before use and were

administered via the brain-implanted cannulae. To examine whether ICV β-END administration can recapitulate the metabolic phenotype of POMC *Crif1* heterodeficient mice, β-END (0.1 μg, Sigma) was ICV-injected twice a day (in the early light phase and 1 h before light-off) in C57 mice for 4 days. Food intake and body weight were monitored just before injections and the EE was measured on treatment day 3. In β-END feeding study, *ad libitum*-fed C57 mice received a single ICV injection of either saline or β-END (0.03 μg/2 μl) during the early light phase and food intake was monitored for 24 h. For ICV MOTS-c continuous infusion, MOTS-c peptide (generated by Changhan Lee's lab) was infused into HFD-fed mice via an ICV-implanted cannula using an Alzet osmotic minipump placed in the interscapular area (3 μg/2.6 μl per day for 28 days). Food intake and body weight were monitored daily whilst the EE were measured on treatment day 20. In an additional set of experiments, either anti-MOTS-c antibody (from Changhan Lee' lab) or IgG (0.2 μg/μl, 1 μl injection each side) was injected daily into the bilateral ARH of 7–8 weeks-old $Crif1^{f/f}$ or Pomc-Cre; $Crif1^{f/+}$ mice for 1 week. For ICV IL-6 treatment, IL-6 peptide (R&D Systems) was ICV-infused in C57 mice using an osmotic minipump (0.4 μg per day for 5 days). At the end of the treatments, the mice were sacrificed in the early light phase under freely-fed conditions. The hypothalamus, iWAT and BAT were collected for histological examination and for real time PCR analysis of thermogenic and UPR^{mt} genes.

2.14. Exercise study

Mice belonging to the regular exercise group were subjected to treadmill

running for 2 weeks between 1800 and 2000 hours. Each exercise section consisted of a 15 min warm-up (treadmill speed gradually increased from 5 to 18 meters/min over 15 min) followed by 50 min of running (18 meters/min, no incline) and a 5 min cooling-down period. The mice were euthanized by decapitation 24 h after last running training. In another group, the mice were acclimated on the treadmill as previously described (Reynolds et al., 2019) and four days later were subjected to high-intensity running till exhausted as follows: (Stage 1) 5 min run at 13 meters/min, (Stage 2) another 5 min run with increasing speed (1 meters/min), (Stage 3) 30 min run at a fixed speed of 18 meters/min, and (Stage 4) open running until exhaustion at 23 meters/min (no incline). Mice were sacrificed immediately after exercise.

2.15. Hypothalamic ROS measurement and blockade

Hypothalamic ROS production was assessed using dihydroethidium (DHE) following a previously described methodology (Andrews et al., 2008; Toda et al., 2016). Briefly, DHE (10 mg/kg, Invitrogen) was administered into the tail vein 2 h prior to sacrifice. To block hypothalamic ROS formation, I injected 2 μl of ROS-scavenging cocktail containing ascorbic acid (10 μM), N-acetyl-L-cysteine (NAC, 10 μM) and Tempo (1 μM) via a cerebroventricle-implanted cannulae 10 min before each running session in the second week of the regular exercise program.

2.16. MOTS-c nuclear translocation study

N1 cells were treated with H_2O_2 (100 nM) with or without NAC (1 mM) for 24 h before fixation. In separate experiments, the cells were treated with IL-6 (100

nM) with or without NAC (1 mM) for 24 h.

Cells were fixed with 4% PFA for 10 min at RT, washed with PBS, permeabilized in 0.2% PBST at RT for 10 min. The samples were then blocked with 3% BSA in 0.1% PBST and incubated with anti-MOTS-c antibody (1:200) at 4°C overnight, followed by incubation with anti-rabbit secondary antibody for 1 h. Samples were then washed three times with 0.2% PBST and incubated with DAPI (1:10,000) for 10 min at RT to visualize the nuclei. After three washes in PBST, the coverslips were mounted in mounting medium. The cellular images were obtained using a Zeiss LSM700 confocal microscope system and software.

2.17. Gene overexpression and knockdown

Mots-c- or *Stat3*-expressing plasmids at indicated doses were transfected into 60~70% confluent cells using Lipofectamine. For small interfering RNA (siRNA)-mediated gene knockdown, cells were transfected using Lipofectamine with siRNA targeting murine *Stat3* (Ambion) or *Crif1* (targeting nucleotide positions +520 to +545: 5'-GGAGUGCUCGCUUCCAGGAACUAUU-3'). Controls were transfected with a non-targeting scrambled siRNA. Successful gene overexpression or knockdown was confirmed by real time PCR (for *Crif1*), immunoblotting (for STAT3) or ELISA (for MOTS-c) in cells collected at 48 h post-transfection.

2.18. Pomc promotor activity

AtT20 cells were cultured in 12-well plates and were transfected with

plasmids expressing murine *Pomc* promoter-luciferase reporter (*pPomc-luc*; nucleotides −1040 to +60, 200 ng) or *pCMV-β-gal* (25 ng) with or without human *MOTS-c*-expressing plasmid (*pMOTS-c*, 0.1 to 10 ng) using Lipofectamine. To study the interaction between MOTS-c and STAT3 in regulating *Pomc* promotor activity, cells were transfected with *pPomc-luc*, *pCMV-β-gal*, *pMOTS-c* plus *pStat3* or mock plasmid. In a separate experiment, cells were transfected with *pMOTS-c* and *Stat3* siRNA or non-targeting siRNA. The total amount of DNA used for transfection in each condition was corrected by the addition of mock DNA. At 48 h after transfection, cells were harvested to measure luciferase activities, which were normalized to β-galactosidase activities. Transfections were performed in triplicate and the experiments were repeated at least three times.

2.19. Chromatin immunoprecipitation study

N1 cells were transfected with *MOTS-c*-expressing plasmid or mock plasmid. After 48 h of transfection, cells were fixed with formaldehyde, lysed, and sonicated. Soluble chromatin was immunoprecipitated with either 1 μg of anti-STAT3 antibody (Cell Signaling) or an equivalent amount of rabbit IgG. After de-crosslinking of the DNA, the samples were subjected to PCR to amplify the region containing a potential STAT3 binding site on the mouse *Pomc* promoter (nucleotide positions –679 to –688) (Figure 5) using the primers: 5'-TCTCAAAACGGAACTGAGAT-3' and 5'-ATAGGTAATTCCACTCCGA-3'. The PCR band intensity of immunoprecipitated DNA sample was corrected by the band intensity of the input sample.

2.20. Quantification and statistical analysis

Data values in this study are presented as the mean ± SEM. Statistical analysis was performed using SPSS-PC (version 22) or Graph Pad Prism software (version 7.0). Statistical significance between groups was tested using one-way, two-way or repeated measures analysis of variance (ANOVA) tests followed by a *post-hoc* LSD (least significant difference) test, or an unpaired Student's t-test when appropriate. Significance was defined by a p value < 0.05.

Table 1. Primers for qRT-PCR

Gene	Forward	Reverse
Agrp	5'-ACAACTGCAGACCGAGCA-3'	5'-GACGCGGAGAACGAGACT-3'
Atp23	5'-GACTGCTCCCTTGTGAACGA-3'	5'-CGCACGCAAGTCTGATGATG-3'
Atp5a1	5'-CATTGGTGATGGTATTGCGC-3'	5'-TCCCAAACACGACAACTCC-3'
Cidea1	5'-TGCTCTTCTGTATCGCCCAGT-3'	5'-GCCGTGTTAAGGAATCTGCTG-3'
Clpp1	5'-GCCATTCACTGCCCAATTCC-3'	5'-TGCTGACTCGATCACCTGTAG-3'
Cpe	5'-CAGCAAGAGGACGGCATCTC-3'	5'-GTCCAACCGCCTCATTACCAT-3'
Crif1	5'-TATCTCCTGCGGCTCTCTGT-3'	5'-CTTCTGCTTTCGCCAGTTTT-3'
Gapdh	5'-CCTGTTGCTGTAGCCGTAT-3'	5'-ACTCTTCCACCTTCGATGC-3'
Gfap	5'-CACCTACAGGAAATTGCTGGAGG-3'	5'-CCACGATGTTCCTCTTGAGGTG-3'
Hspd1	5'-GAGCTGGGTCCCTCACTCG-3'	5'-AGTCGAAGCATTTCTGCGGG-3'
Hsp60	5'-GACGTTGACGGAGAAGCTCTAA-3'	5'-CACTGCACCACCAGTAGCAATA-3'
Hsp90	5'-AGGTCCTCGGAGTCAACCAC-3'	5'-TCAAATTGTATGTCCGCCGT-3'
Htra2	5'-TCCCCGGAGCCAGTACAAT-3'	5'-GAAAGGGTGCCGGTCTAGG-3'
Iba1	5'-TCTGCCGTCCAAACTTGAAGCC-3'	5'-CTCTTCAGCTCTAGGTGGGTCT-3'
Immp1l	5'-ATGACCCATGCACGCTTTGA-3'	5'-TCTGCTACCACCAGCCATAA-3'
Immp2l	5'-ACATGTGGGTTGAAGGCGAT-3'	5'-CCCAGAGAAACCGGTCCAAA-3'
Insr	5'-AGATGAGAGGTGCAGTGTGGCT-3'	5'-GGTTCCTTTGGCTCTTGCCACA-3'
Lepr	5'-CTTTCCTGTGGACAGAACCAGC-3'	5'-AGCACTGAGTGACTCCACAGCA-3'
Lonp1	5'-AGCCCTATGTTGGCGTCTTC-3'	5'-CCGGCTGATGTGAATCCTTCT-3'
Mtco1	5'-CCCAGATATAGCATTCCCACG-3'	5'-ACTGTTCATCCTGTTCCTGC-3'
mtDNA	5'-AAGACACCTTGCCTAGCCACAC-3'	5'-TGGCTGGCACGAAATTTACC-3'
nDNA	5'-AACTTTCGATGGTAGTCGCCG-3'	5'-CCTTGGATGTGGTAGCCGTTT-3'
Npy	5'-GGACTGACCCTCGCTCTA-3'	5'-TCGCAGAGCGGAGTAGTA-3'
Pam	5'-CTGGGGTCACACCTAAAGAGT-3'	5'-ATGAGGGCATGTTGCATCCAA-3'
Parl	5'-TCACCATTGGGTTCACAGGC-3'	5'-TCCTTTTGTGGCCGTATGCT-3'
Pcsk1	5'-AGTTGGAGGCATAAGAATGCTG-3'	5'-GCCTTCTGGGCTAGTCTGC-3'
Pcsk2	5'-AGAGAGACCCCAGGATAAAGATG-3'	5'-CTTGCCCAGTGTTGAACAGGT-3'
Pomc	5'-CAGGTCCTGGAGTCCGAC-3'	5'-CATGAAGCCACCGTAACG-3'
Ppargc1a	5'-CCCTGCCATTGTTAAGACC-3'	5'-TGCTGCTGCTCCTGTTTTC-3'
Prcp	5'-CCGCATTTGTCAGCCAGTC-3'	5'-CCAAAGTGGTCAACCTTCTGTTC-3'
Prdm16	5'-AGCTACTGGTGGAACGGAGA-3'	5'-TTAAGCCAATGCTCGCTTCT-3'
Sf1	5'-GTGCATGGTCTTTAAGGAGCTGG-3'	5'-GGATGCTGTCTTCCTTGCCGTA-3'

3. Results

3.1 Severe mitoribosomal stress in POMC neurons causes maturity-onset obesity

CRIF1 is a mitoribosomal protein that coordinates the insertion of mitochondrial-encoded proteins into the ETC complexes (Kim et al., 2012). To study mitoribosomal stress in POMC neurons, I generated mice lacking *Crif1* in POMC neurons using the Cre-loxP system. FACS sorting of POMC-eGFP cells and real time PCR analysis confirmed successful *Crif1* depletion in the hypothalamic POMC neurons, but not in non-POMC cells (Figures 1A and 1B). I compared the metabolic phenotype of Pomc-Cre; $Crif1^{f/f}$ mice to the $Crif1^{f/f}$ littermates (*i.e.* control group) as $Crif1^{f/f}$ and Pomc-Cre mice were metabolically indistinguishable (Figure 2). Pomc-Cre; $Crif1^{f/f}$ mice were born and developed normally until around 10 weeks of age when they started to show accelerated weight gain under chow diet (CD)-fed conditions (Figure 3). By 25 weeks, all Pomc-Cre; $Crif1^{f/f}$ mice gained considerably more weight, but the effect was more pronounced in females compared to males (Figure 3). Body composition analysis revealed that both male and female Pomc-Cre; $Crif1^{f/f}$ mice had normal lean mass at 8 and 14 weeks of age, but increased fat mass at 14 weeks, but not 8 weeks, of age (Figures 4A and 4B). These findings suggest that *Crif1* homodeficiency in POMC neurons leads to maturity-onset obesity in both males and females.

Monitoring of food intake revealed that Pomc-Cre; $Crif1^{f/f}$ males consumed more food before 10 weeks of age but showed normal food intake thereafter

(Figure 5), whereas females showed delayed-onset hyperphagia starting after 15 weeks of age. Energy expenditure (EE) was significantly higher in 8-week old male, but not female, Pomc-Cre; Crif1$^{f/f}$ mice (Figure 6). However, at 20 weeks of age, both sexes exhibited significantly reduced EE (Figure 6).

Glucose and insulin tolerance tests showed that male Pomc-Cre; Crif1$^{f/f}$ mice were insulin resistant by 8 weeks, but also developed hyperglycemia by 24 weeks of age (Figures 7). Similarly, female Pomc-Cre; Crif1$^{f/f}$ mice were also insulin resistant and hyperglycemic at 15 weeks of age (Figure 7). Hence, hypothalamic POMC neuron-specific *Crif1* homodeficiency leads to glucose intolerance resembling features of human type 2 diabetes.

In the previous study, *Crif1* deficiency in CaMKII-expressing neurons caused neuronal death in the hippocampus, leading to locomotor disability and early death prior to 24 weeks of age (Kim et al., 2012). Here, I show that, by 14 weeks of age, *Crif1* deficiency in POMC neurons (Pomc-Cre; Crif1$^{f/f}$ male mice) significantly reduced (i) the number of POMC neurons in the hypothalamic ARH as determined by β-endorphin (β-END) staining (Figure 8), (ii) the level of *Pomc* transcripts (Figure 9), and (iii) POMC neuronal activity as determined by c-Fos expression (Figure 10). These findings suggest that *Crif1* homodeficiency in POMC neurons reduces *Pomc* expression and neuronal activity after ~10 weeks of age and accelerates the loss of POMC neurons, resulting in severe obesity.

A

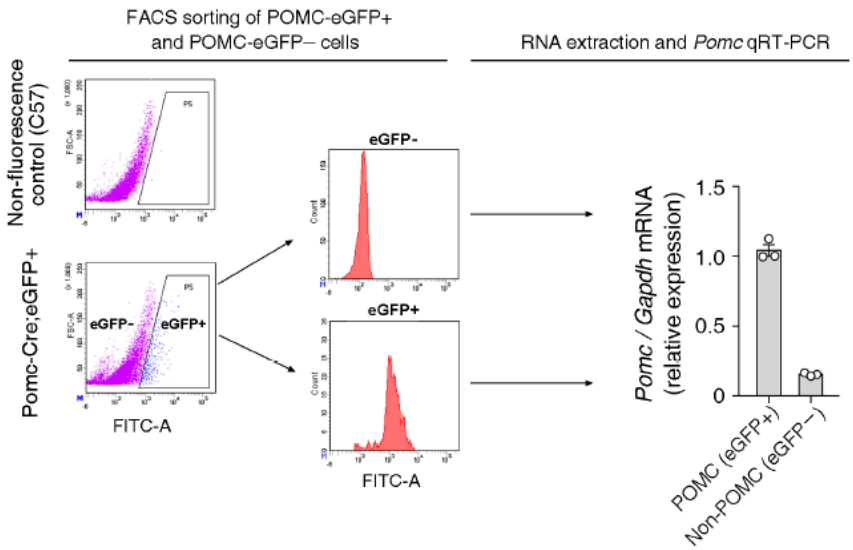

B

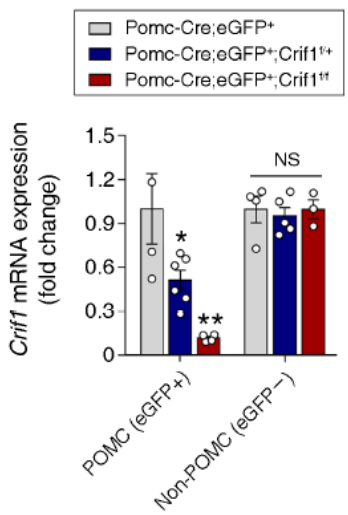

Figure 1. (A) The representative dot plot depicting FACS sorting of eGFP+ and eGFP─ cells isolated from the hypothalamus of Pomc-Cre; eGFP+ mice and confirmation of successful FACS sorting using real-time PCR analysis of Pomc expression in eGFP+ and eGFP─ cells. (B) Comparison of Crif1 mRNA expression among the mice groups in hypothalamic POMC-eGFP+ and POMC-eGFP— cells (n = 3─6). Results presented as mean ± SEM. *p < 0.05 and **p < 0.01 vs. Pomc-Cre; eGFP+ or Crif1$^{f/f}$ littermates. NS: not significant.

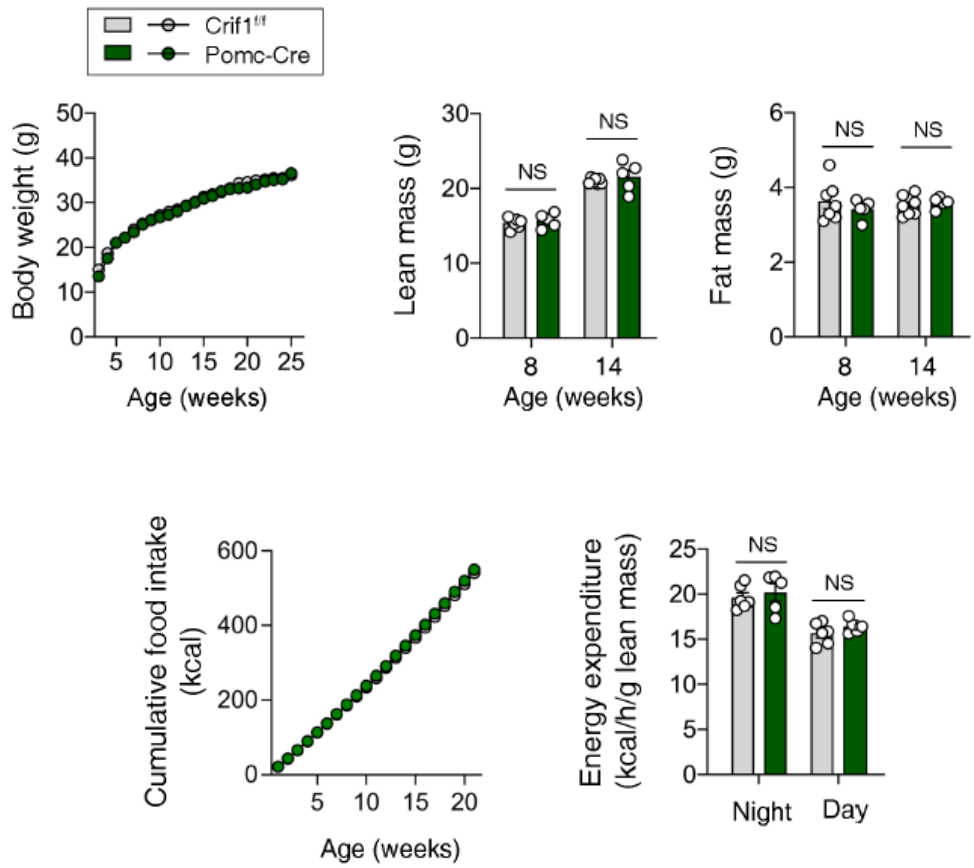

Figure 2. No differences in body weight, lean and fat mass, cumulative food intake, and energy expenditure between Pomc-Cre mice and Crif1f/f mice (n = 5─7). Results presented as mean ± SEM. NS: not significant.

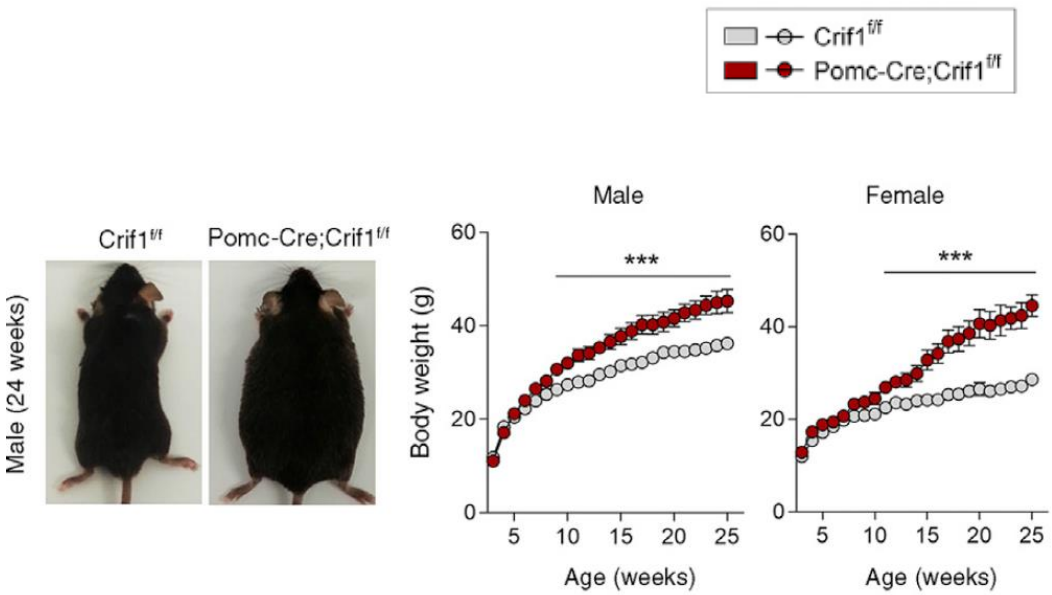

Figure 3. Representative body images and body weights in Crif1$^{f/f}$ and Pomc-Cre; Crif1$^{f/f}$ mice at the indicated ages (n = 7–8). Results are presented as a mean ± SEM. ***p < 0.001 vs. Crif1$^{f/f}$ littermates.

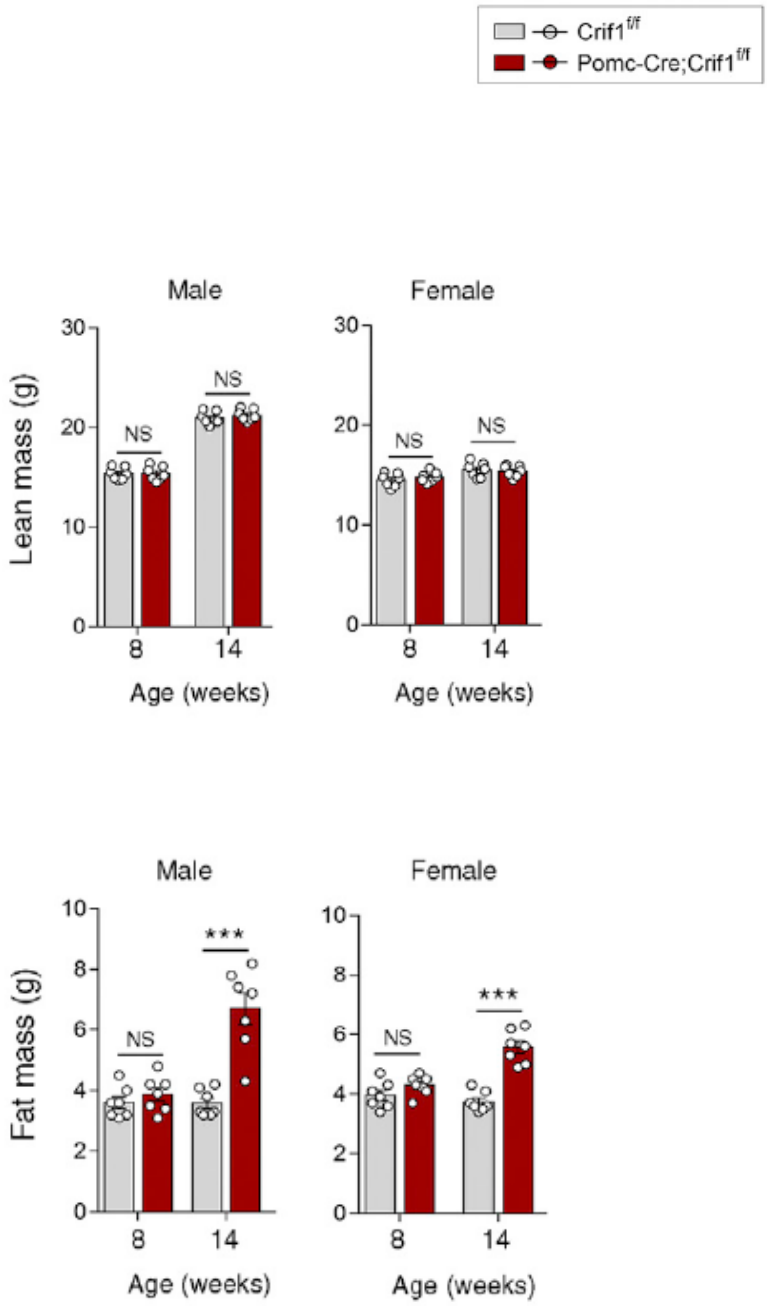

Figure 4. (A) Lean mass and (B) fat mass in Crif1$^{f/f}$ and Pomc-Cre; Crif1$^{f/f}$ mice at the indicated ages (n = 7–8). Results are presented as a mean ± SEM. ***p < 0.001 vs. Crif1$^{f/f}$ littermates. NS, not significant.

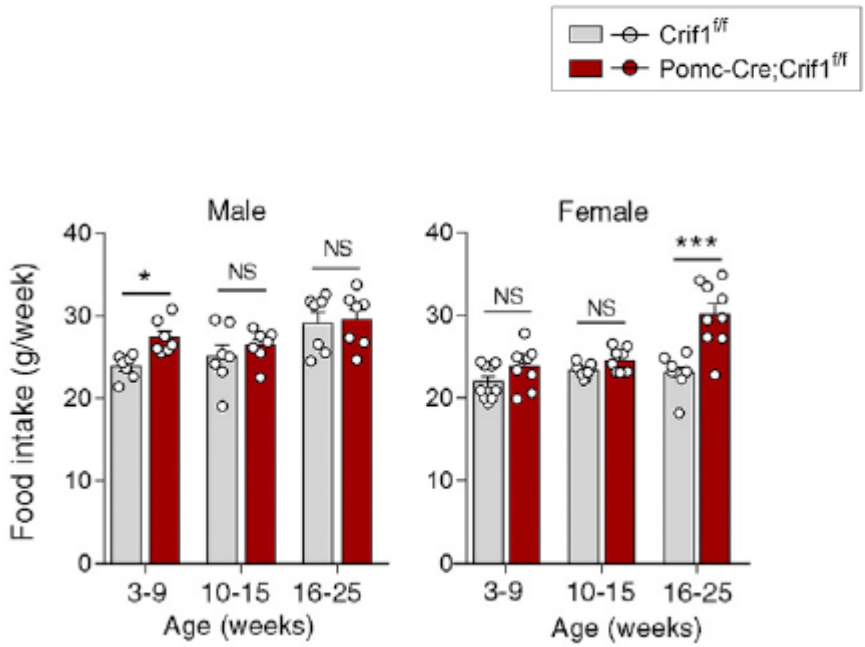

Figure 5. Food intakes measured at the indicated ages (n = 6–9). Results are presented as a mean ± SEM. *p < 0.05, and ***p < 0.001 vs. Crif1$^{f/f}$ littermates. NS, not significant.

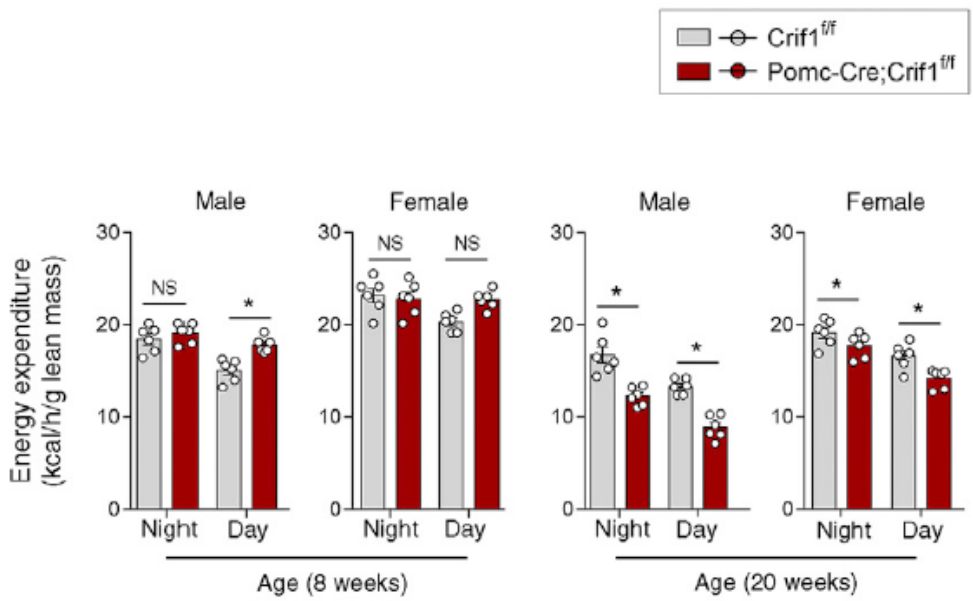

Figure 6. Energy expenditure measured at the indicated ages (n = 6–9). Results are presented as a mean ± SEM. *$p < 0.05$ vs. Crif1$^{f/f}$ littermates. NS, not significant.

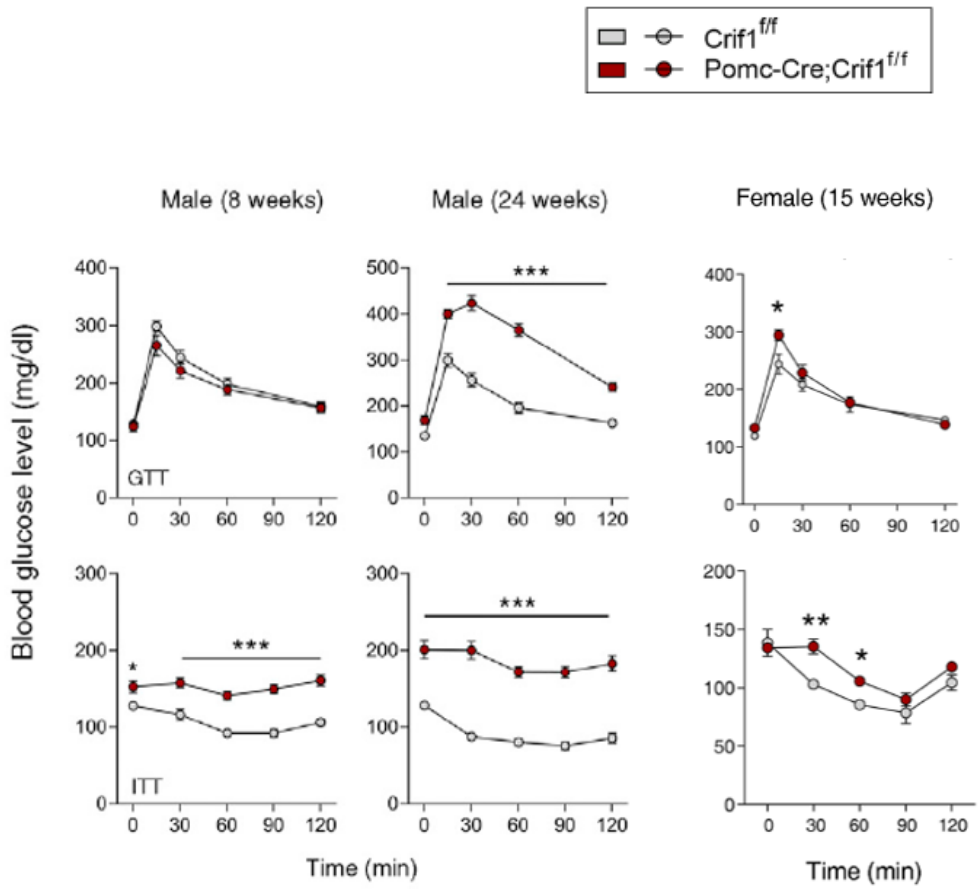

Figure 7. Results of glucose tolerance tests (GTT) and insulin tolerance tests (ITT) in Crif1$^{f/f}$ and Pomc-Cre; Crif1$^{f/f}$ mice at indicated age (n = 5–8). Results are presented as a mean ± SEM. *p < 0.05, and ***p < 0.001 vs. Crif1$^{f/f}$ littermates.

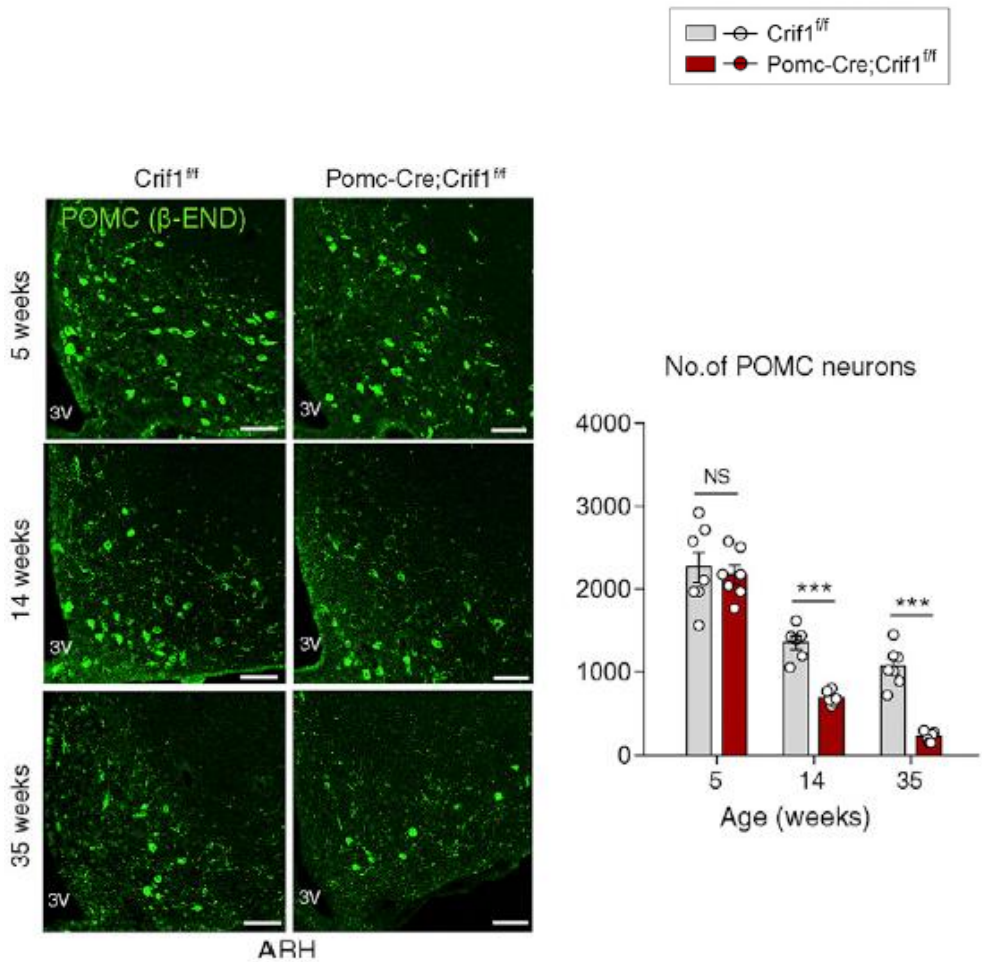

Figure 8. Immunohistochemistry of POMC neurons using β-endorphin (β-END) antibody at 5, 14 and 35 weeks of age (n = 6–7). 3V, third ventricle; ARH, hypothalamic arcuate nucleus. Scale bars, 50 μm. Results are presented as a mean ± SEM. ***$p < 0.001$ vs. Crif1$^{f/f}$ littermates. NS, not significant.

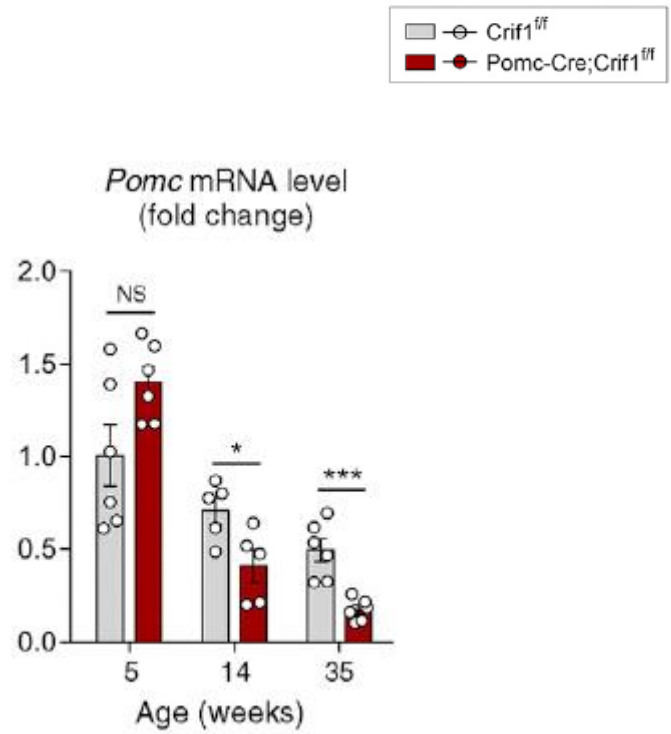

Figure 9. Hypothalamic *Pomc* mRNA expression measurement at 5, 14 and 35 weeks of age (n = 6–7). Results are presented as a mean ± SEM. *p < 0.05, and ***p < 0.001 vs. Crif1$^{f/f}$ littermates. NS, not significant.

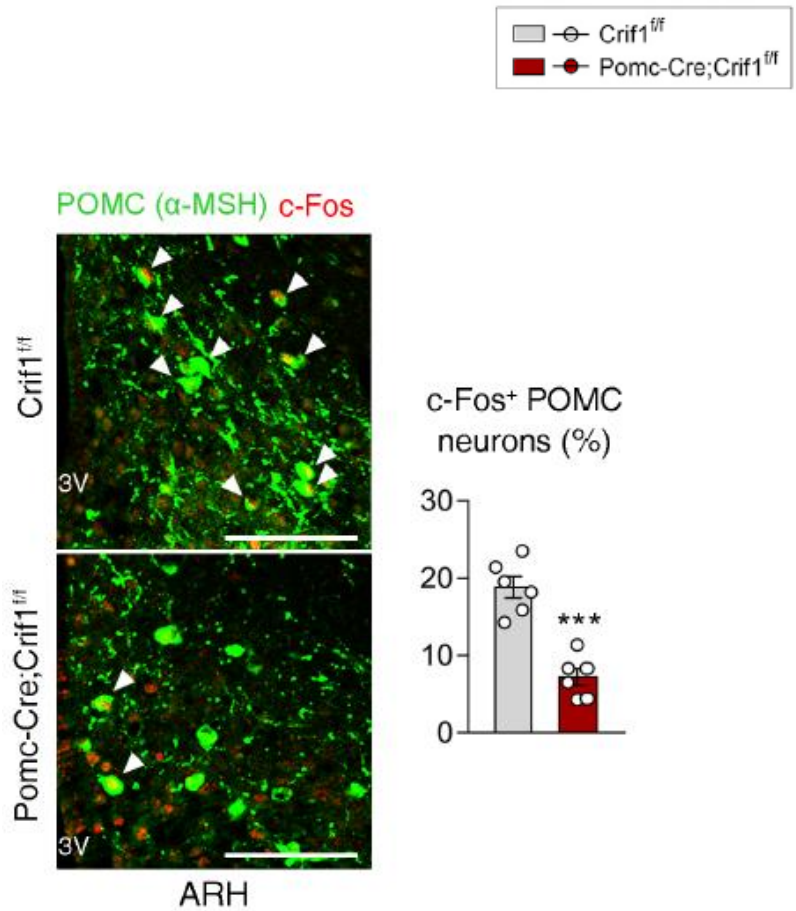

Figure 10. POMC (α-MSH) and c-Fos double staining in 14-week-old Pomc-Cre;Crif1f/f mice showing reduced POMC neuronal activity (n = 6). 3V, 3rd cerebroventricle; ARH, hypothalamic arcuate nucleus. Scale bars, 100 μm. Results are presented as a mean ± SEM. ***$p < 0.001$ vs. Crif1$^{f/f}$ littermates.

3.2. Mild mitoribosomal stress in POMC neurons promotes a high-turnover metabolism and resistance to diet-induced obesity

I next assessed the metabolic phenotype of mice with POMC-specific *Crif1* heterodeficiency. In the CD-fed condition, Pomc-Cre; Crif1$^{f/+}$ males and females showed no alteration in body weight, lean mass, nor fat mass (Figures 11 and 12). Yet, young male Pomc-Cre; Crif1$^{f/+}$ mice exhibited higher food intake, night-time EE, and overall locomotor activity compared to Crif1$^{f/f}$ littermates (Figure 13) while maintaining normal body weight/composition (Figures 11 and 12), glucose tolerance, and insulin sensitivity (Figure 14). Because POMC neurons control adipose tissue thermogenesis (Dodd et al., 2015), I assessed the thermogenic capacity of Pomc-Cre; Crif1$^{f/+}$ mice and found that they held rectal temperature much better during a 3-hour cold (4°C) challenge (Figure 15). Infrared thermal imaging also displayed higher skin temperature in these mice (Figure 16).

I metabolically challenged Pomc-Cre; Crif1$^{f/+}$ males by feeding them a 60% high fat diet (HFD) starting at 8 weeks of age. Pomc-Cre; Crif1$^{f/+}$ mice on a HFD gained significantly less weight compared to Crif1$^{f/f}$ controls despite consuming more calories, indicating a reduction in food efficiency (Figures 17A and 17B). Pomc-Cre; Crif1$^{f/+}$ mice had higher EE during the night (Figure 17C), which may have contributed to the resistance to diet-induced obesity.

Gene deletion using Pomc-Cre transgenic mice starts during the mid-embryonic period (Padilla et al., 2010). Moreover, during embryogenesis, POMC is transiently expressed in immature hypothalamic neurons, some of which adopt a non-POMC fate later in life (Padilla et al., 2010). To avoid *Crif1* deletion in non-

POMC neurons and the developmental defects caused by embryonic gene deletion, I induced *Crif1* depletion specifically in POMC neurons during young adulthood by injecting tamoxifen in 7 week-old Pomc-ERT2-Cre; Crif1$^{f/+}$ mice. Notably, Pomc-ERT2-Cre; Crif1$^{f/+}$ mice recapitulated the metabolic phenotype of the Pomc-Cre; Crif1$^{f/+}$ mice (Figures 18A-18E). Thus, the induction of POMC-specific partial *Crif1* deficiency in young adult mice also caused high turnover metabolism with enhanced thermogenesis.

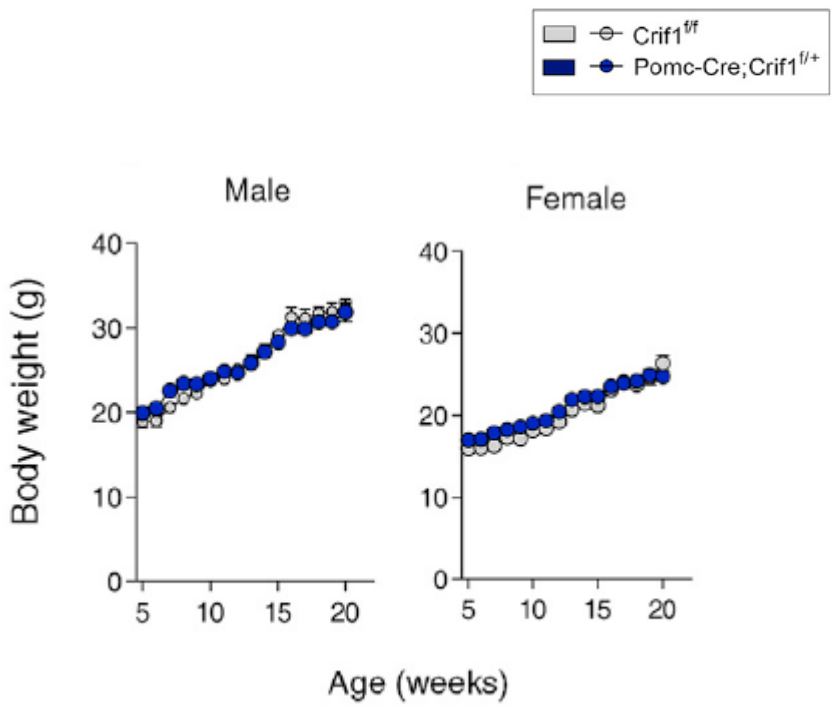

Figure 11. Body weights of Crif1$^{f/f}$ and Pomc-Cre; Crif1$^{f/+}$ mice, determined at the indicated ages (n = 6–8). Results are presented as a mean ± SEM.

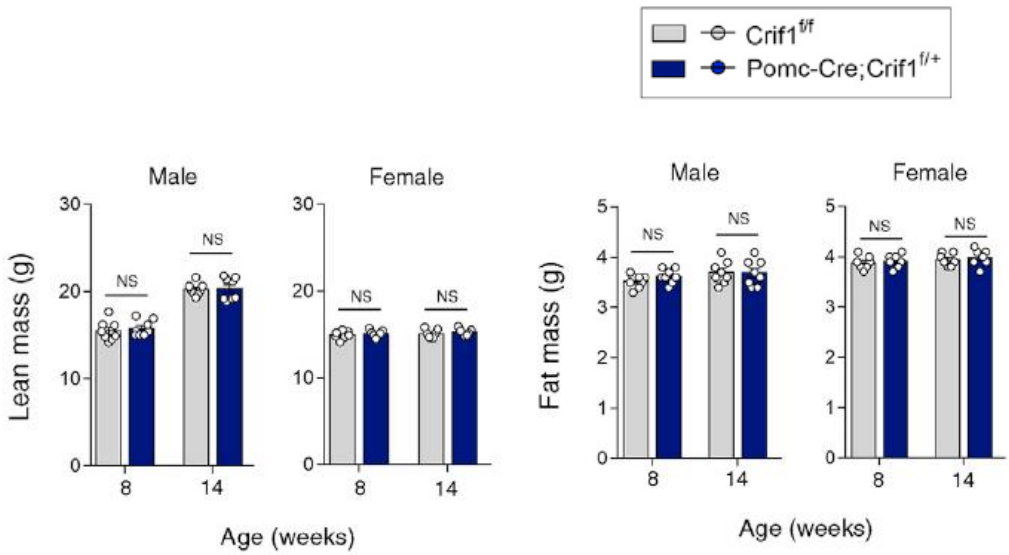

Figure 12. Lean mass and fat mass of Crif1$^{f/f}$ and Pomc-Cre; Crif1$^{f/+}$ mice, determined at the indicated ages (n = 6–8). Results are presented as a mean ± SEM. NS, not significant.

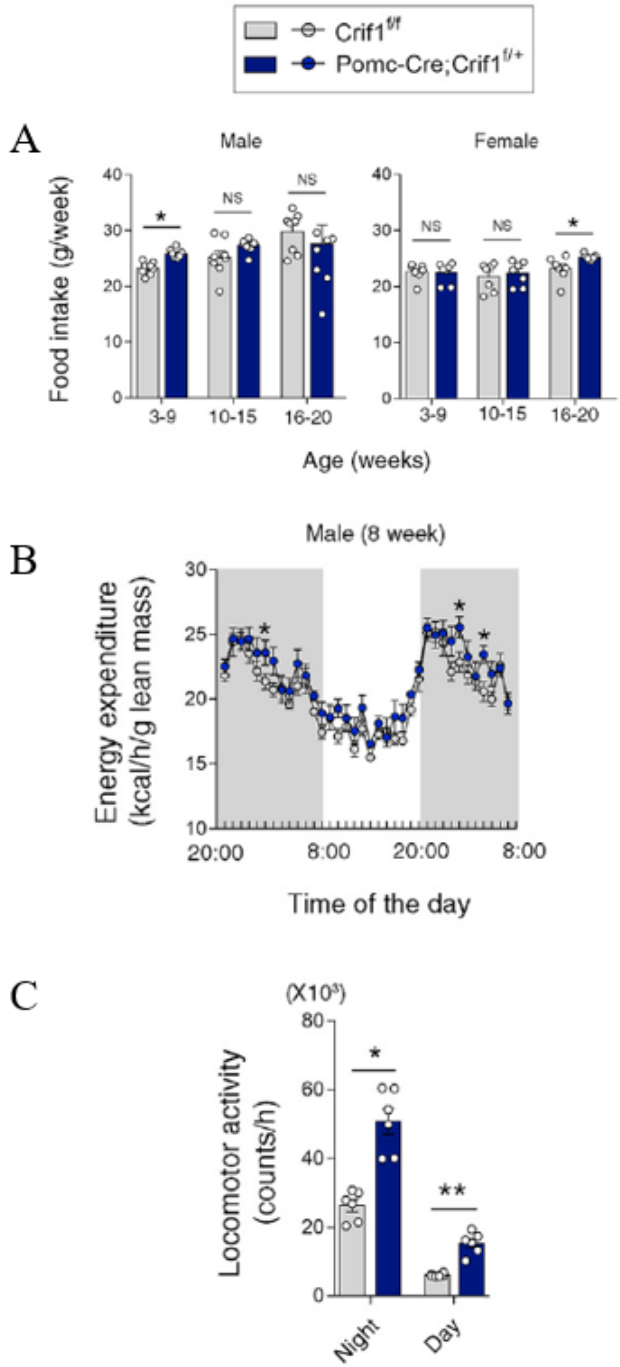

Figure 13. (A) Food intakes, (B) energy expenditure, and (C) locomotor activity in Crif1$^{f/f}$ and Pomc-Cre; Crif1$^{f/+}$ males at indicated age (n = 6). Results are presented as a mean ± SEM. *p < 0.05, **p < 0.01 vs. Crif1$^{f/f}$ controls.

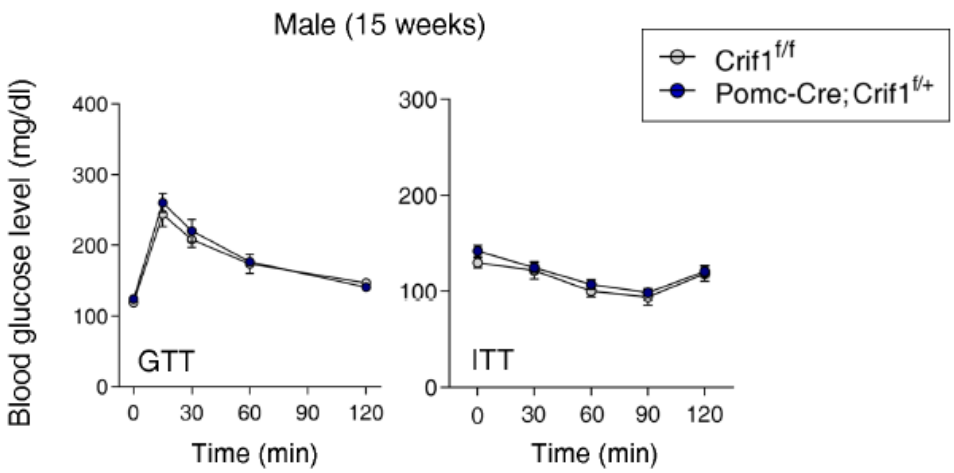

Figure 14. Glucose tolerance test (GTT) and insulin tolerance test (ITT) in 15 week-old Crif1$^{f/f}$ and Pomc-Cre; Crif1$^{f/+}$ male mice (n = 4─6).

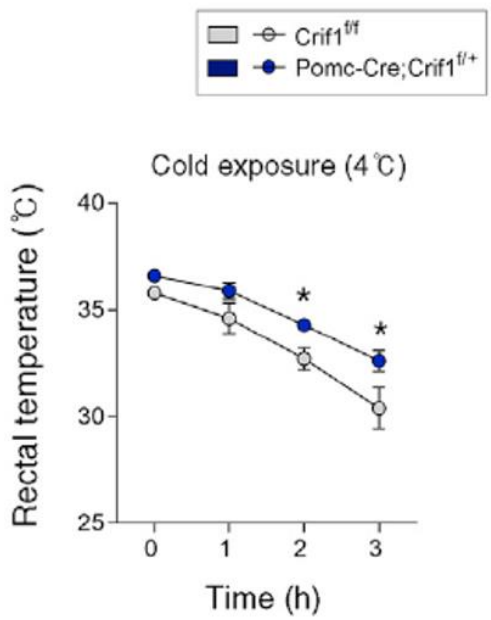

Figure 15. Rectal temperatures during 4°C cold exposure in young Crif1$^{f/f}$ and Pomc-Cre; Crif1$^{f/+}$ males (n = 5–8). Results are presented as a mean ± SEM. *p < 0.05 vs. Crif1$^{f/f}$ controls.

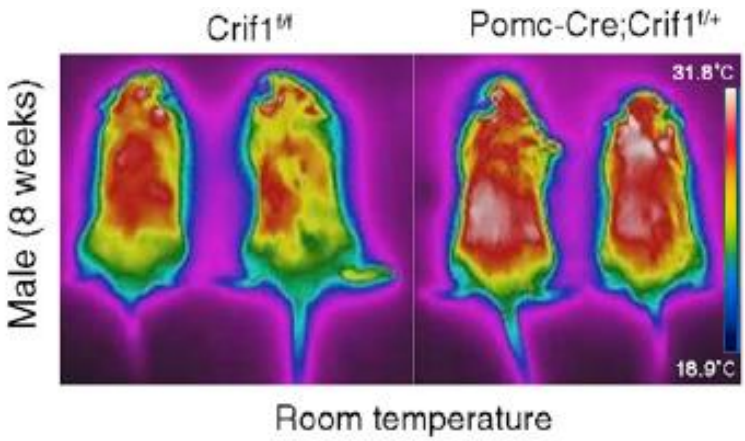

Figure 16. Skin temperature in young Crif1$^{f/f}$ and Pomc-Cre; Crif1$^{f/+}$ males (*n* = 5–8).

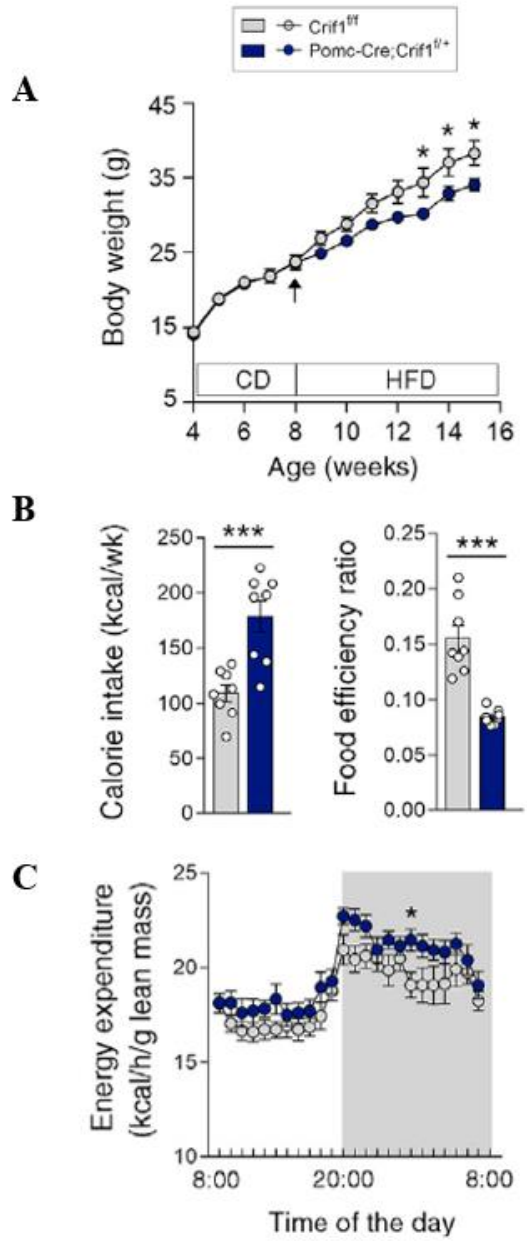

Figure 17. Comparison of body weights, food intake, and energy expenditure during a high fat diet (HFD, 60% fat) challenge between Pomc-Cre; Crif1$^{f/+}$ males and Crif1$^{f/f}$ controls (n = 7–8). Results are presented as a mean ± SEM. *p < 0.05 and ***p < 0.001 vs. Crif1$^{f/f}$ controls.

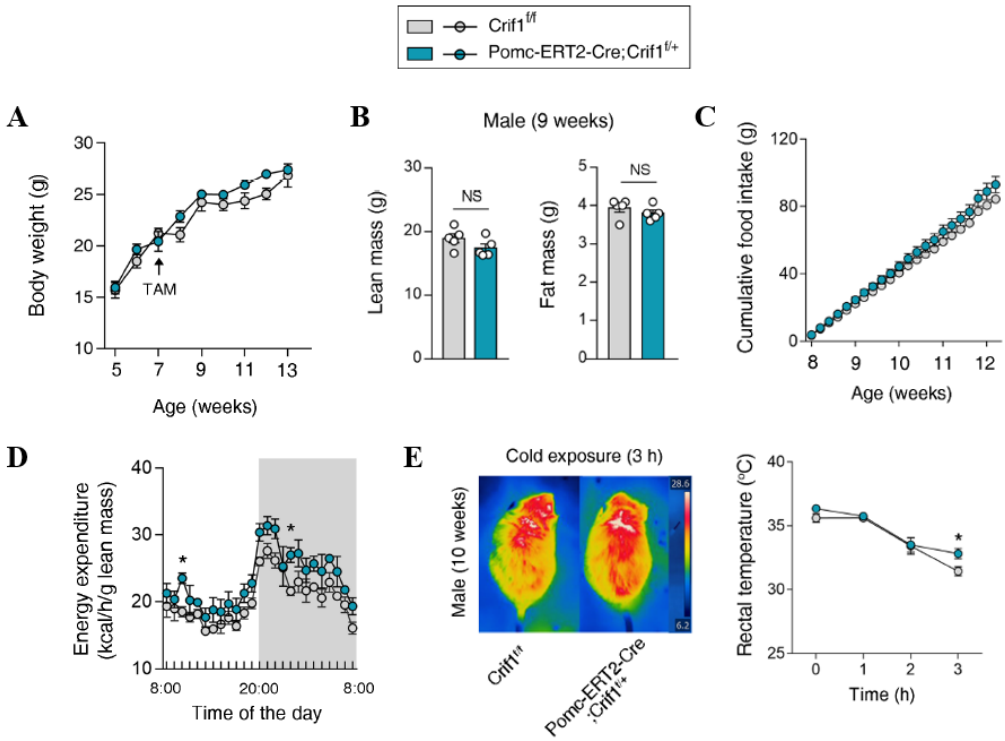

Figure 18. (A) Body weights, (B) lean and fat mass, (C) food intakes, (D) energy expenditure, and (E) skin and rectal temperature during 4 °C cold exposure in mice with adult-onset POMC neuron-specific Crif1 partial deficiency. Gene deletion was induced by intraperitoneal injection of tamoxifen (TAM, 75 mg/kg for 5 days) at 7 weeks of age (n = 6).Results presented as mean ± SEM. *p < 0.05 vs. $Crif1^{f/f}$ littermates. NS: not significant.

3.3 Mild mitoribosomal stress in POMC neurons activates a thermogenic program and UPR^{mt} in adipose tissues

To further decipher the mechanisms underlying increased EE and thermogenesis in the Pomc-Cre; Crif1$^{f/+}$ mice, I first histologically examined brown adipose tissue (BAT), the primary site of non-shivering thermogenesis in rodents. Hematoxylin and eosin staining revealed increased eosin staining and smaller fat droplets in the Pomc-Cre; Crif1$^{f/+}$ mice (Figure 19), indicating increased mitochondrial mass and enhanced lipolysis and/or lipid oxidation. Indeed, electron micrographs (EM) of Pomc-Cre; Crif1$^{f/+}$ BAT showed increased mitochondrial density (number) and coverage (Figure 20), suggesting increased mitochondrial biogenesis. Consistently, mtDNA/nDNA ratio was increased in BAT, reflecting increased mitochondrial mass (Figure 21). The aspect ratio (AR), an index of mitochondrial elongation, was also increased (Figure 20), consistent with increases in mitochondrial fusion and OXPHOS (Mishra et al., 2014). A histological examination of inguinal white adipose tissue (iWAT) revealed BAT-like multilocular fat droplets in Pomc-Cre; Crif1$^{f/+}$ mice, reflecting inducible thermogenesis through the “browning/beigeing” phenotype (Ikeda et al., 2018) (Figure 19). Mitochondrial biogenesis determined by mtDNA/nDNA ratio was also increased in iWAT (Figure 21). In line with these findings, the mRNA expression levels of thermogenesis-related genes such as *Cidea1*, *Ppargc1a*, and *Ucp1* were markedly elevated in iWAT of Pomc-Cre; Crif1$^{f/+}$ mice and in BAT to a lesser degree (Figure 22). Epididymal WAT (eWAT) showed a significant reduction in adipocyte size without browning (Figure 19). Taken together, these results indicate that POMC neuron-*Crif1* heterodeficiency induces remarkable changes in iWAT

mitochondrial context, lipid utilization, and thermogenesis.

In *C. elegans*, UPR^{mt} can occur in a cell-non-autonomous fashion (Durieux et al., 2011; Lan et al., 2019; Taylor et al., 2014; Zhang et al., 2018). I therefore examined whether the *Crif1* partial deletion-induced mitochondrial stress in POMC neurons can induce UPR^{mt} in peripheral adipose tissues. The expression levels of mitochondrial proteases (*Immp2l, Spg7, Parl* and *Htra2*) and chaperones (*Hspd1* and *Tid1*) were significantly elevated in iWAT and BAT of Pomc-Cre; Crif1$^{f/+}$ mice (Figures 23A and 23B). Notably, UPR^{mt} was more pronounced in iWAT compared to BAT. In contrast, UPR^{mt} in eWAT was less distinct (Figure 23C). An imbalance in the stoichiometric ratio between nDNA- and mtDNA-encoded ETC proteins (*i.e.* mitonuclear protein imbalance) extends the lifespan in worms through UPR^{mt} induction (Houtkooper et al., 2013). Therefore, I tested whether mitonuclear protein imbalance in iWAT and BAT occurred in the mouse model. The ratio between ATP5A1 (ATP synthase subunit α, nDNA-encoded ETC component) and MTCO1 (cytochrome c oxidase subunit 1, mtDNA-encoded ETC protein) expression was significantly higher in both fat depots of the Pomc-Cre; Crif1$^{f/+}$ mice (Figure 24). Consistently, *Crif1* partial deficiency in POMC neurons induced during young adulthood caused iWAT browning, thermogenesis, and UPR^{mt} (Figures 25 and 26). Together, these data demonstrate that mild mitoribosomal stress in hypothalamic POMC neurons enhances thermogenesis and elicits mitochondrial stress responses in distal adipose tissues.

POMC neurons regulate adipose tissue thermogenesis through the sympathetic nervous system (SNS) (Yang and Ruan, 2015). I thus postulated that the SNS may mediate cell-non-autonomous mitochondrial stress responses in adipose tissues.

Tyrosine hydroxylase (TH) staining, which labels sympathetic nerve terminals, revealed a dramatic increase in sympathetic fiber density in iWAT of Pomc-Cre; Crif1$^{f/+}$ mice compared to the Crif1$^{f/f}$ littermates (Figure 27). These data suggested that POMC-specific *Crif1* partial deficiency may stimulate thermogenesis via increasing sympathetic innervation in iWAT. Consistently, multiple microinjections of neurotoxin 6-hydroxydopamine (OHDA) in one side of iWAT of Pomc-Cre; Crif1$^{f/+}$ mice significantly reversed browning, thermogenic gene expression, UPR^{mt}, and mitonuclear protein imbalance (Figures 27 and 28). These findings demonstrate that the SNS mediates the communication of mitochondrial stress responses between the central nervous system and peripheral organs.

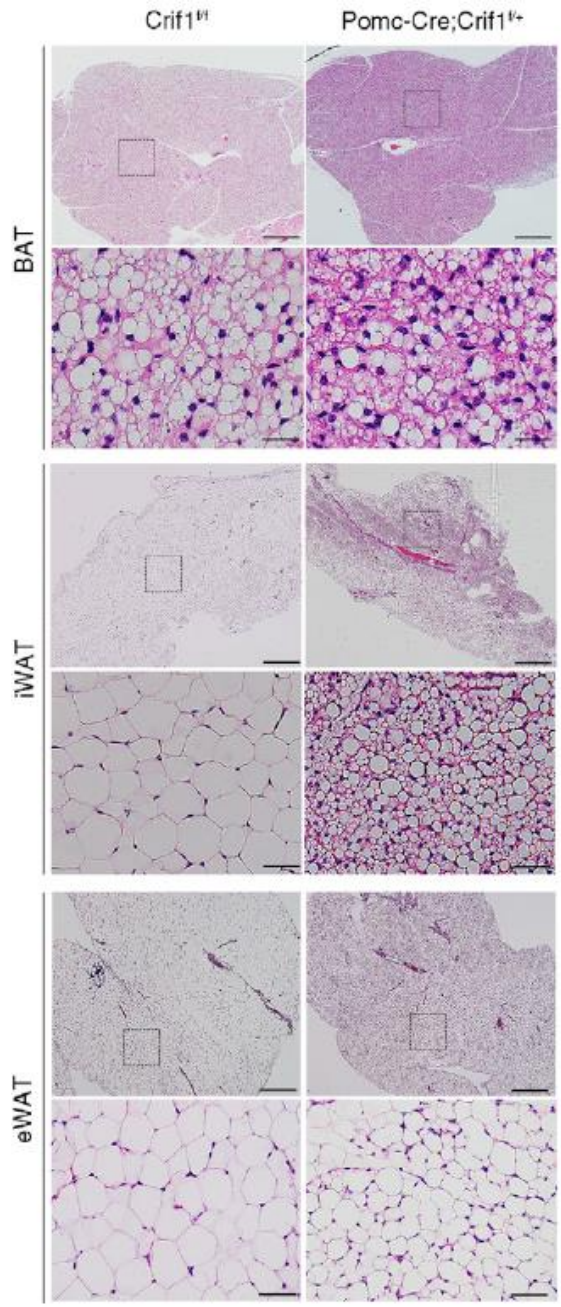

Figure 19. Histology of brown adipose tissue (BAT), inguinal white adipose tissue (iWAT) and epididymal white adipose tissue (eWAT) in Crif1$^{f/f}$ and Pomc-Cre; Crif1$^{f/+}$ males. Scale bars, 500 μm (upper) and 50 μm (lower).

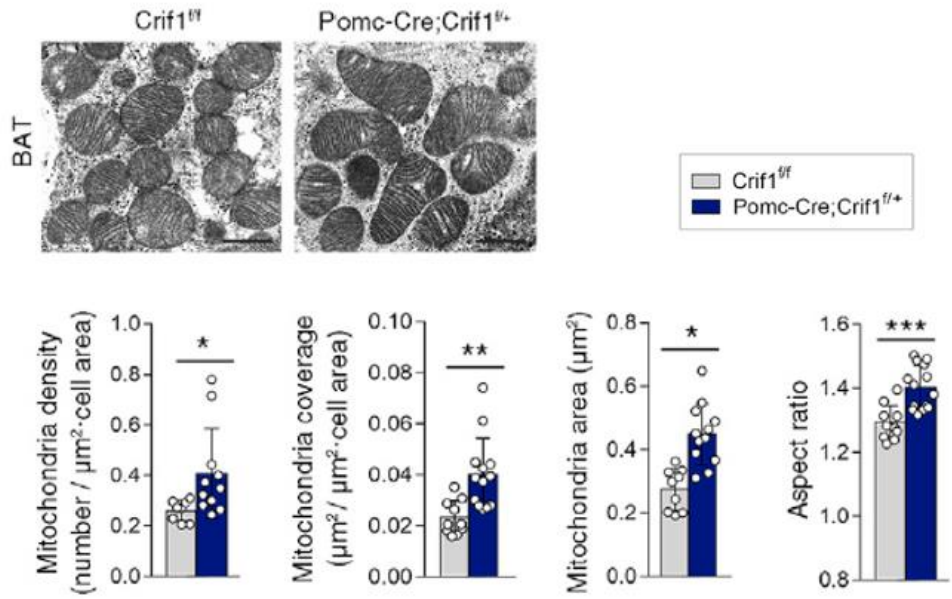

Figure 20. Electron microscopic examination of the BAT from 8 week-old Crif1$^{f/f}$ and Pomc-Cre; Crif1$^{f/+}$ males (n = 8–13 cells). Scale bars, 0.5 μm. Results are presented as a mean ± SEM. *p < 0.05, **p < 0.01, and ***p < 0.001 between indicated groups.

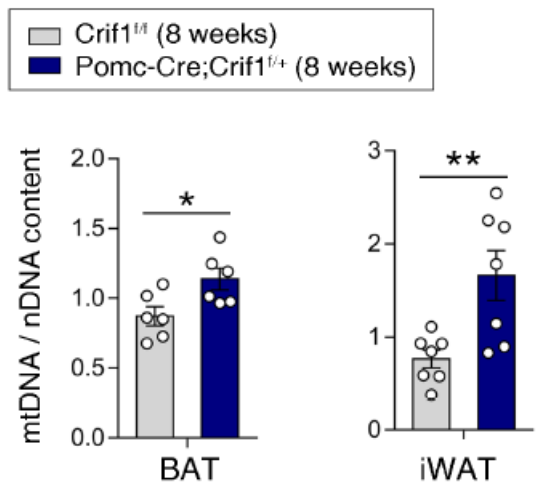

Figure 21. The mtDNA / nDNA ratio in BAT and iWAT of 8-week-old Crif1$^{f/f}$ and Pomc-Cre; Crif1$^{f/+}$ male mice (n = 6─7). Results presented as mean ± SEM. *p < 0.05, **p < 0.01, and **p < 0.01 between indicated groups.

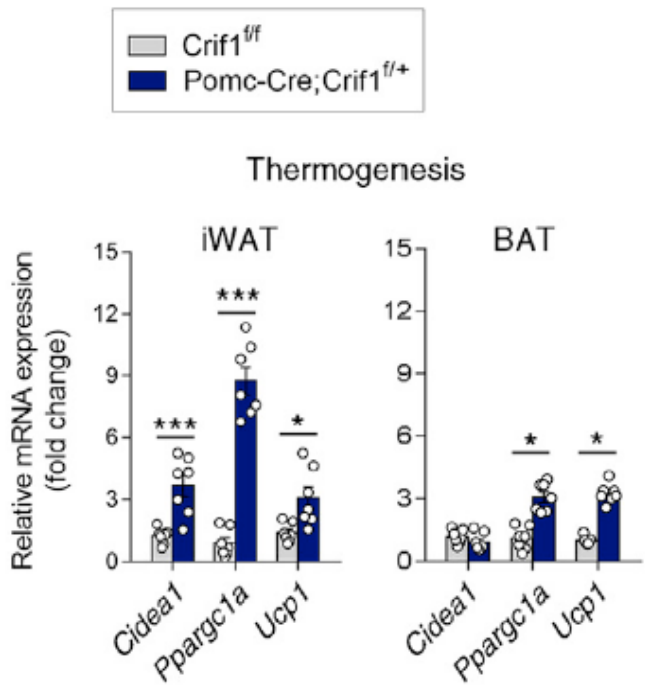

Figure 22. Thermogenesis-related gene expression in the iWAT and BAT at 8 weeks (n = 7). Results are presented as a mean ± SEM. *p < 0.05 and ***p < 0.001 between indicated groups.

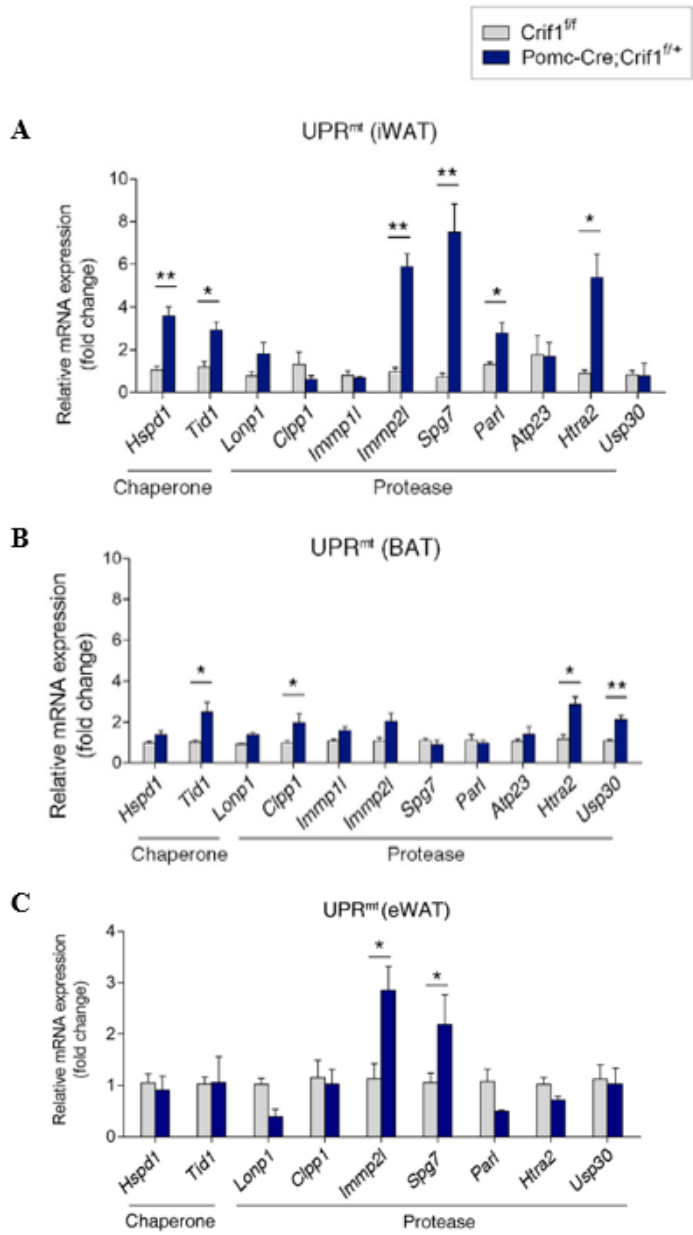

Figure 23. Increased mitochondrial chaperone and protease expression in the iWAT, BAT, and eWAT of Pomc-Cre; Crif1$^{f/+}$ males, indicating a mitochondrial unfolded protein response (UPR^{mt}) (n = 4). Results are presented as a mean ± SEM. *p < 0.05 and **p < 0.01 between indicated groups.

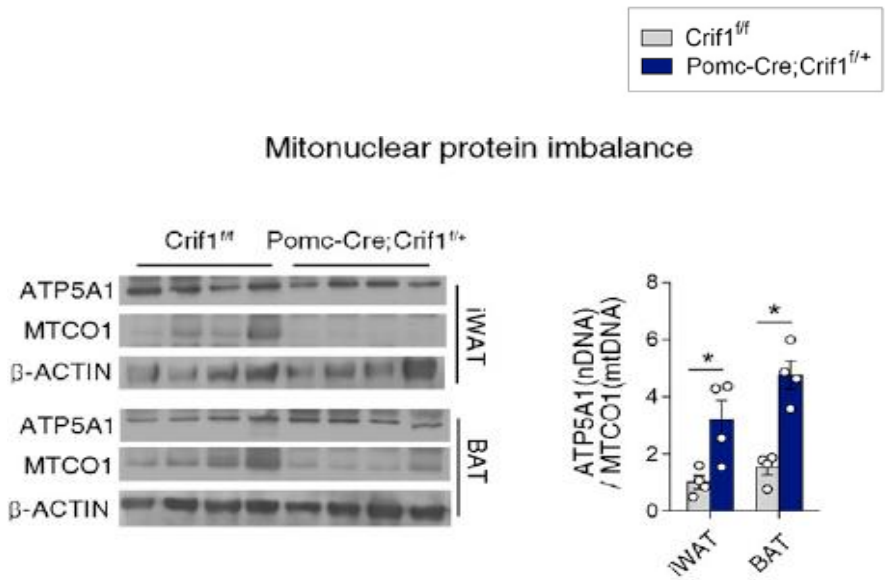

Figure 24. Mitonuclear protein imbalance between nuclear DNA (nDNA)-encoded ETC protein (ATP5A1) versus mitochondrial DNA (mtDNA)-encoded protein (MTCO1) in the iWAT and BAT (n = 4). Results are presented as a mean ± SEM. *$p < 0.05$ between indicated groups.

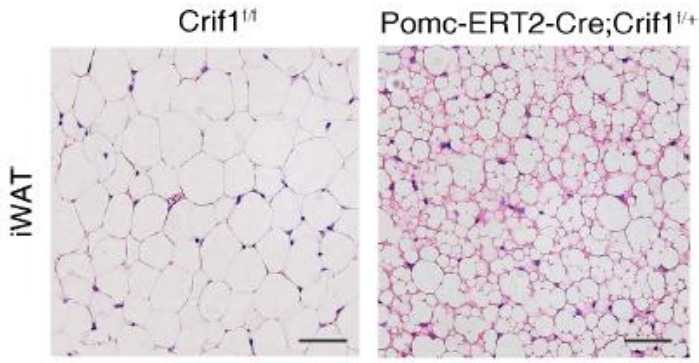

Figure 25. BAT-like changes in iWAT of 11-week-old mice with adult (at 7 weeks)-induced *Crif1* partial deletion in POMC neurons (n = 6). Scale bars, 50 μm.

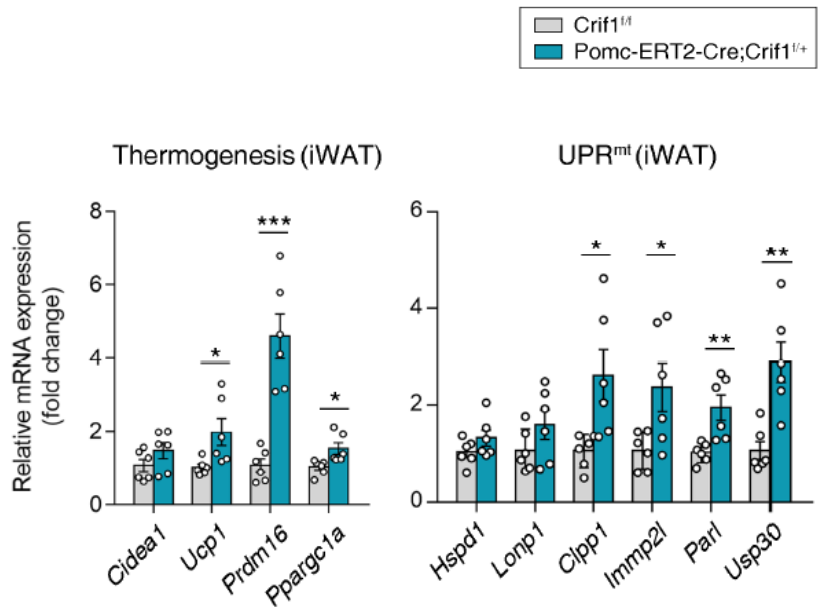

Figure 26. Thermogenesis-related gene expression and UPRmt in iWAT of 11-week-old mice with adult (at 7 weeks)-induced *Crif1* partial deletion in POMC neurons (n = 6). Results presented as mean ± SEM. *$p < 0.05$, **$p < 0.01$, and ***$p < 0.001$ between indicated groups.

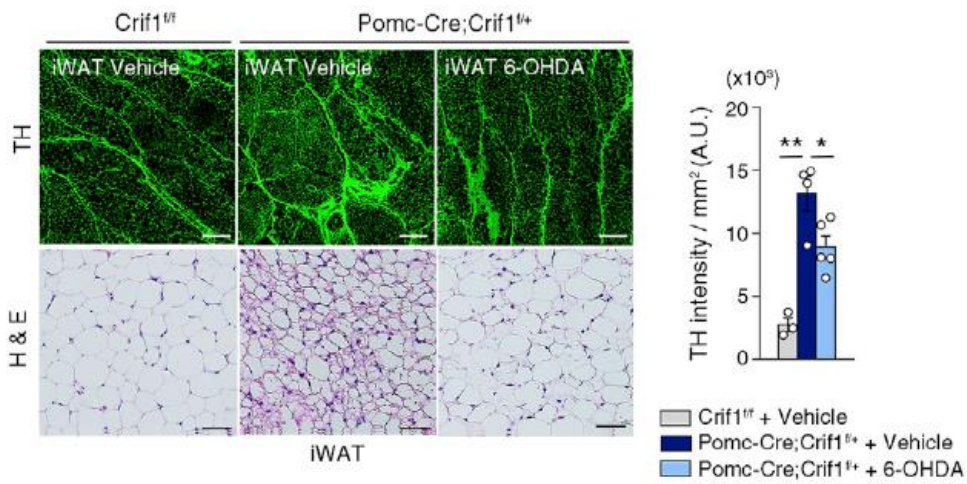

Figure 27. Reversal of iWAT browning and increased sympathetic innervation in Pomc-Cre; Crif1$^{f/+}$ males following an intra-iWAT injection of neurotoxin 6-hydroxydopamine (OHDA). Tyrosine hydroxylase (TH) staining of sympathetic innervation in the iWAT is shown. Scale bars, 200 μm (upper) and 50 μm (lower) (n = 6–7). Results are presented as a mean ± SEM. *p < 0.05 and **p < 0.01 between indicated groups.

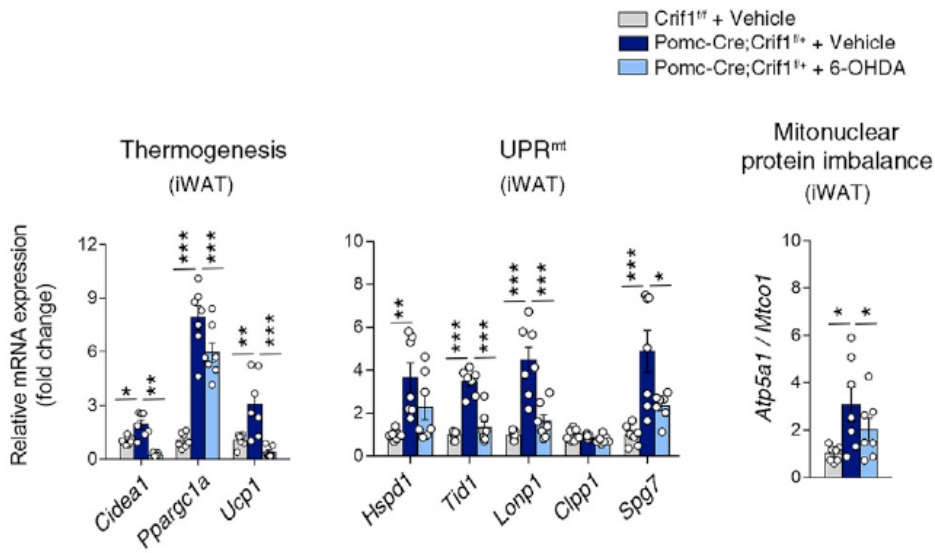

Figure 28. Reversal of thermogenic gene expression, the UPR^{mt}, and the mitonuclear protein imbalance in Pomc-Cre; Crif1$^{f/+}$ males following an intra-iWAT injection of neurotoxin 6-hydroxydopamine (OHDA). Tyrosine hydroxylase (TH) staining of sympathetic innervation in the iWAT is shown (n = 6–7). Results are presented as a mean ± SEM. *p < 0.05, **p < 0.01, and ***p < 0.001 between indicated groups.

3.4. Mitochondrial changes and the UPR^{mt} in POMC neurons with a *Crif1* deficiency

To investigate the effects of *Crif1* deficiency on mitochondria in hypothalamic POMC neurons, I conducted immuno-EM analysis on 11 week-old male Crif1$^{f/f}$ mice, Pomc-Cre; Crif1$^{f/+}$ mice and Pomc-Cre; Crif1$^{f/f}$ mice. *Crif1* heterodeficient POMC neurons showed no changes in mitochondrial mass and morphology except for a reduced mitochondrial coverage in the cytosol (Figure 29). In contrast, *Crif1* homodeficiency induced evident mitochondrial changes (Figure 29). Mitochondrial density (number) was reduced without changes in mitochondrial coverage, indicating mitochondrial enlargement. Consistently, mitochondrial area and perimeter were proportionally increased without altering the aspect ratio. Notably, the fraction of mitochondria with morphological disruption of the inner membrane significantly increased and the mitochondria-endoplasmic reticulum contacts were reduced. Hence, POMC neurons that are *Crif1* homodeficient already undergo mitochondrial dysfunction in 11 week-old mice.

I also evaluated the UPR^{mt} and mitonuclear protein imbalance in the ARH POMC neurons. For this analysis, I generated RiboTag mice in which a hemagglutinin-tagged ribosomal subunit (Rpl22^{HA}) was specifically expressed in POMC neurons to measure mRNA translation (Sanz et al., 2009). *Crif1* homodeficient POMC neurons had apparent UPR^{mt} activation and mitonuclear protein imbalance (Figure 30). By contrast, *Crif1* heterodeficiency caused a mild cell-autonomous mitochondrial stress response in POMC neurons (Figure 30).

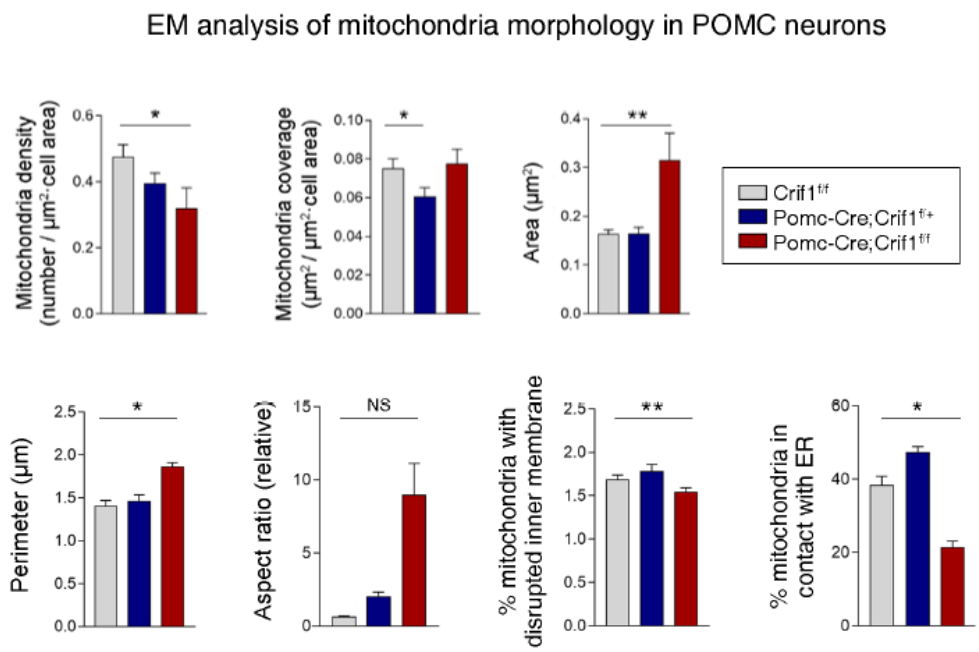

Figure 29. Mitochondrial analysis in *Crif1* deficient POMC neurons using POMC immune-EM in 11 weeks-old mice (n = 5). Results presented as mean ± SEM. *p < 0.05 and **p < 0.01 between indicated groups. NS: not significant.

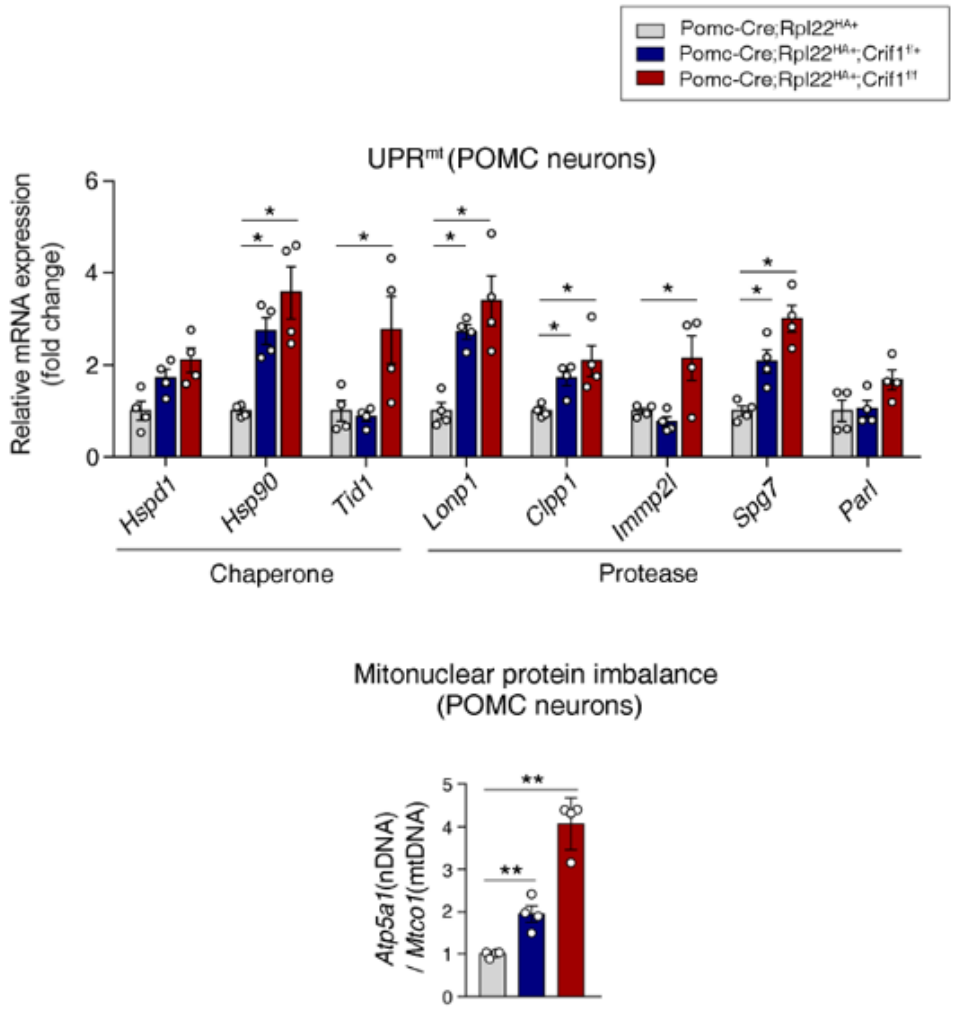

Figure 30. Measurement of UPR^{mt} and mitonuclear protein imbalance in *Crif1*-depleted POMC neurons using RiboTag (Rpl22HA) mice at 7─8 weeks (n = 4). Results presented as mean ± SEM. *p < 0.05 and **p < 0.01 between indicated groups.

3.5. Mild mitoribosomal stress increases β-END expression in POMC neurons

I further investigated how POMC neurons promoted adipose tissue changes in Pomc-Cre; Crif1$^{f/+}$ mice. *Pomc* in situ hybridization revealed no alteration in the total number of POMC neurons whereas the percentage of c-Fos^{+} activated POMC neurons were markedly increased in the ARH of Pomc-Cre; Crif1$^{f/+}$ mice (Figure 31). I next immunostained ARH POMC neurons with antibodies against β-END or α-melanocyte stimulating hormone (α-MSH), which are cleaved peptide products of POMC. The number of β-END^{+} neurons was increased but that of α-MSH^{+} neurons was unaltered in the Pomc-Cre; Crif1$^{f/+}$ mice (Figure 32). Moreover, Pomc-Cre; Crif1$^{f/+}$ mice showed increased β-END^{+} axonal fiber intensity and unaltered α-MSH^{+} fiber intensity in the hypothalamic paraventricular nucleus (PVH) and dorsomedial nucleus (DMH) (Figure 33). I also measured hypothalamic β-END and α-MSH contents using enzyme-linked immunosorbent assay (ELISA) and a radioimmunoassay (RIA), respectively, and confirmed selective elevation in β-END expression (Figure 34). Similar changes in hypothalamic β-END and α-MSH expression were observed in Pomc-ERT2-Cre; Crif1$^{f/+}$ mice (Figures 35A and 35B). Together, these data indicate that *Crif1* heterodeficiency specifically increases β-END levels in the ARH POMC neurons.

In addition, I found that *Pomc* mRNA expression was markedly elevated specifically in the hypothalamus of Pomc-Cre; Crif1$^{f/+}$ mice (Figures 36), but not in the brainstem and pituitary gland (Figure 37), indicating region-specific differential *Pomc* expression. I next asked how α-MSH expression was unaltered despite higher *Pomc* mRNA expression. I assessed the alterations in the enzymes involved

in α-MSH production and degradation. Biologically active α-MSH (1-13) is produced from precursor polypeptide POMC via multiple enzymatic steps catalyzed by prohormone convertase (PC)-1, PC-2 (encoded by *Pcsk1* and *Pcsk2*), carboxypeptidase E (CPE, encoded by *Cpe1*), and peptidyl α-amidating monooxygenase (PAM). α-MSH (1-13) is degraded by prolyl carboxypeptidase (PRCP, encoded by *Prcp*) to the inactive α-MSH (1-12) form (Wallingford et al., 2009). I detected a significant elevation in the hypothalamic expression of *Pcsk1*, *Pcsk2*, *Pam*, and *Prcp* in Pomc-Cre; Crif1$^{f/+}$ mice compared to the Crif1$^{f/f}$ controls (Figure 36). Hence, α-MSH production and degradation may have both increased, providing a steady-state level of hypothalamic α-MSH.

I further tested the possibility that increased hypothalamic β-END expression may induce the WAT changes observed in the Pomc-Cre; Crif1$^{f/+}$ mice. For this analysis, I administered β-END (1-13) (0.1 μg twice a day) intracerebroventricularly (ICV) into C57BL/6J (C57) mice for 4 days. Chronic β-END treatment did increase EE especially during daytime (Figures 38). Moreover, it markedly increased sympathetic innervation, thermogenic gene expression, and UPR^{mt} in iWAT and induced its browning (Figures 39 and 40). Chronic β-END treatment did not significantly alter body weight nor food intake during the treatment period (Figure 41A). As the orexigenic effect of β-END are short-lasting (Dutia et al., 2012, Figure 41B), twice-a-day-injection may not induce a continuous hyperphagic behavior over the course of the chronic treatment period as determined by cumulative food intake. These data support the potential role of β-END in mediating the cell-non-autonomous mitochondrial stress response and inducible thermogenesis in the iWAT of Pomc-Cre; Crif1$^{f/+}$ mice.

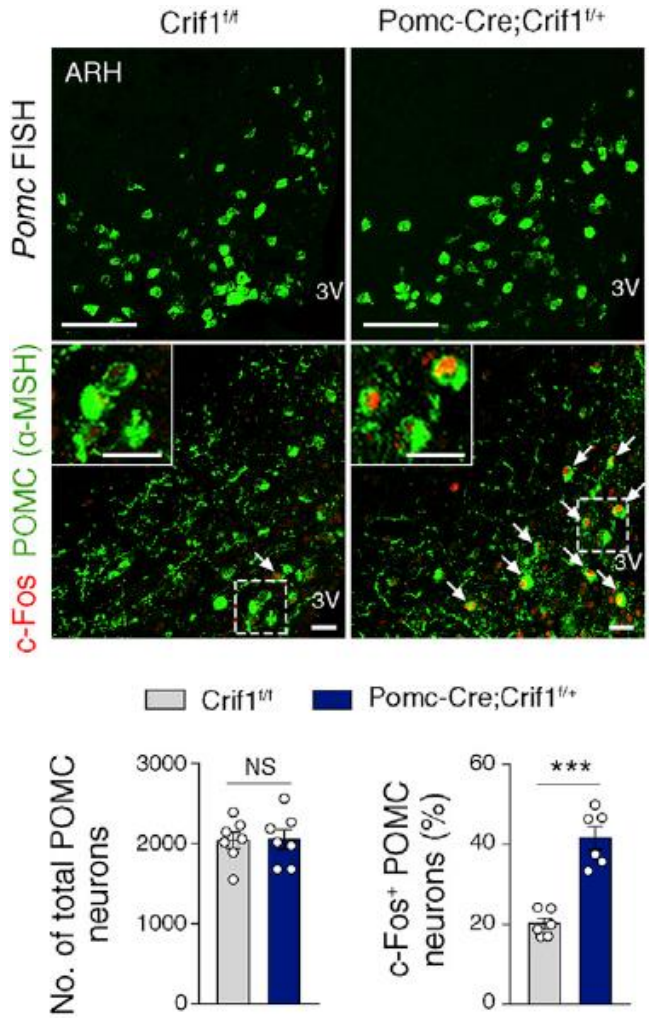

Figure 31. *Pomc* fluorescence in situ hybridization (FISH) showing no alteration in ARH POMC neuron numbers (upper panel) and an increase in the percentage of c-Fos^{+} POMC neurons (lower panel) in 8 week-old Pomc-Cre; Crif1$^{f/+}$ males compared to Crif1$^{f/f}$ controls (n = 6–7). Scale bars, 25 μm. Arrowheads indicate c-Fos^{+} POMC neurons. Results are presented as a mean ± SEM. ***p < 0.001 between indicated groups. NS, not significant.

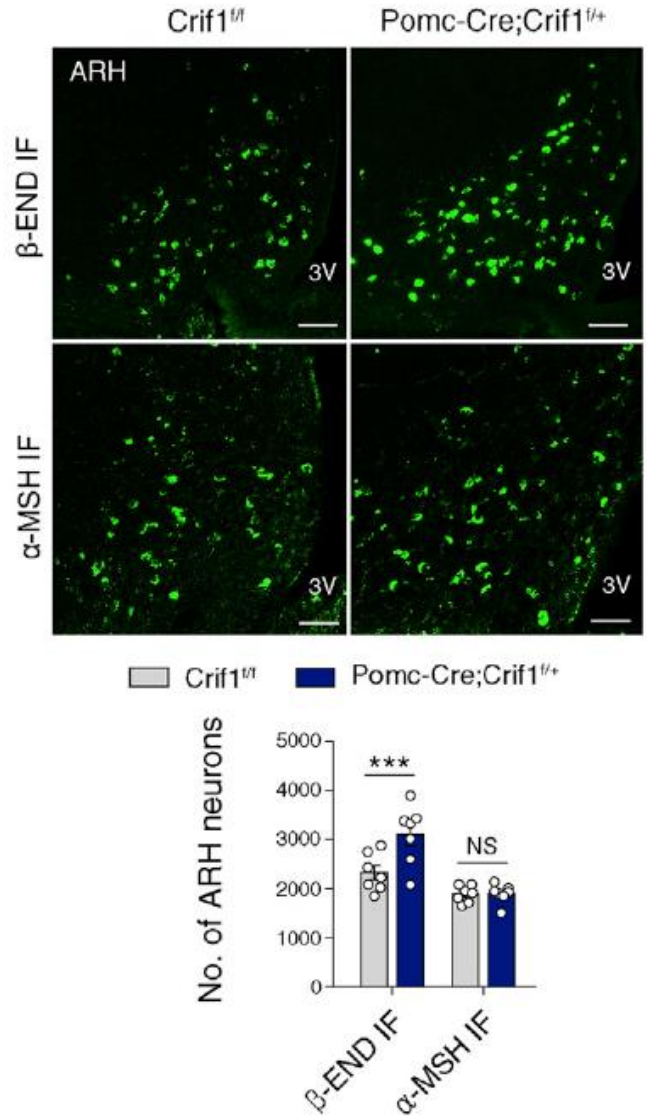

Figure 32. Increased numbers of β-END^{+} neurons, but no change in the α-MSH^{+} neuron population, in the hypothalamic ARH of Pomc-Cre; Crif1$^{f/+}$ male mice at 8 weeks (n = 6–7). Scale bars, 50 μm. IF, immunofluorescence staining. Results are presented as a mean ± SEM. ***p < 0.001 between indicated groups. NS, not significant.

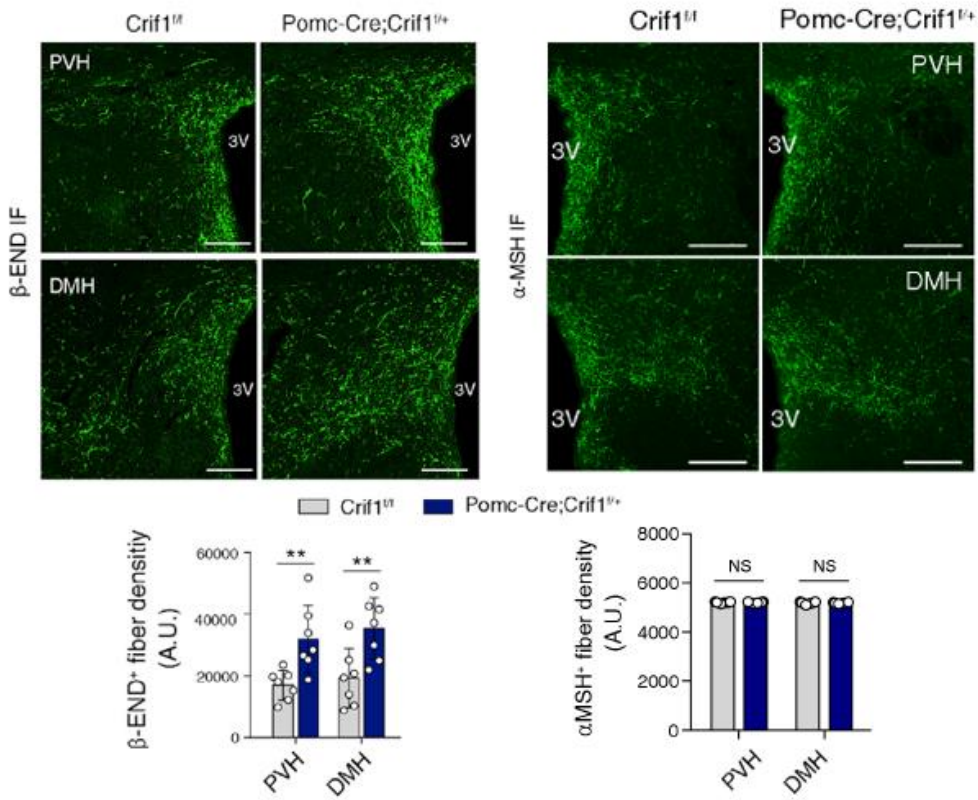

Figure 33. Increase in β-END^{+} and α-MSH^{+} axonal projections in the hypothalamic paraventricular (PVH) and dorsomedial nucleus (DMH) of Pomc-Cre; Crif1$^{f/+}$ males (n = 7). Scale bars, 100 μm. Results are presented as a mean ± SEM. **$p < 0.01$ between indicated groups. NS, not significant.

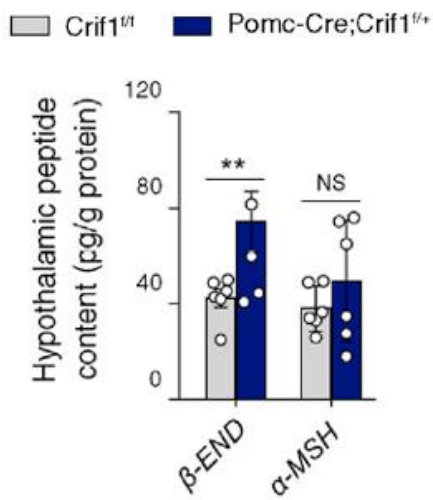

Figure 34. Quantitation of the hypothalamic β-END and α-MSH protein contents at 8 weeks of age (n =4–6). Results are presented as a mean ± SEM. $^{**}p < 0.01$ between indicated groups. NS, not significant.

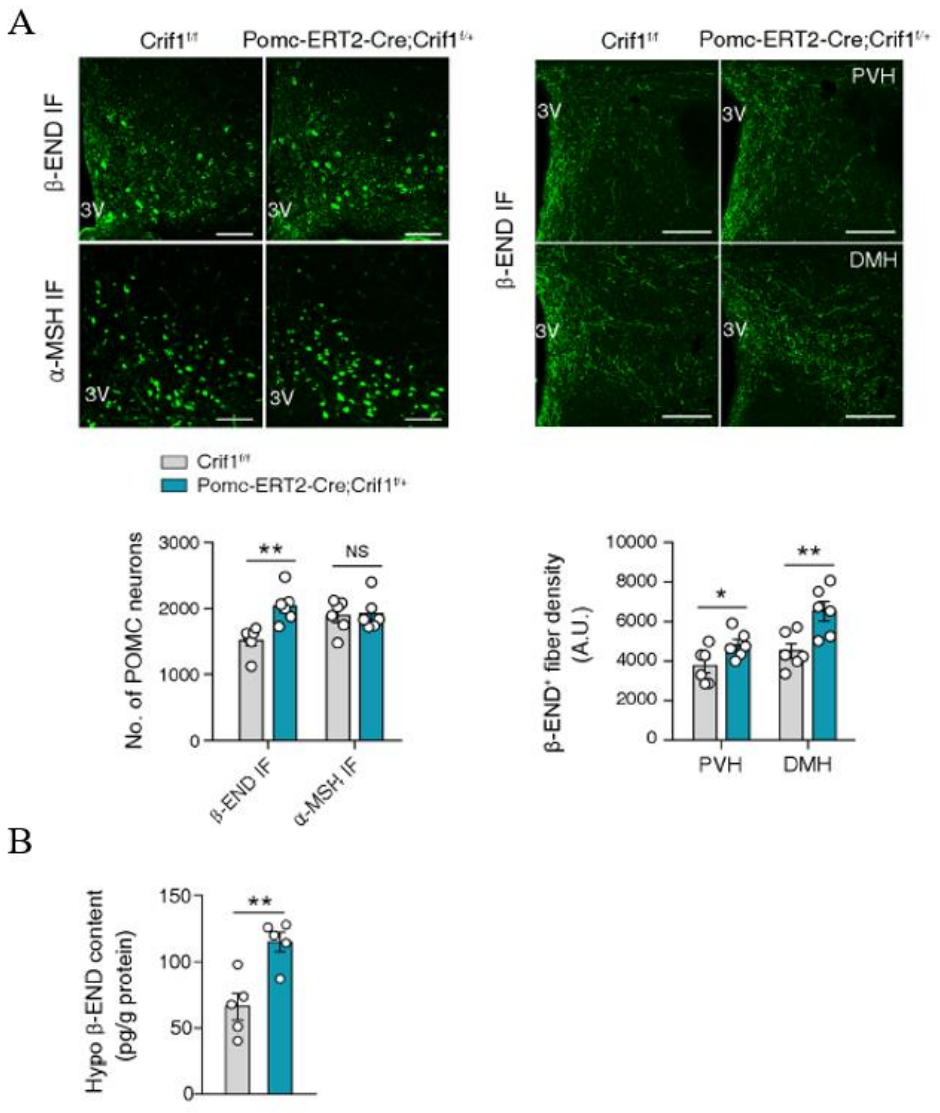

Figure 35. (A) Increased β-END+ neuron numbers and axonal fiber density, but unaltered α-MSH+ neuron numbers in Pomc-ERT2-Cre; Crif1f/+ mice (n = 6). Gene knockout was induced by injecting tamoxifen at 7 weeks. Scale bars, 100 μm. (B) Increased hypothalamic β-END contents in Pomc-ERT2-Cre; Crif1f/+ mice (n = 5). Results presented as mean ± SEM. *p < 0.05, **p < 0.01 between indicated groups. NS: not significant.

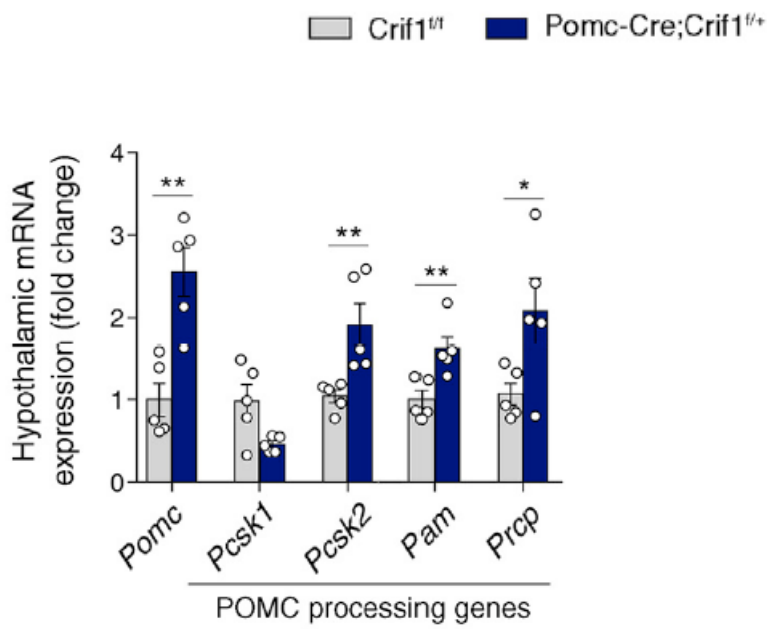

Figure 36. Changes in the hypothalamic mRNA expression levels of *Pomc* and of enzymes involved in the production and degradation of POMC-derived peptides in Pomc-Cre; Crif1$^{f/+}$ mice (n = 5). Results are presented as a mean ± SEM. *p < 0.05 and **p < 0.01 between indicated groups.

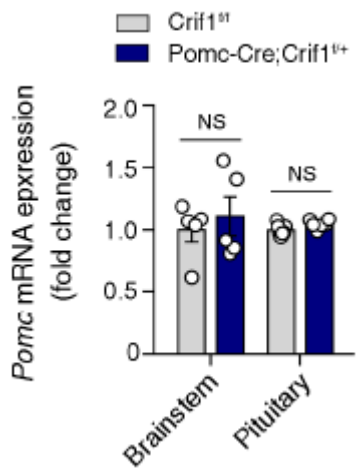

Figure 37. *Pomc* mRNA expression in the brainstem and pituitary gland of Pomc-Cre; Crif1$^{f/+}$ mice and Crif1$^{f/f}$ littermates (n = 5). Results presented as mean ± SEM. NS: not significant.

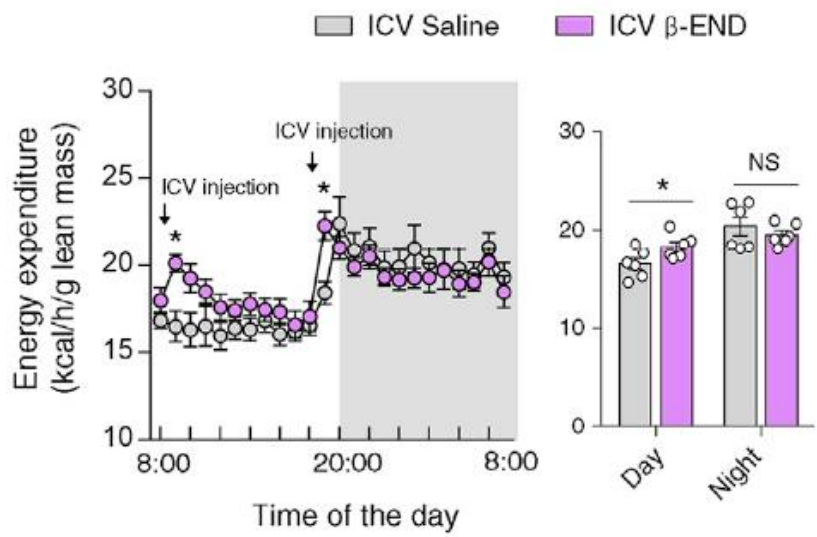

Figure 38. Repeated ICV injection of β-END (0.1 μg twice a day for 4 days) increases EE in C57 mice (n = 5–6). Results are presented as a mean ± SEM. *p < 0.05 between indicated groups. NS, not significant.

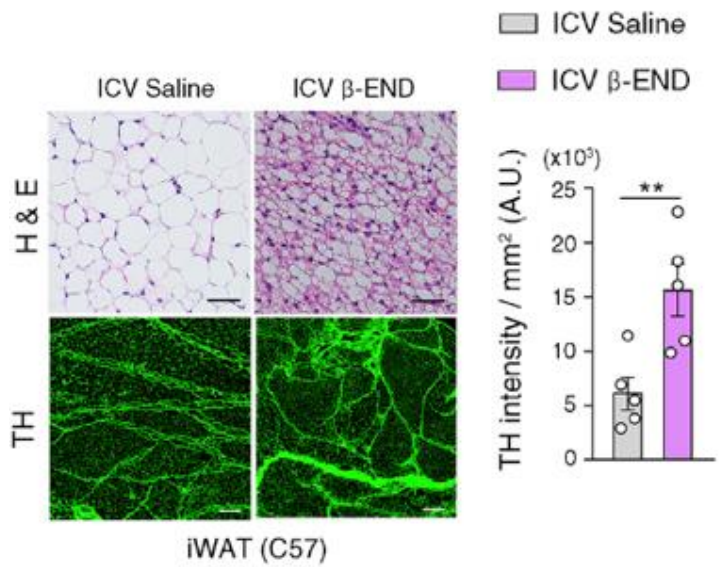

Figure 39. Repeated ICV injection of β-END (0.1 μg twice a day for 4 days) induces browning and enhanced sympathetic innervation in the iWAT of C57 mice (n = 5–6). Scale bars, 200 μm (upper) and 50 μm (lower). Results are presented as a mean ± SEM. ** $p < 0.01$ between indicated groups.

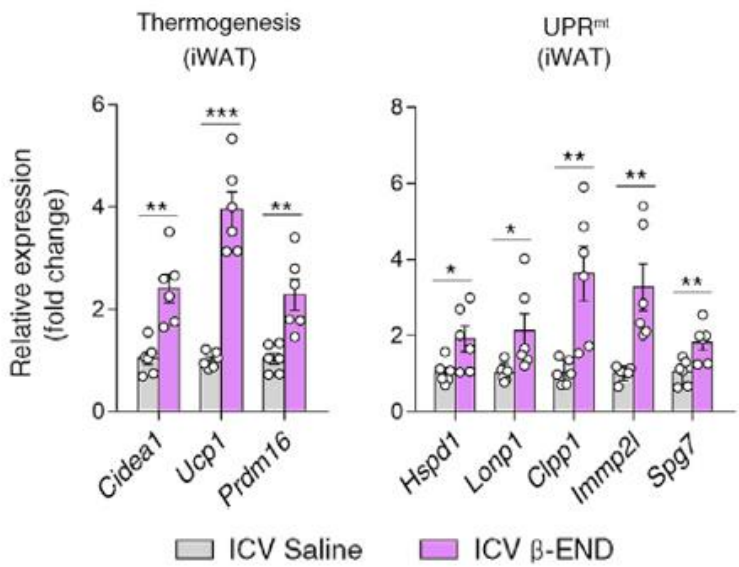

Figure 40. Repeated ICV injection of β-END (0.1 μg twice a day for 4 days) enhanced thermogenic gene expression and the UPR^{mt} in the iWAT of C57 mice (n = 5–6). Results are presented as a mean ± SEM. *p < 0.05, **p < 0.01, and ***p < 0.001 between indicated groups.

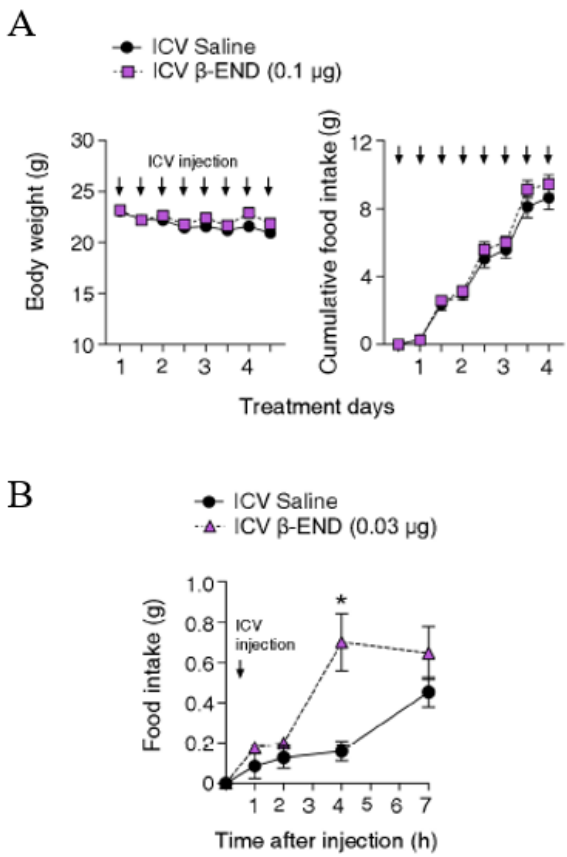

Figure 41. (A) Measurements of body weight and cumulative food intake during repeated ICV injection of saline or β-END (0.1 μg twice a day for 4 days) (*n* = 8─10). Arrows indicate times of ICV injection. (B) Food intakes following single ICV injection of β-END in freely-fed C57 mice (*n* = 4─5). Results presented as mean ± SEM. *p < 0.05 vs. ICV saline.

3.6. The mitochondrial-derived peptide MOTS-c coordinates mitoribosomal stress response in POMC neurons

I explored the downstream mediator of mitoribosomal stress in POMC neurons. I found that N1 hypothalamic neuronal cells significantly increased the expression of a mtDNA-encoded peptide, MOTS-c, upon *Crif1* knockdown using small interfering RNA (siRNA) (Figure 42). Moreover, MOTS-c and α-MSH double immunohistochemistry revealed that Pomc-Cre; $Crif1^{f/+}$ mice showed increased MOTS-c expression in POMC neurons in ARH (Figure 43). *Pomc* and MOTS-c double staining showed unaltered MOTS-c expression in the solitary tract nucleus POMC neurons of Pomc-Cre; $Crif1^{f/+}$ mice whilst MOTS-c expression was negligible in mouse pituitary POMC cells (Figure 44). The specificity of the MOTS-c antibody I used had been validated in the previous study (Kim et al., 2018) and also in hypothalamic tissues using a peptide competition antibody test (Figure 45). MOTS-c ELISA also confirmed the elevation of hypothalamic MOTS-c content in both Pomc-Cre; $Crif1^{f/+}$ mice and Pomc-ERT2-Cre; $Crif1^{f/+}$ mice (Figure 46). These findings suggested that mitoribosomal stress stimulates MOTS-c expression in hypothalamic POMC neurons.

As previously reported, MOTS-c translocates to the nucleus upon metabolic stress and regulates adaptive nuclear gene expression in an ROS-dependent manner (Kim et al., 2018). I confirmed that MOTS-c translocates to the nucleus in N1 hypothalamic neurons upon H_2O_2-induced oxidative stress, which was completely prevented by co-treatment with the antioxidant N-acetylcysteine (Figure 47). Further, I assessed ROS levels in *Crif1*-depleted POMC neurons. For this, I intravenously injected dihydroethidium (DHE), a fluorescent probe used to detect

tissue superoxide and hydrogen peroxide, into 14 week-old *Crif1* heterodeficient mice and their age-matched controls 2 h prior to euthanasia. Indeed, the level of ROS in POMC neurons was significantly elevated in *Crif1* heterodeficient mice (Figure 48). Thus, mitoribosomal stress induced by *Crif1* partial deficiency may increase ROS levels in POMC neurons. Interestingly, ROS production was also elevated in non-POMC cells in the ARH (Figure 48). Thus, mitoribosomal stress in POMC neurons may cause oxidative stress in neighboring neurons and glia via currently unclear inter-cellular communication mechanisms.

Then, I tested whether MOTS-c regulates nuclear-encoded *Pomc* transcription. Indeed, *Mots-c* overexpression in POMC-producing AtT20 cells significantly increased *Pomc* mRNA expression and *Pomc* promoter activity (Figures 49A and 49B). Hence, elevated MOTS-c expression can stimulate *Pomc* transcription. As previously reported, once in the nucleus, MOTS-c interacts with transcription factors (Kim et al., 2018). As STAT3 is a well-known transcriptional regulator of *Pomc* (Munzberg et al., 2003), I examined its involvement in MOTS-c-dependent *Pomc* transcription. Indeed, at sub-effective doses (0.1 ng each), *Mots-c* and *Stat3* co-expression synergistically stimulated *Pomc* promotor activity whilst *Stat3* depletion by siRNA treatment blocked MOTS-c-induced *Pomc* promotor activity (Figures 50A and 50B). Chromatin immunoprecipitation experiments revealed that STAT3 binding to the *Pomc* promotor was enhanced in cells overexpressing *Mots-c* (Figure 51). These findings indicate that MOTS-c upregulates *Pomc* transcription in coordination with STAT3.

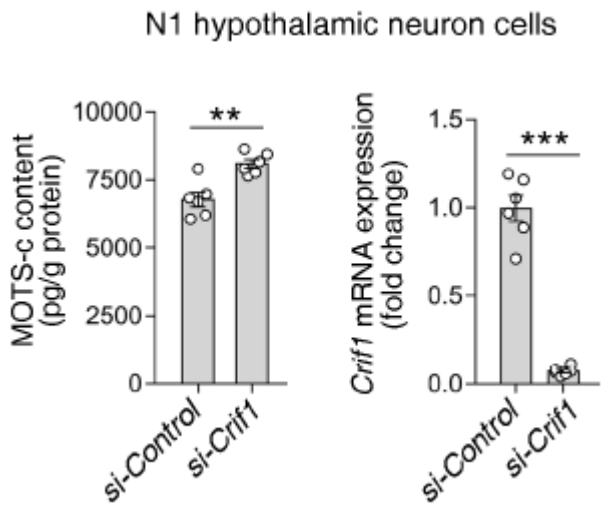

Figure 42. *Crif1* knockdown with Crif1 siRNA in N1 hypothalamic neuron cells increases cellular MOTS-c protein contents (n = 5 wells). Results presented as mean ± SEM. $^{**}p < 0.01$, and $^{***}p < 0.001$ vs. controls.

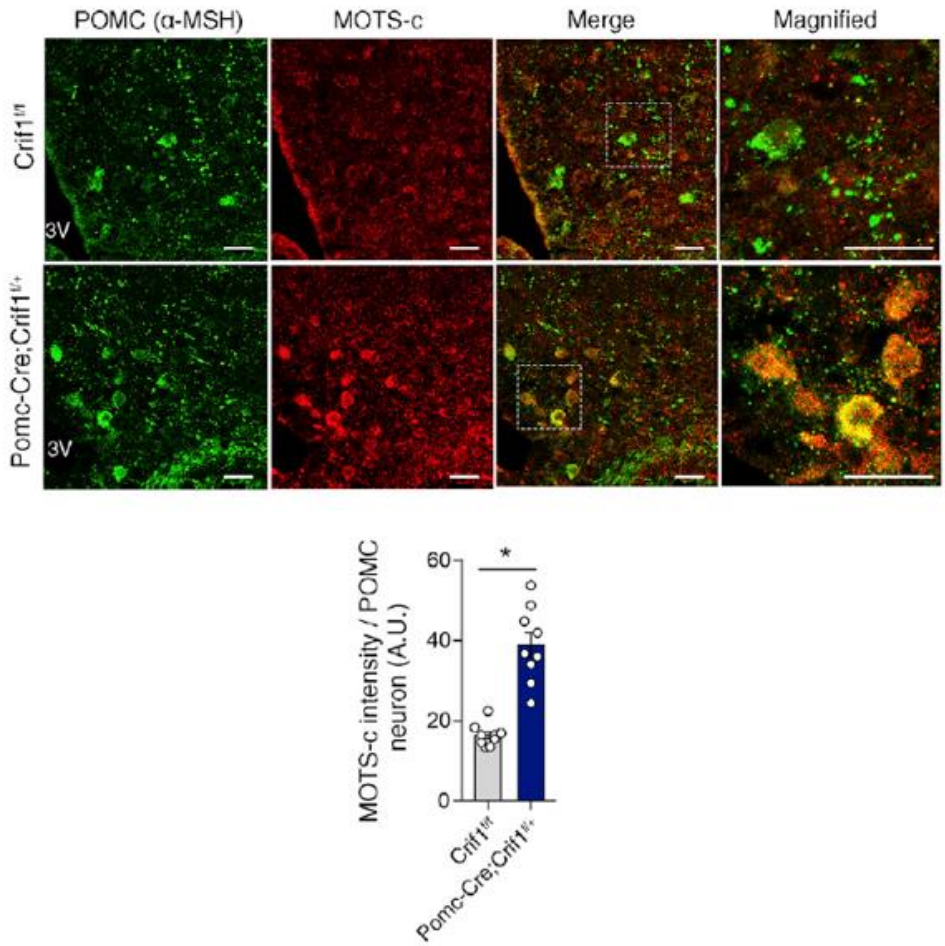

Figure 43. αMSH and MOTS-c double immunohistochemistry showing increased MOTS-c expression in the POMC neurons of Pomc-Cre; Crif1$^{f/+}$ mice compared to Crif1$^{f/f}$ controls (n = 9). Scale bars, 25 μm. Results are presented as a mean ± SEM. *p < 0.05 between indicated groups.

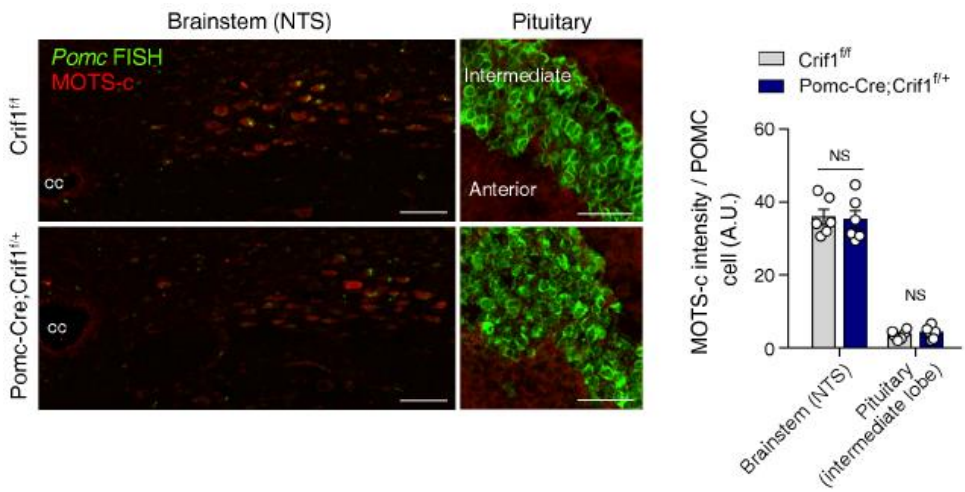

Figure 44. *Pomc* FISH and MOTS-c immunofluorescence double staining showing MOTS-c expression in brainstem solitary tract nucleus (NTS) and pituitary POMC cells of Crif1$^{f/f}$ and Pomc-Cre; Crif1$^{f/+}$ mice (n = 6). cc, central canal. Scale bars, 50 μm**.** Results presented as mean ± SEM. NS: not significant.

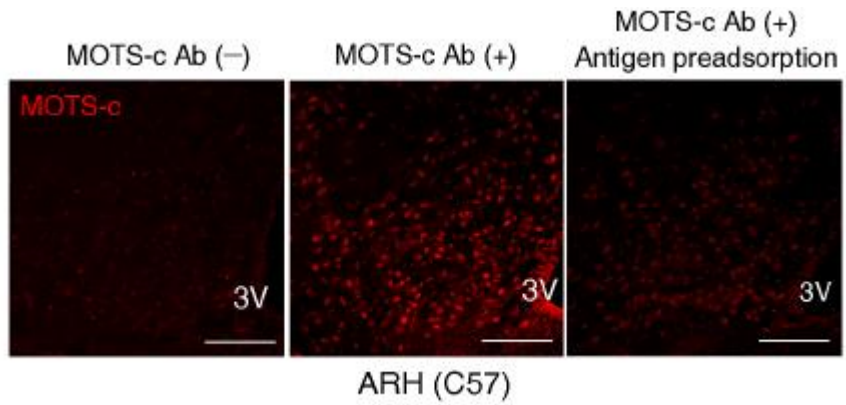

Figure 45. The MOTS-c antibody specificity test for hypothalamic MOTS-c immunohistochemistry using antigen preadsorption. Scale bars, 50 μm.

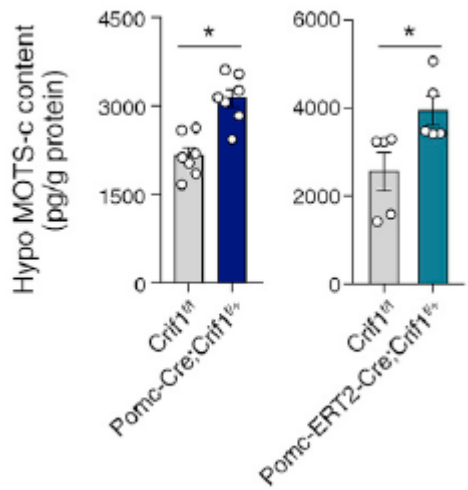

Figure 46. Increased hypothalamic MOTS-c contents in Pomc-Cre; Crif1$^{f/+}$ mice and Pomc-ERT2-Cre; Crif1$^{f/+}$ mice compared to Crif1$^{f/f}$ mice (n = 5–7). Results are presented as a mean ± SEM. *p < 0.05 between indicated groups.

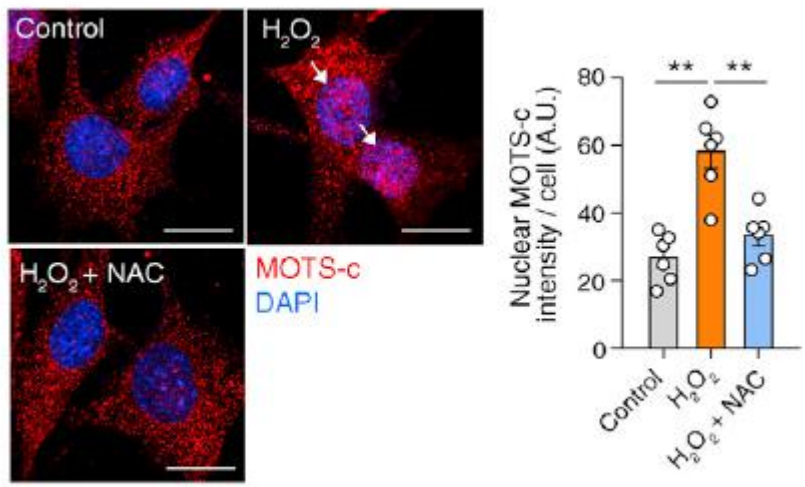

Figure 47. Oxidative stress (H_2O_2 treatment) induces MOTS-c nuclear localization (white arrows) which is blocked by a cotreatment with antioxidant N-acetylcysteine (NAC) in N1 hypothalamic neurons (n = 6 wells). Scale bars, 25 μm. Results are presented as a mean ± SEM. **$p < 0.01$ between indicated groups.

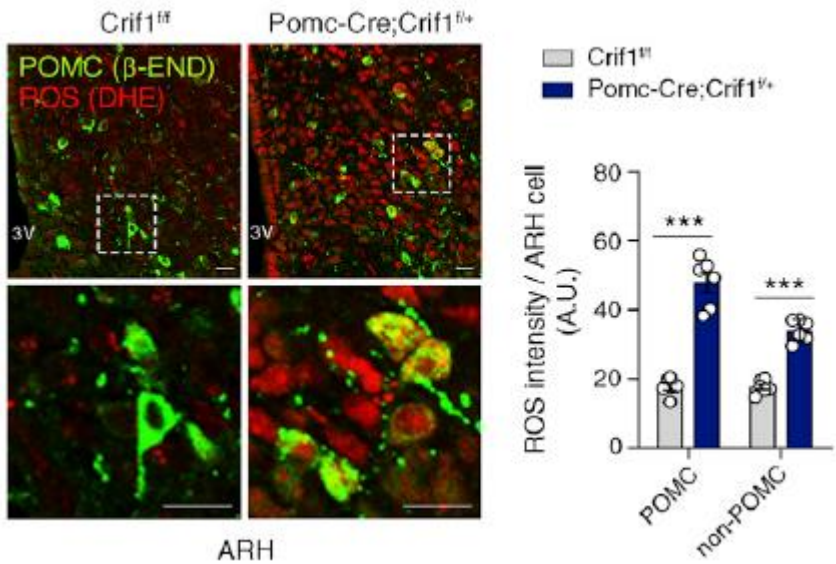

Figure 48. Dihydroethidium (DHE) and β-END double staining showing increased ROS production in the ARH of Pomc-Cre; Crif1$^{f/+}$ mice (n = 6). Scale bars, 10 μm. Results are presented as a mean ± SEM. ***p < 0.001 between indicated groups.

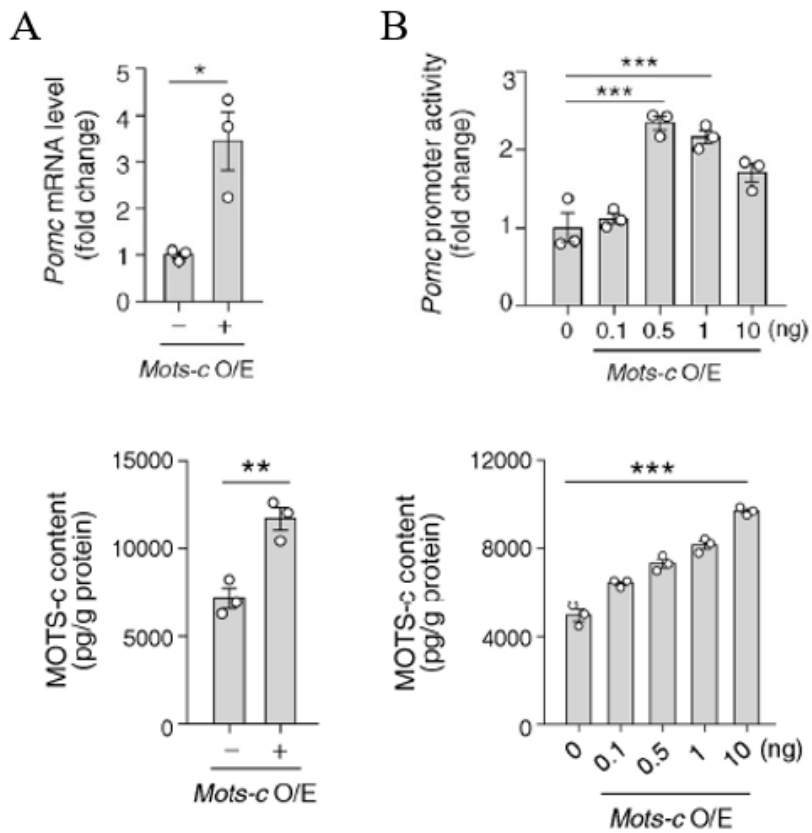

Figure 49. Effect of *Mots-c* overexpression (O/E) on *Pomc* mRNA and *Pomc* transcriptional activity ($n = 3$). Results are presented as a mean ± SEM. *$p < 0.05$, **$p < 0.01$, and ***$p < 0.001$ between indicated groups.

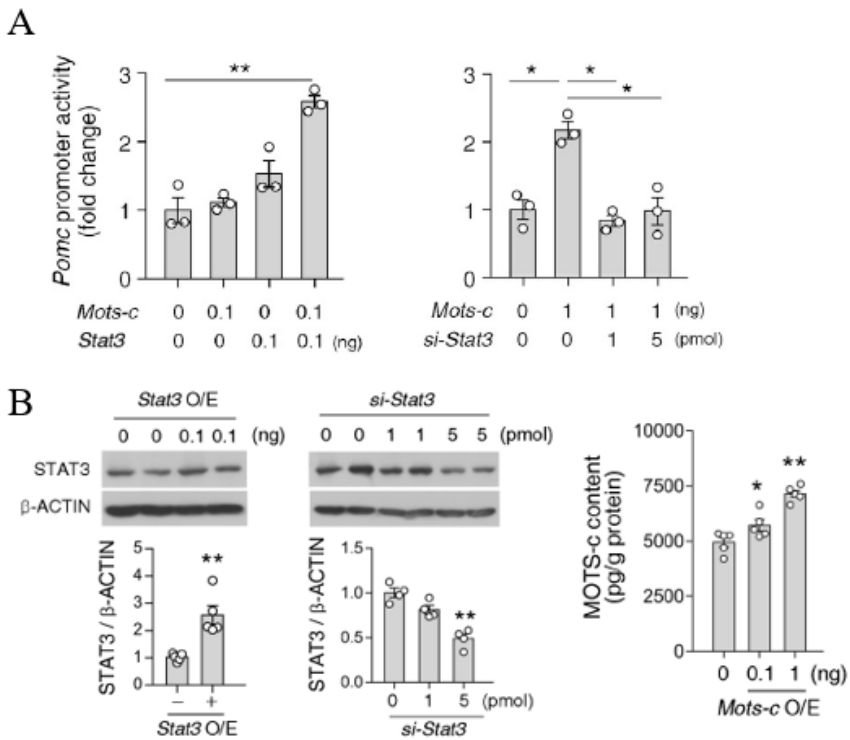

Figure 50. (A) Effects of *Stat3* coexpression and depletion via siRNA on the MOTS-c-mediated regulation of *Pomc* transcription (n = 3). (B) Confirmation of *Stat3* overexpression/knockdown and *Mots-c* overexpression in *Pomc* promotor experiments (n = 4—6). Results are presented as a mean ± SEM. *p < 0.05, **p < 0.01 between indicated groups.

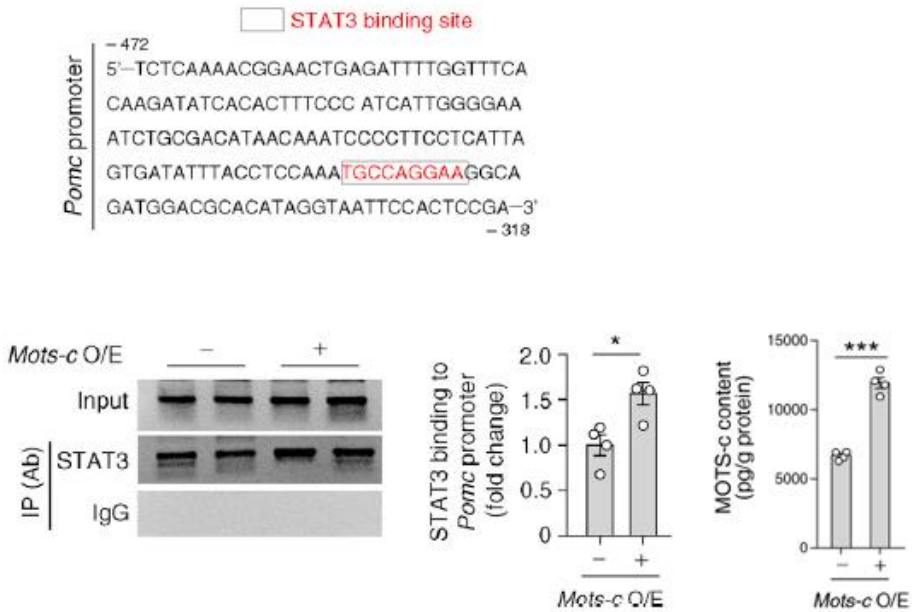

Figure 51. Chromatic immunoprecipitation assay showing increased STAT3 binding to the *Pomc* promotor area under conditions of *Mots-c* overexpression (n = 4) IP, immunoprecipitation; Ab, antibody. Results are presented as a mean ± SEM. *$p < 0.05$ and ***$p < 0.001$ between indicated groups.

3.7. Central MOTS-c administration recapitulates the phenotypes of mice with mild mitoribosomal stress in POMC neurons

I tested whether hypothalamic MOTS-c treatment could recapitulate the metabolic and adipose phenotypes of the Pomc-Cre; Crif1$^{f/+}$ mice. To this end, MOTS-c peptide (3 μg/day) was ICV-infused for 28 days using an osmotic minipump to young C57 mice. Chronic MOTS-c treatment increased nighttime EE and food intake without body weight changes (Figure 52). In addition, ICV-infused MOTS-c caused significant iWAT browning, smaller BAT fat droplets, greater sympathetic innervation as well as increased thermogenic gene expression, UPR^{mt} activation, and mitonuclear protein imbalance in the iWAT and BAT (Figures 53–55). These findings support the potential role of MOTS-c in mediating communication between the hypothalamus and adipose tissues as observed in *Crif1* heterodeficient mice.

I next examined whether the inhibition of hypothalamic MOTS-c expression or action could reverse the fat tissue changes in Pomc-Cre; Crif1$^{f/+}$ mice. The specific inhibition of *Mots-c* transcript was technically challenging due to the short open reading frame within the mitochondrial 12S rRNA gene. As an alternative strategy, I infused MOTS-c neutralizing antibody into the bilateral ARH of Pomc-Cre; Crif1$^{f/+}$ mice using an osmotic pump to block MOTS-c actions if it was secreted extracellularly from POMC neurons and acted in an autocrine and/or paracrine manner within the ARH. Intra-ARH infusion of MOTS-c antibody did not reverse iWAT browning in Pomc-Cre; Crif1$^{f/+}$ mice (Figure 56), supporting intracellular actions of hypothalamic MOTS-c.

Consistent with the *in vitro* findings, ICV MOTS-c infusion elevated hypothalamic *Pomc* mRNA and β-END expression in mice but α-MSH levels did not alter and were at a steady-state with increased expression of hypothalamic α-MSH–producing/degrading enzymes (Figures 57 and 58). The percentage of c-Fos^{+} POMC neurons and the expression of ARH UPR^{mt} genes were also upregulated by ICV MOTS-c treatment (Figures 59 and 60). Therefore, ICV MOTS-c infusion recapitulated the phenotypes of POMC *Crif1* heterodeficient mice. On the other hand, MOTS-c-treatment did not affect hypothalamic transcript levels of other neuronal markers (*Agrp*, *Npy*, *Sf1*), astrocyte marker (*Gfap)*, microglia marker (*Iba1*) and leptin and insulin receptors (*Lepr*, *Insr*) (Figure 61), supporting a specific regulatory role of MOTS-c on POMC neurons.

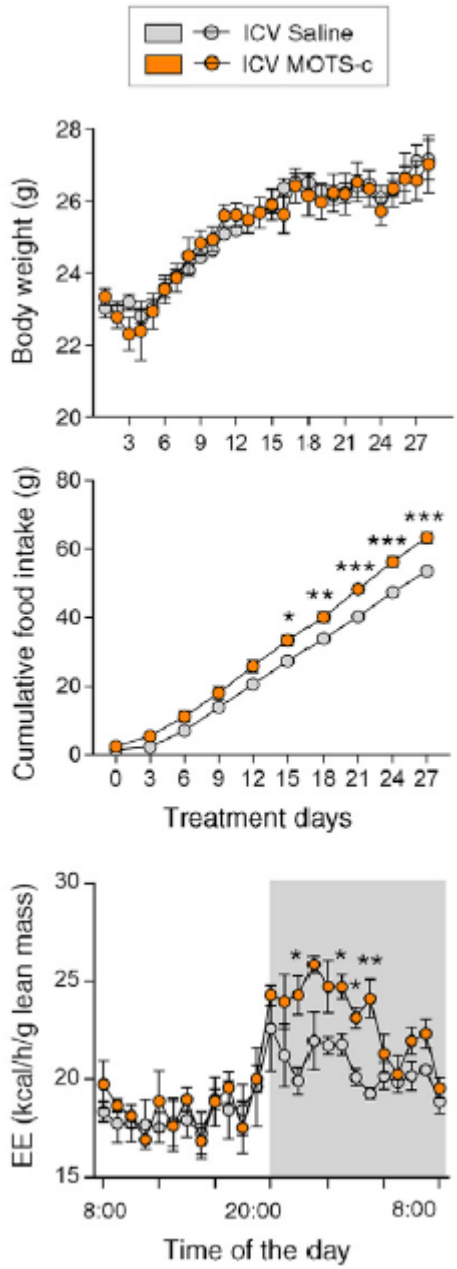

Figure 52. Body weight, cumulative food intake, and energy expenditure during ICV infusion of MOTS-c in C57 mice (n = 6–9). Results are presented as a mean ± SEM. *p < 0.05, **p < 0.01, and ***p < 0.001 between indicated groups.

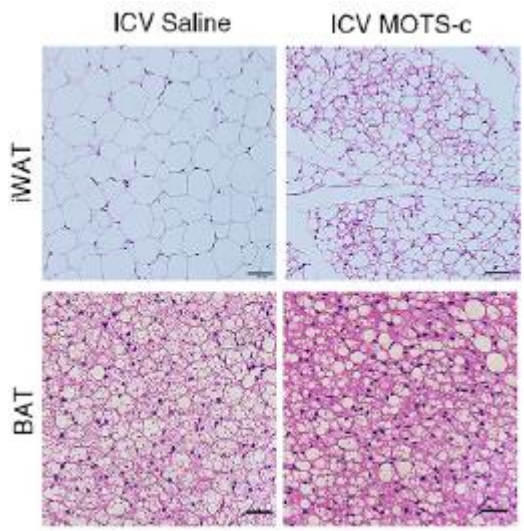

Figure 53. ICV MOTS-c-treated mice show iWAT browning and smaller fat droplets in the BAT (n = 6). Scale bars, 50 μm.

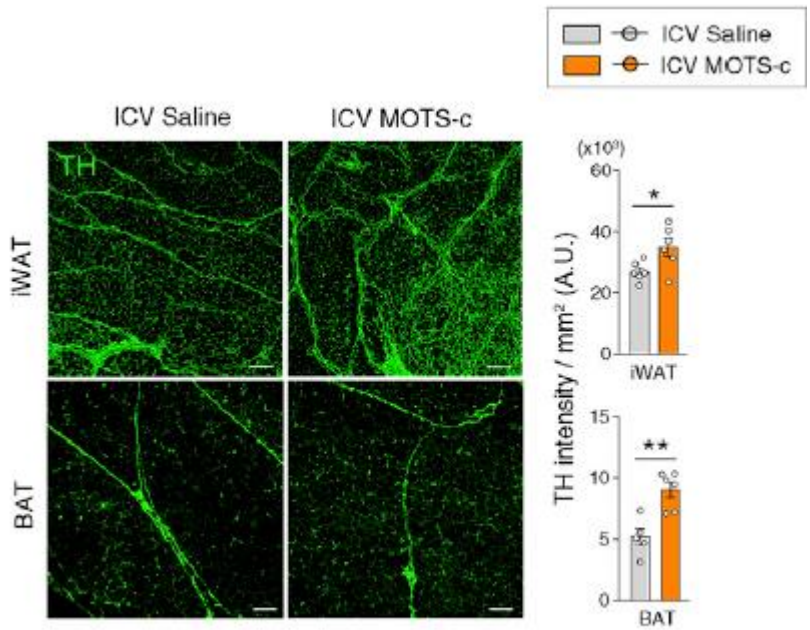

Figure 54. ICV MOTS-c-induces enhanced sympathetic innervation in the iWAT and BAT (n = 5–6). Scale bars, 200 μm (upper) and 50 μm (lower). Results are presented as a mean ± SEM. *p < 0.05 between indicated groups.

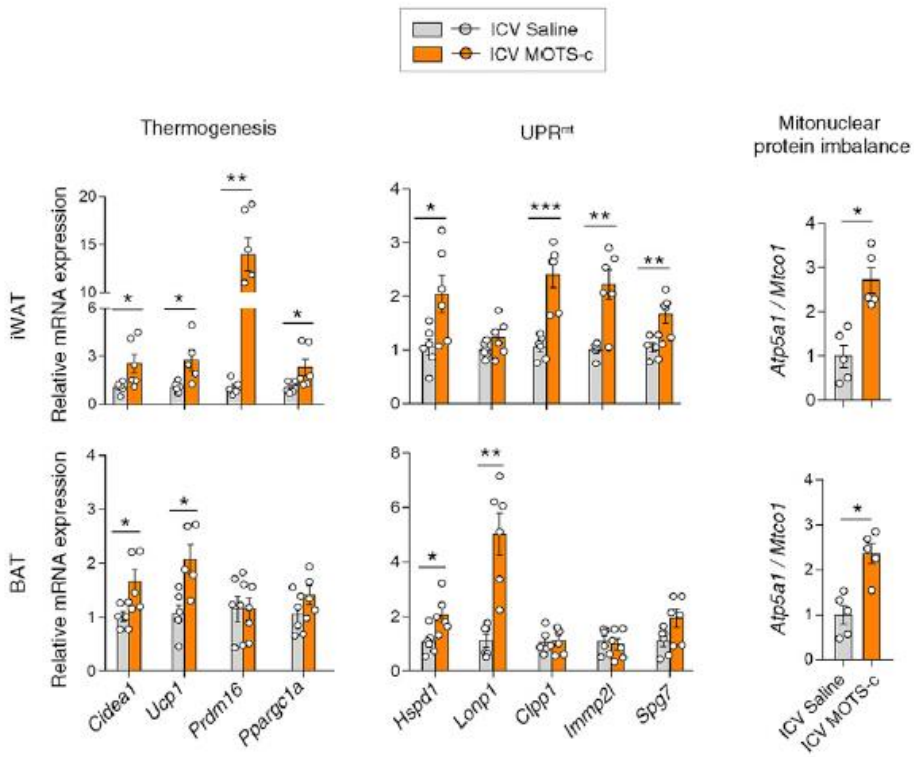

Figure 55. ICV MOTS-c-induces enhanced thermogenesis, the UPR^{mt}, and a mitonuclear protein imbalance in the iWAT and BAT (n = 5–6). Results are presented as a mean ± SEM. *p < 0.05, **p < 0.01, and ***p < 0.001 between indicated groups.

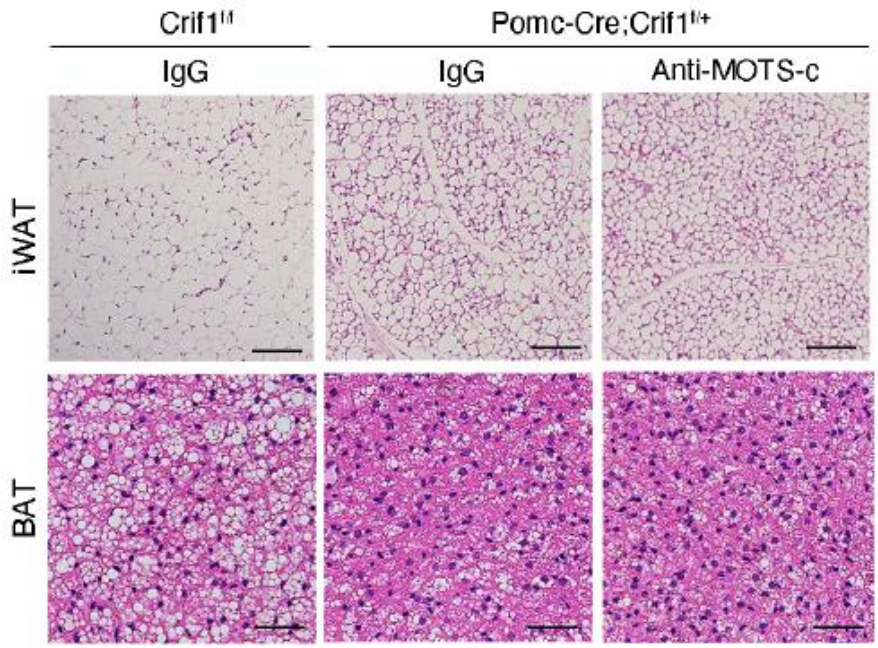

Figure 56. Histology of iWAT and BAT in Pomc-Cre; Crif1f/+ mice receiving intra-ARH infusion of either IgG or anti-MOTS-c antibody for 7 days. As a control, $Crif1^{f/f}$ mice were infused with IgG in their ARH (n = 4─5). Scale bars, 50 μm.

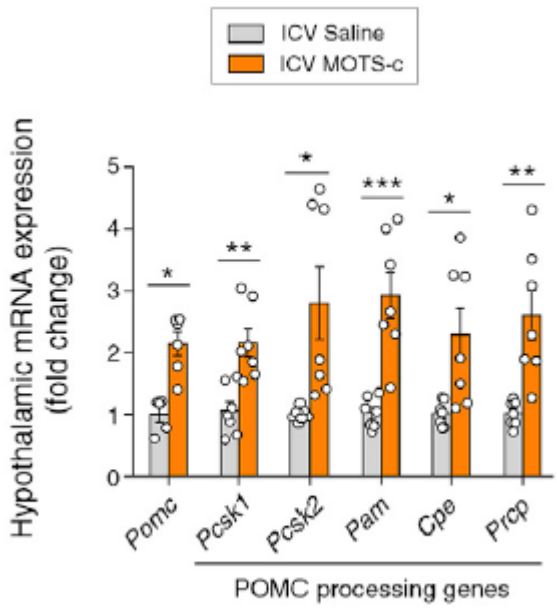

Figure 57. Increased hypothalamic expression of *Pomc* and its processing enzymes in mice with ICV MOTS-c administration (n = 7). Results are presented as a mean ± SEM. *$p < 0.05$, **$p < 0.01$, and ***$p < 0.001$ between indicated groups.

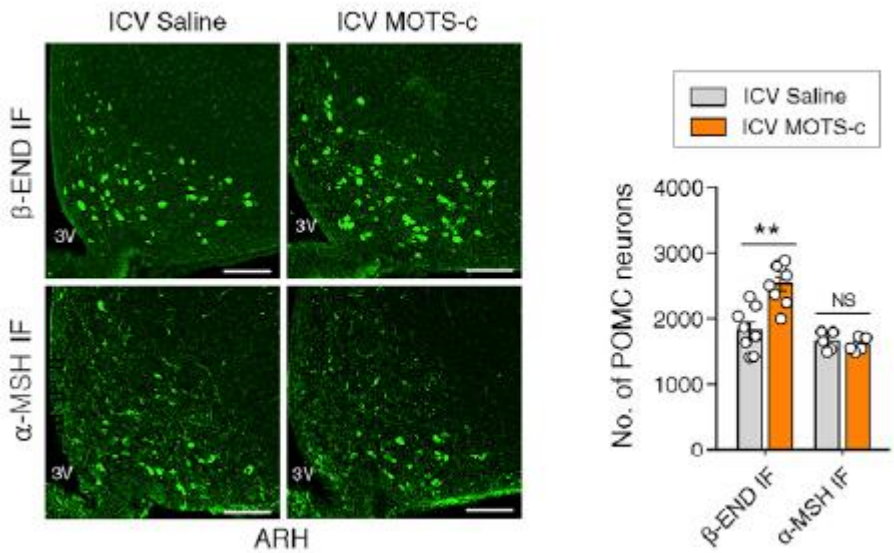

Figure 58. Increased numbers of the hypothalamic β-END$^+$ neurons but no change in the α-MSH$^+$ neuron numbers following ICV MOTS-c infusion (n = 5–8). Scale bars, 50 μm. Results are presented as a mean ± SEM. **$p < 0.01$ between indicated groups. NS, not significant.

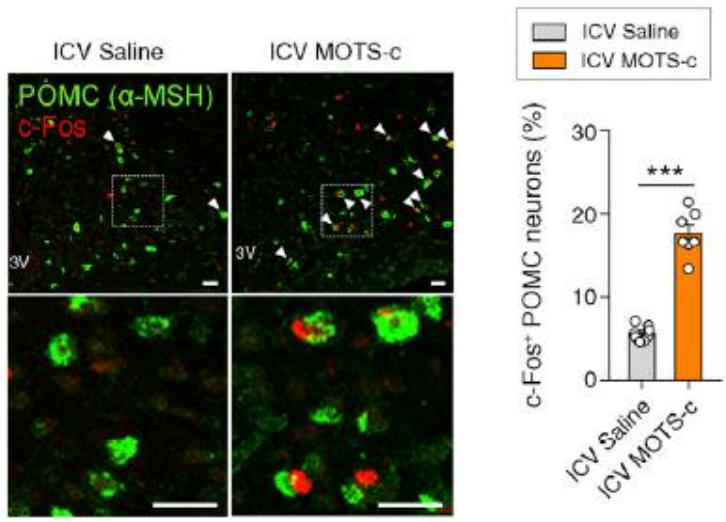

Figure 59. Increase in the percentage of c-Fos$^+$ POMC neurons in MOTS-c-treated mice (n = 6–8). Scale bars, 25 μm. Arrowheads indicate c-Fos$^+$ POMC neurons. Results are presented as a mean ± SEM. ***$p < 0.001$ between indicated groups.

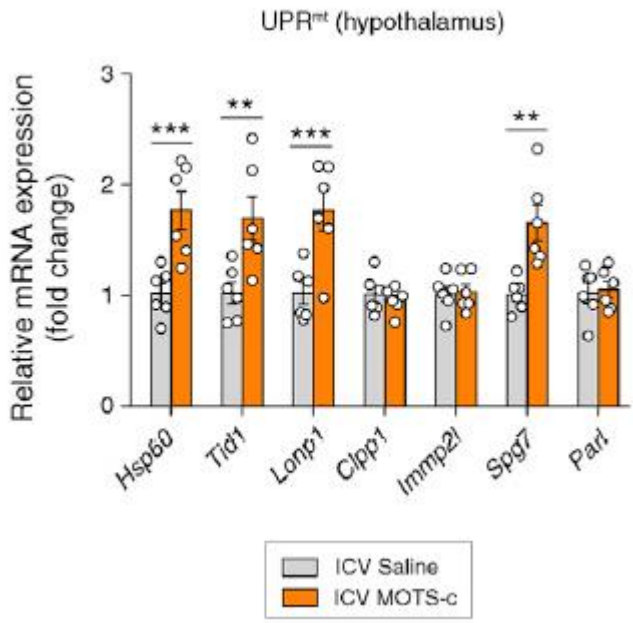

Figure 60. Increase in hypothalamic UPR^{mt} gene expression in MOTS-c-treated mice (n = 6–8). Results are presented as a mean ± SEM. **p < 0.01 and ***p < 0.001 between indicated groups.

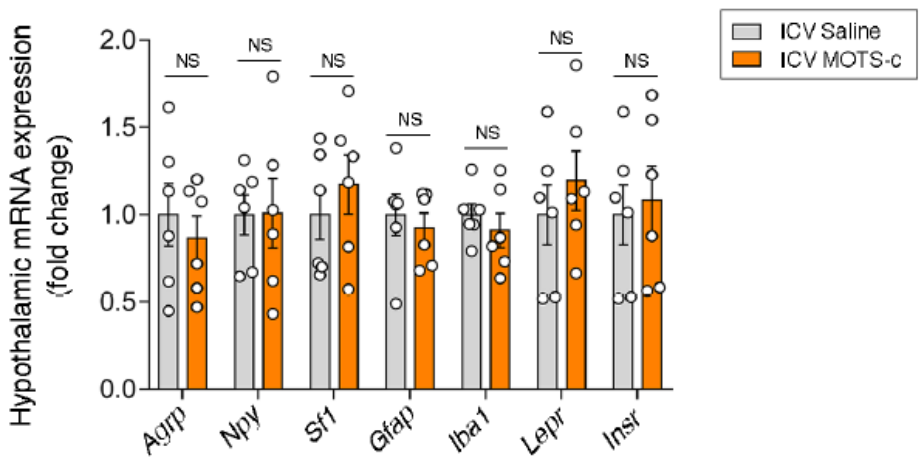

Figure 61. No alteration in the hypothalamic expression levels of neuronal markers, glial markers, and hormonal receptors by ICV MOTS-c treatment (n = 6). Results presented as mean ± SEM. NS: not significant.

3.8. Regular exercise and the myokine interleukin-6 stimulate hypothalamic MOTS-c and β-END production

I next searched for a physiological regulator or condition related to POMC neuronal mitoribosomal stress. I first examined the involvement of leptin in this regard as it stimulates *Pomc* transcription via STAT3 and activates adipose tissue thermogenesis (Dodd et al., 2015). In contrast to the expectation, a single ICV leptin (1 μg) administration decreased MOTS-c expression in the hypothalamus of C57 mice as determined by immunohistochemistry (Figure 62A) and ELISA (Figure 62B), indicating that leptin may act as a negative regulator of hypothalamic MOTS-c.

I hypothesized that regular moderate-intensity exercise may induce high metabolic turnover and beneficial metabolic changes without marked weight changes via hypothalamic mitoribosomal stress responses. To test whether regular exercise increases hypothalamic MOTS-c expression, young C57 mice were subjected to moderate-intensity running (13 meters/min on a treadmill for 50 min/day) for 2 weeks. This regular exercise robustly increased hypothalamic MOTS-c expression (Figures 63A and 63B), whereas a single bout of high-intensity running until exhaustion did not cause this elevation (Figure 64). These data highlighted the importance of exercise duration or intensity in inducing hypothalamic MOTS-c.

Regular running also increased hypothalamic β-END expression and ROS production, particularly in POMC neurons (Figure 65 and 66). It also induced histological changes, elevated sympathetic innervation, and increased thermogenic

gene expression and UPR^{mt} especially in iWAT of the mice (Figures 67, 68 and 69). Notably, a blockade of hypothalamic ROS production with a prior ICV injection of an antioxidant cocktail significantly inhibited regular exercise-induced hypothalamic MOTS-c/β-END expression as well as iWAT thermogenesis and UPR^{mt} (Figures 65-68), consistent with the prior results indicating coordination between ROS and MOTS-c (Figure 47 and 48). Hence, hypothalamic ROS production may be critical for exercise-induced changes in the hypothalamic and adipose tissues.

I finally investigated bioactive molecules that mediate exercise-induced hypothalamic mitochondrial stress responses. Because interleukin-6 (IL-6) is an exercise-related myokine (Pedersen et al., 2001), I tested its ability to induce hypothalamic MOTS-c expression. For this purpose, I ICV infused IL-6 peptide (400 ng/day) in young C57 mice for 5 days and found that it significantly elevated hypothalamic MOTS-c and β-END expression (Figure 70). Furthermore, ICV IL-6 treatment stimulated browning, sympathetic innervation, thermogenesis, and mitochondrial stress responses in iWAT (Figures 71 and 72). Further, in N1 hypothalamic neurons, IL-6 (100 nM) treatment induced the nuclear translocation of MOTS-c in an ROS-dependent manner (Figure 73). These findings collectively indicate that IL-6 promotes mitohormesis in hypothalamic neurons upon regular moderate-intensity exercise.

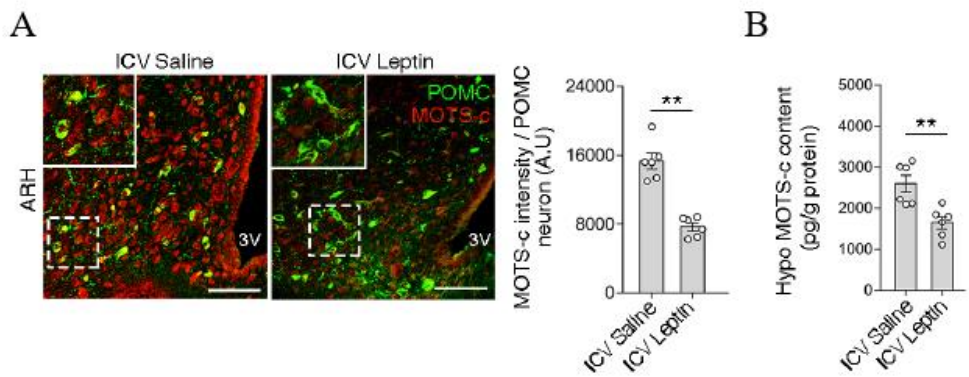

Figure 62. (A) MOTS-c / POMC (α-MSH) immunohistochemistry and (B) MOTS-c ELISA assay showing a reduction in hypothalamic MOTS-c expression following ICV leptin administration (n = 6). Scale bars, 50 μm. Results presented as mean ± SEM. ** $p < 0.01$ between indicated groups.

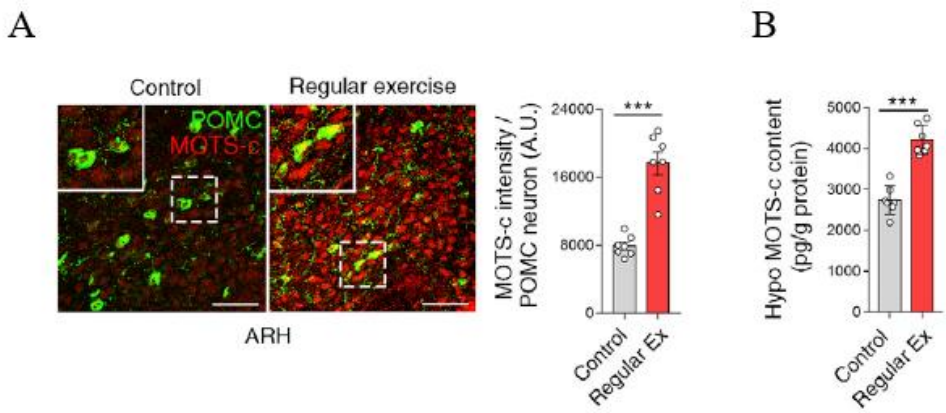

Figure 63. Increased MOTS-c expression in the mouse hypothalamus, including POMC neurons following 2 weeks of regular treadmill exercise (n = 7). Scale bars, 50 μm. Results are presented as a mean ± SEM. ***p < 0.001 between indicated groups.

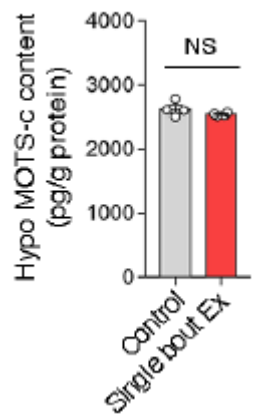

Figure 64. No alteration in hypothalamic MOTS-c content after single bout high-intensity running exercise (n = 5). Results are presented as a mean ± SEM. NS, no significant.

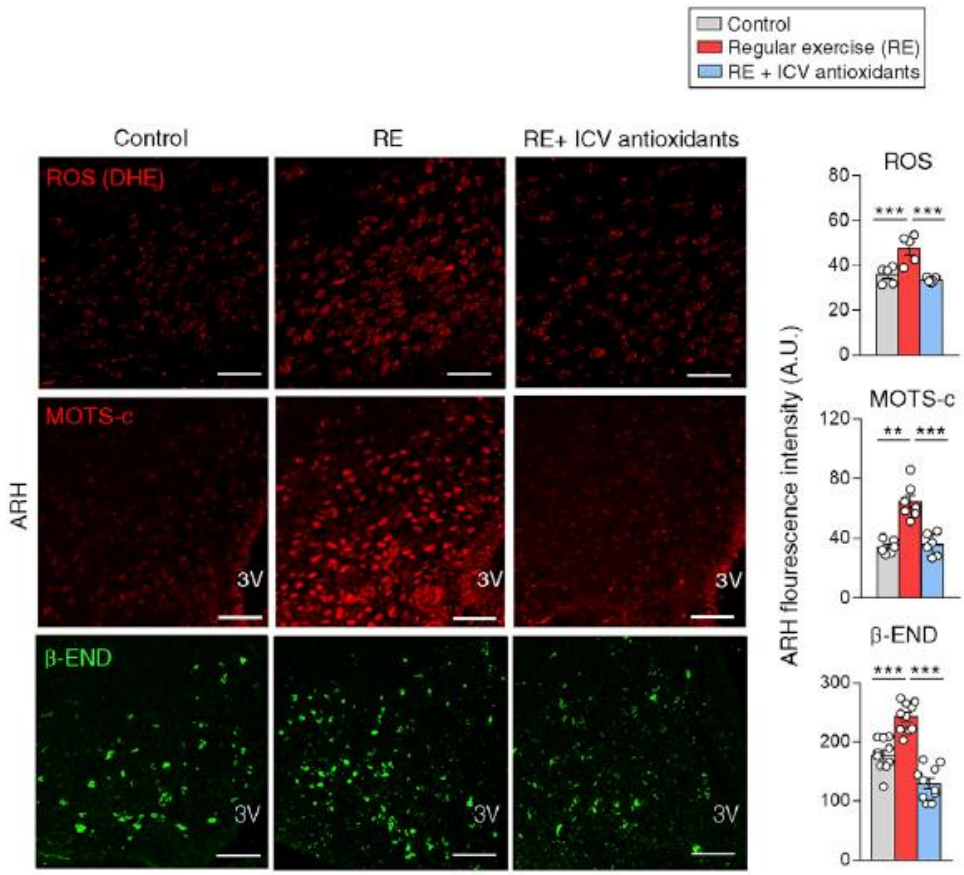

Figure 65. Regular running (RE)–induced increase in hypothalamic ROS production and MOTS-c/β-END expression, is reversed by an ICV injection of antioxidant cocktail prior to exercise (n = 5–10). Scale bars, 50 μm. Results are presented as a mean ± SEM. $^{**}p < 0.01$ and $^{***}p < 0.001$ between indicated groups.

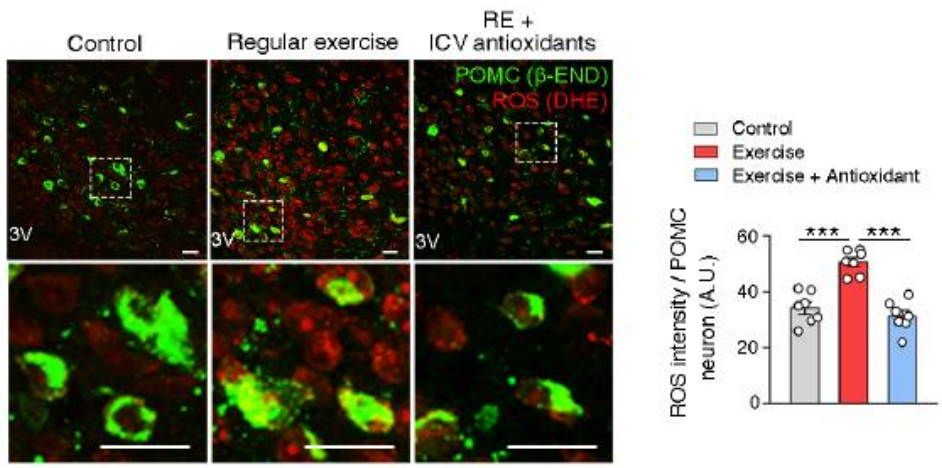

Figure 66. ROS (DHE) and β-END double staining in the hypothalamus of mice which underwent moderate-intensity regular running exercise with or without ICV antioxidant treatment ($n = 7$). Scale bars, 20 μm. Results presented as mean ± SEM. ***$p < 0.001$ between indicated groups.

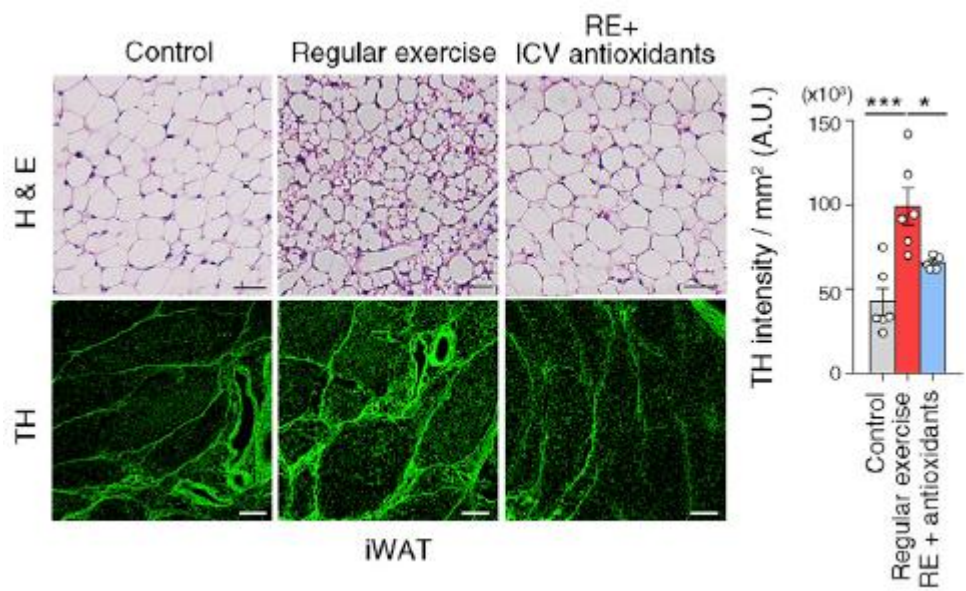

Figure 67. Effects of RE with or without ICV antioxidant treatment on iWAT histology and sympathetic innervation (n = 6–8). Scale bars, 50 μm (upper) and 200 μm (lower). Results are presented as a mean ± SEM. *p < 0.05 and ***p < 0.001 between indicated groups.

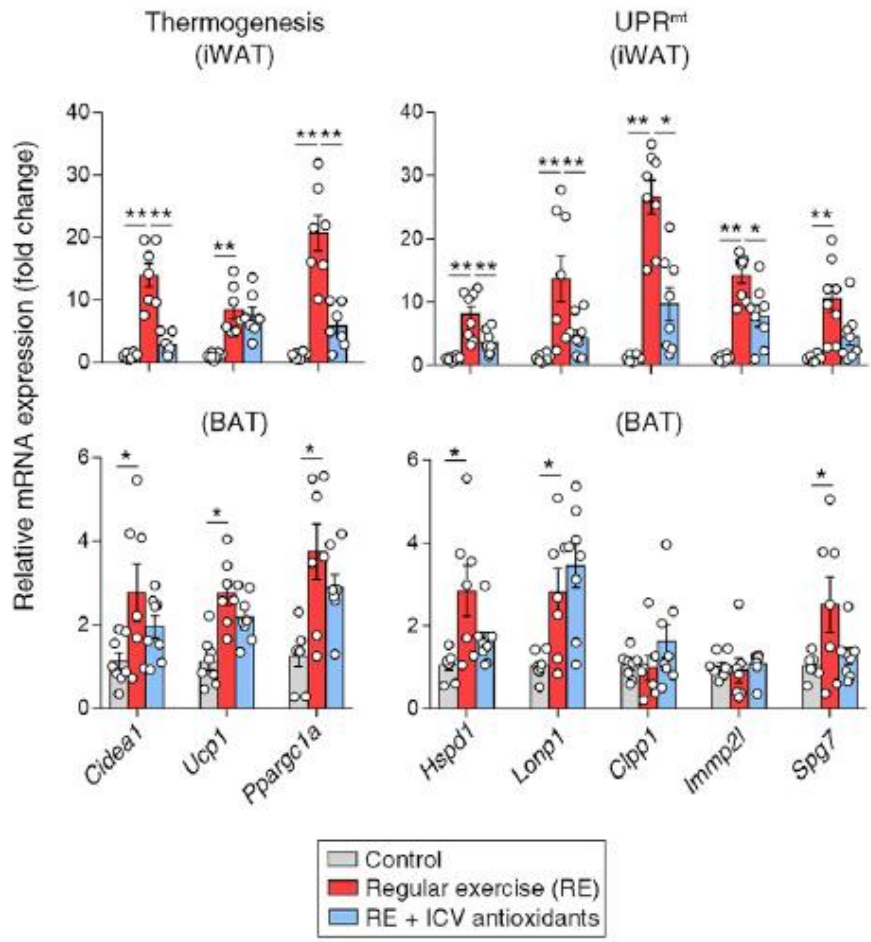

Figure 68. Effects of RE with or without ICV antioxidant treatment on thermogenic gene expression and UPR^{mt} (n = 6–8). Results are presented as a mean ± SEM. *p < 0.05 and **p < 0.01 between indicated groups.

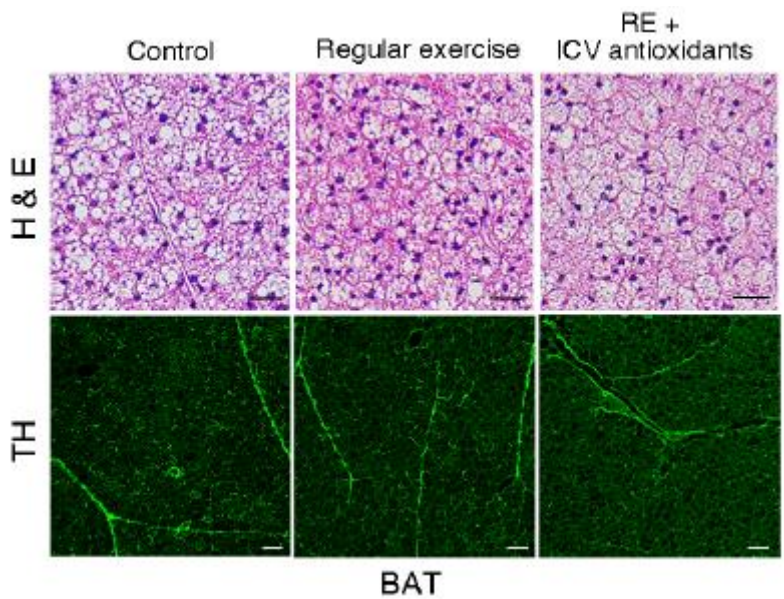

Figure 69. No significant changes in the BAT histology and sympathetic innervation after 2 week-regular running exercise (n = 7). Scale bars, 50 μm (upper) and 200 μm (lower).

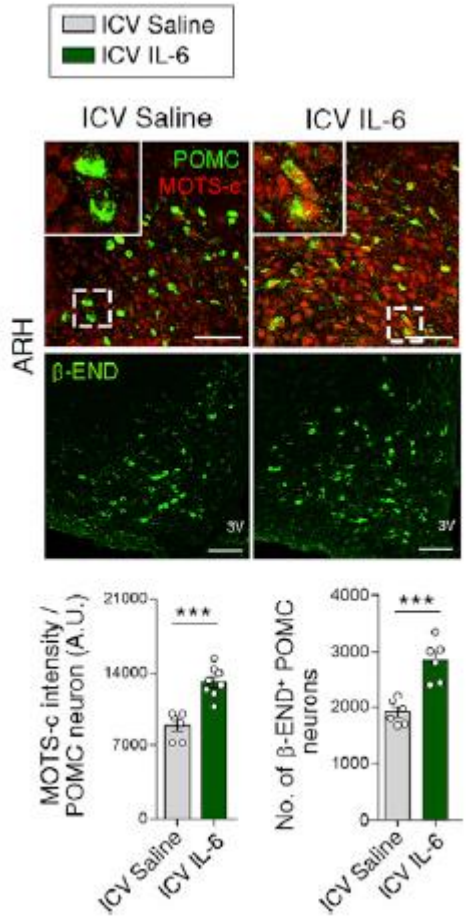

Figure 70. Increased hypothalamic MOTS-c and β-END expression following an ICV IL-6 infusion (400 ng/day for 5 days) (n = 6–8). Scale bars, 50 μm. Results are presented as a mean ± SEM. ***$p < 0.001$ between indicated groups.

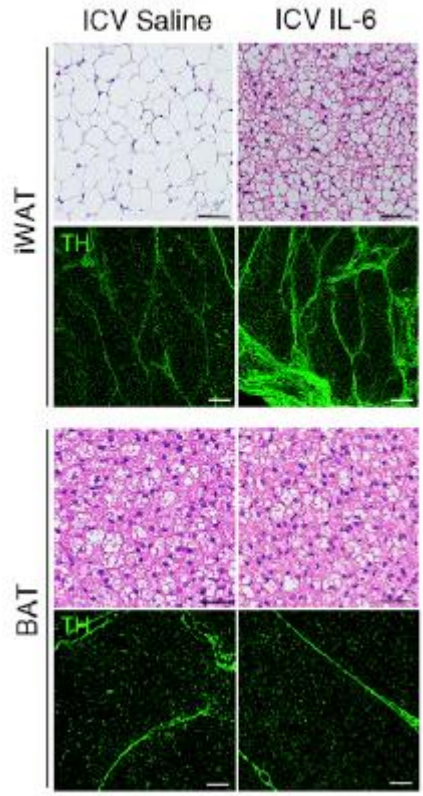

Figure 71. ICV IL-6-induced changes in the iWAT and BAT (*n* = 6). Scale bars, 50 μm (H & E and BAT TH image), and 200 μm (iWAT TH).

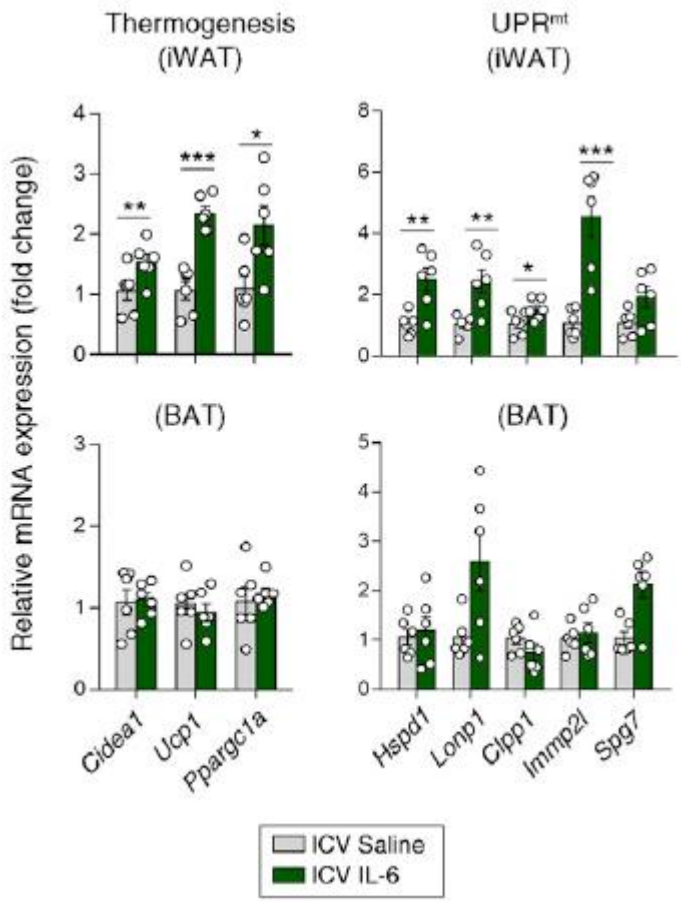

Figure 72. ICV IL-6-induced thermogenic gene expression and UPR^{mt} in the iWAT and BAT (n = 6). Results are presented as a mean ± SEM. *p < 0.05, **p < 0.01, and ***p < 0.001 between indicated groups.

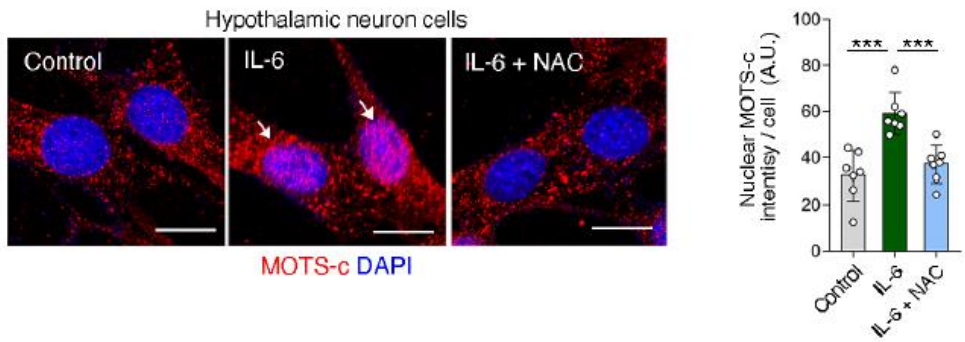

Figure 73. MOTS-c nuclear translocation upon treatment of IL-6 +/- antioxidant N-acetyl cysteine (NAC) in N1 hypothalamic neuron cells (*n* = 10 wells). Scale bars, 25 μm. Arrows indicate nuclear MOTS-c expression. Results presented as mean ± SEM. **p < 0.01, ***p < 0.001 between indicated groups.

4. DISCUSSION

The current study demonstrates the importance of mitoribosomal stress in hypothalamic POMC neurons on whole-body metabolism. *Crif1* homodeficiency in POMC neurons results in the development of adult-onset severe obesity and glucose dysregulation. As demonstrated in the hippocampal neurons of CamKII-Cre: Crif1$^{f/f}$ mice (Kim et al., 2012), *Crif1* homodeficiency in POMC neurons may cause ETC dysfunction, defective ATP production, and eventually cell death. Consistent with this possibility, EM examinations revealed disrupted inner mitochondrial membrane and reduced endoplasmic reticulum-mitochondria contacts in *Crif1* homodeficient POMC neurons.

Contrary to the adverse outcomes of *Crif1* homodeficiency, mice with *Crif1* heterodeficiency showed higher metabolic turnover with a modest increase in energy intake and a higher EE, without changes in body weight. Interestingly, similar metabolic changes were observed in *Crif1* homodeficient males before the development of obesity (prior to 10 weeks of age). During this period, POMC neurons with *Crif1* homodeficiency may be under mitochondrial stress but not critically damaged. The high metabolic turnover induced by partial *Crif1* deficiency may protect against diet-induced obesity. Indeed, *Crif1* heterodeficient mice on a HFD, which consumed more food than the controls, were resistant to weight gain. These findings are in line with previous studies in lower organisms demonstrating that perturbations in mitochondrial ETC and ribosomes increase lifespan and delay ageing-related changes (Durieux et al., 2011; Houtkooper et al.,

2013).

Interestingly, the induction of mitohormesis appears to be dependent on spatial and temporal contexts, whereby cell type and stage of life play critical roles. Neuronal, muscle, and intestinal cells have been shown to elicit mitohormesis (Berendzen et al., 2016; Durieux et al., 2011; Shao et al., 2016) and the findings of current study provide evidence for POMC neurons. The timing of mitochondrial stress may also influence the induction of mitohormesis. In *C. elegans*, mitochondrial perturbation, introduced early in life during development and young adulthood, induced beneficial effects (Cox et al., 2018; Durieux et al., 2011; Schulz et al., 2007). Consistently, the embryonic and young adult-onset partial deletion of *Crif1* in POMC neurons promoted similar metabolic phenotypes.

Mitochondrial stress during development increases resilience throughout life via a retrograde stress response from the mitochondria to the nucleus (Yun and Finkel, 2014). In *C. elegans*, the UPR^{mt} constitutes an important part of mitochondrial stress responses as it helps in the recovery from mitochondrial perturbation by stimulating the production of nDNA-encoded mitochondrial chaperones and proteases. In *C. elegans*, the UPR^{mt} can be induced cell-autonomously or cell-non-autonomously (Shao et al., 2016), mediated by secreted factors such as serotonin (neurotransmitter) and FLP-2 (neuropeptide) (Berendzen et al., 2016; Shao et al., 2016). As previously reported that in mammals, GDF15 acts as a secretory mediator of mitochondrial stress (Chung et al., 2017). Fibroblast growth factor 21, angiopoietin-like peptide 6, and adrenomedullin 2 are also potential candidate mediators of these processes (Kang et al., 2017; Kim et al.,

2013; Lv et al., 2016).

Crif1 partial deficiency in POMC neurons provoked remarkable cell-non-autonomous UPR^{mt} in the iWAT and BAT, whereas it induced relatively mild cell-autonomous UPR^{mt}. These data suggest that cell-non-autonomous UPR^{mt} may have a more sensitive induction threshold than cell-autonomous UPR^{mt} in hypothalamic POMC neurons. I also provide evidence of neural-mediated cell-non-autonomous UPR^{mt} in the iWAT of mice, as shown by chemical sympathetic denervation, in response to mitoribosomal stress in hypothalamic POMC neurons. Although the detailed molecular mechanisms of SNS-mediated adipose tissue UPR^{mt} remain elusive, a mitonuclear protein imbalance may be related to this process as it activates the UPR^{mt} and extends the lifespan in worms (Houtkooper et al., 2013). Indeed, I found that POMC-specific *Crif1* deficiency caused a mitonuclear protein imbalance in POMC neurons as well as in iWAT and BAT. Again, the cell-non-autonomous mitonuclear protein imbalance in iWAT of *Crif1* heterodeficient mice was inhibited by disruption of sympathetic innervation. Hence, mitonuclear protein imbalance can be induced cell-non-autonomously through the autonomic nervous system.

Substantial evidence now shows the role of MDPs as inherent mitochondrial signals that promote the cellular and organismal adaptation to mitochondria stress (Galluzzi et al., 2018; Kim et al., 2017; Lee et al., 2016; Mottis et al., 2019; Quiros et al., 2016; Tan and Finkel, 2020). In the current study, MOTS-c expression was significantly elevated in the POMC neurons with partial *Crif1* deficiency. Furthermore, ICV MOTS-c infusion induced high turnover metabolism observed in the Pomc-Cre: Crif1$^{f/+}$ mice. These data support a role for MOTS-c as a potential

mitochondrial-encoded messenger that propagates mitochondrial stress from POMC neurons to adipose tissue to induce thermogenesis. MOTS-c is detected in circulation and its levels can decrease during aging, cold exposure and type 2 diabetes, but increase upon exercise (Lee et al., 2015; Lu et al., 2019a; Ramanjaneya et al., 2019; Reynolds et al., 2019), evidencing its role as a mitochondrial hormone (Zarse and Ristow, 2015). In addition, intracellular MOTS-c (endogenous and exogenous), directly relays mitochondrial stress conditions to the nucleus, where it coordinates with transcription factors (*e.g.* NRF2 and ATF1) to regulate adaptive nuclear gene expression (Kim et al., 2018; Reynolds et al., 2019). Consistently, in the hypothalamic neurons, MOTS-c entered the nucleus upon oxidative stress and stimulated *Pomc* transcription by enhancing STAT3 binding to the *Pomc* promotor.

POMC is cleaved by multiple enzymes to yield β-END and α-MSH. Intriguingly, I found that partial *Crif1* deficiency and ICV MOTS-c infusion selectively increased hypothalamic β-END, but not α-MSH levels. This differential regulation of POMC processing by partial *Crif1* deficiency or MOTS-c can be, in part, explained by a marked increase in the expression of PRCP, which degrades biologically active α-MSH (1-13). Interestingly, α-MSH and β-END, despite being derived from the same precursor POMC, have opposing effects on food intake; β-END has orexigenic effect although this effect is short-lasting and antagonizes the anorexigenic effect of α-MSH (Dutia et al., 2012). Indeed, POMC neurons mediate cannabinoid-induced hyperphagia by releasing β-END (Koch et al., 2015). Considering that ICV β-END administration induced iWAT browning, both β-END and α-MSH may have similar thermogenesis-promoting effects (Fan et al., 2005).

The current study demonstrated that moderate-intensity regular exercise increased hypothalamic MOTS-c expression through a ROS-dependent mechanism. Consistently, MOTS-c levels were increased in human skeletal muscle and plasma following exercise (Reynolds et al., 2019). Exercise-related myokine IL-6 elevated hypothalamic MOTS-c expression whereas leptin lowered it. Both leptin and IL-6 activate hypothalamic STAT3 signaling (Munzberg et al., 2003; Wrighting and Andrews, 2006). Thus, further studies are crucial to discover the downstream signaling pathways leading to differential regulation of MOTS-c. Also, it will be worthwhile to examine whether ICV MOTS-c treatment regulates skeletal muscle metabolism and function as recent study reported that exercise performance and aging-related decline in physical capacity were improved by systemic MOTS-c treatment (Reynolds et al., 2019).

In human, there are substantial evidence of the role of mitochondrial dysfunction in the pathogenesis of chronic metabolic diseases including obesity, diabetes, and neurodegenerative disorders. Severe mitochondrial dysfunction either due to nutrition overload and excessive ROS generation contributes to systemic inflammation and oxidative stress, which are associated with pathogenesis of metabolic syndrome. In particular, abdominal obesity has been associated with impaired mitochondrial biogenesis accompanied by decreased mitochondrial function, oxidative metabolism, low mitochondrial gene expression, and ATP generation in human (Nisoli et al, 2007). This might be due to reduced mtDNA, respiratory protein, mitochondrial dynamics and expressions of mtDNA transcription factor such as Tfam (Bhatti et al, 2017). However, so far, there is little evidence that mild mitochondrial stress improves metabolic fitness in human.

Calorie restriction, temperature stress, and physical exercise have been suggested as hormetic conditions that could evoke metabolic stress but potentially be of great benefit to humans. These conditions, in part, might be associated with mitochondrial stress adaptive response. Many different mitochondrial haplotypes exist in humanity, implying rapid evolution of mitochondrial genes and adaptation to different environments (Wallace, 2008). For instance, in hot countries where thermogenesis is less important, tight coupling might result in high ATP phenotypes, where as in cold countries, increased uncoupling might help generating heat. Moreover, some haplotypes may be better protected against type II diabetes, while others are associated with extreme longevity (Nunn et al, 2010).

However, so far, there are no effective method to measure mitochondrial adaptive response or degree of mitochondrial stress in human. Therefore, we suggest that MOTS-c, which is highly conserved among species, could be the potential indicator of mitochondrial adaptive response in perspective of progression of metabolic diseases. Indeed, there are several studies on the relationship between MOTS-c and human metabolic diseases. In a cross-sectional study conducted by Ramanjaneya et al., serum MOTS-c in T2DM patients was significantly lower in compared to controls (Ramanjaneya et al., 2019). Meanwhile, Du et al reported that MOTS-c levels are significantly lower in obese male children and adolescents compared to females, and also showed a negative correlation with BMI, HOMA, HbA1c, and fasting insulin in male subjects (Du et al., 2018). Recently, Reynolds et al. reported that exercise induces endogenous MOTS-c expression in skeletal muscle and in circulation (Reynolds et al., 2021). However, since the value of the circulating MOTS-c levels are more than 1000 times different among the studies

depending on which measurement kit they used, more accurate and consistent measurement methods for measurement of human MOTS-c are required. Moreover, it is also necessary to check whether the MOTS-c produced by diverse tissues will have a different roles.

Although this study provides strong evidence for the role of MOTS-c in communicating low-grade mitoribosomal stress in hypothalamic POMC neurons and leading to high-turnover metabolism and resistance to obesity, the effect of *Mots-c* gene ablation remains unexplored. Targeted mtDNA editing tools that can precisely alter nucleotide sequences of interest are currently unavailable, but opportunities may emerge in the near future based on active ongoing research on mitochondrial genome editing technology (Bacman et al., 2013; Gammage et al., 2018; Mok et al., 2020). Moreover, whether mitoribosomal stress induces a differential metabolic effect in hypothalamic *vs.* hindbrain POMC neurons remains to be addressed. However, at least, I observed POMC and MOTS-c expression were not changed in brainstem NTS and pituitary gland in current rodent model, hence the metabolic phenotypes in the study appears to be mainly attributable to changes driven by mitoribosomal stress in hypothalamic POMC cells. Further, the absolute degree of mitoribosomal stress that might induce whether detrimental or beneficial metabolic impact could not be measured, which could be expanded in further researches.

In conclusion, regular exercise-induced low-level mitoribosomal stress in POMC neurons causes high metabolic turnover via interorgan communication of mitochondrial stress. These findings provide a novel neuroendocrine mechanism of exercise physiology that may provide new venues for future therapeutic

development of exercise-mimetics.

ACKNOWLEDGEMENT

Gil Myoung Kang and Chan Hee Lee also contributed to this study and published the results as co-first authors (Cell Metab. 2021 Feb 2;33(2):334-349).

References

Anderson, N.S., and Haynes, C.M. (2020). Folding the Mitochondrial UPR into the Integrated Stress Response. Trends in cell biology *30*, 428-439.

Andrews, Z.B., Liu, Z.W., Walllingford, N., Erion, D.M., Borok, E., Friedman, J.M., Tschop, M.H., Shanabrough, M., Cline, G., Shulman, G.I., et al. (2008). UCP2 mediates ghrelin's action on NPY/AgRP neurons by lowering free radicals. Nature *454*, 846-851.

Bacman, S.R., Williams, S.L., Pinto, M., Peralta, S., and Moraes, C.T. (2013). Specific elimination of mutant mitochondrial genomes in patient-derived cells by mitoTALENs. Nature medicine *19*, 1111-1113.

Berendzen, K.M., Durieux, J., Shao, L.W., Tian, Y., Kim, H.E., Wolff, S., Liu, Y., and Dillin, A. (2016). Neuroendocrine Coordination of Mitochondrial Stress Signaling and Proteostasis. Cell *166*, 1553-1563.e1510.

Bhatti, J.S., Bhatti, G.K., Reddy, P.H. (2017). Mitochondrial dysfunction and oxidative stress in metabolic disorders - A Step towards mitochondria based therapeutic strategies. Biochimica et Biophysica Acta *1863*, 1066–1077.

Bouret, S.G., Draper, S.J., and Simerly, R.B. (2004). Trophic action of leptin on hypothalamic neurons that regulate feeding. Science (New York, N.Y.) *304*, 108-110.

Chandel NS. (2015). Evolution of mitochondria as signaling organelles. Cell Metabolism *22*:204–206.

Chao, P.T., Yang, L., Aja, S., Moran, T.H., and Bi, S. (2011). Knockdown of NPY expression in the dorsomedial hypothalamus promotes development of brown

adipocytes and prevents diet-induced obesity. Cell metabolism *13*, 573-583.

Chung, H.K., Ryu, D., Kim, K.S., Chang, J.Y., Kim, Y.K., Yi, H.S., Kang, S.G., Choi, M.J., Lee, S.E., Jung, S.B., et al. (2017). Growth differentiation factor 15 is a myomitokine governing systemic energy homeostasis. The Journal of cell biology *216*, 149-165.

Costa-Mattioli, M., and Walter, P. (2020). The integrated stress response: From mechanism to disease. Science (New York, N.Y.) *368*.

Cox, C.S., McKay, S.E., Holmbeck, M.A., Christian, B.E., Scortea, A.C., Tsay, A.J., Newman, L.E., and Shadel, G.S. (2018). Mitohormesis in Mice via Sustained Basal Activation of Mitochondrial and Antioxidant Signaling. Cell metabolism *28*, 776-786.e775.

Diano, S., Liu, Z.W., Jeong, J.K., Dietrich, M.O., Ruan, H.B., Kim, E., Suyama, S., Kelly, K., Gyengesi, E., Arbiser, J.L., et al. (2011). Peroxisome proliferation-associated control of reactive oxygen species sets melanocortin tone and feeding in diet-induced obesity. Nature medicine *17*, 1121-1127.

Dietrich, M.O., Liu, Z.W., and Horvath, T.L. (2013). Mitochondrial dynamics controlled by mitofusins regulate Agrp neuronal activity and diet-induced obesity. Cell *155*, 188-199.

Dodd, G.T., Decherf, S., Loh, K., Simonds, S.E., Wiede, F., Balland, E., Merry, T.L., Munzberg, H., Zhang, Z.Y., Kahn, B.B., et al. (2015). Leptin and insulin act on POMC neurons to promote the browning of white fat. Cell *160*, 88-104.

Du, C., Zhang, C., Wu, W., Liang, Y., Wang, A., Wu, S., Zhao, Y., Hou, L., Ning, Q., and Luo, X. (2018). Circulating MOTS-c levels are decreased in obese male children and adolescents and associated with insulin resistance. Pediatric diabetes.

Durieux, J., Wolff, S., and Dillin, A. (2011). The cell-non-autonomous nature of electron transport chain-mediated longevity. Cell *144*, 79-91.

Dutia, R., Meece, K., Dighe, S., Kim, A.J., and Wardlaw, S.L. (2012). beta-Endorphin antagonizes the effects of alpha-MSH on food intake and body weight. Endocrinology *153*, 4246-4255.

Fan, W., Voss-Andreae, A., Cao, W.H., and Morrison, S.F. (2005). Regulation of thermogenesis by the central melanocortin system. Peptides *26*, 1800-1813.

Friedman JR, Nunnari J. (2014). Mitochondrial form and function. Nature *505*:335–343.

Galluzzi, L., Yamazaki, T., and Kroemer, G. (2018). Linking cellular stress responses to systemic homeostasis. Nature reviews. Molecular cell biology *19*, 731-745.

Gammage, P.A., Viscomi, C., Simard, M.L., Costa, A.S.H., Gaude, E., Powell, C.A., Van Haute, L., McCann, B.J., Rebelo-Guiomar, P., Cerutti, R., et al. (2018). Genome editing in mitochondria corrects a pathogenic mtDNA mutation in vivo. Nature medicine *24*, 1691-1695.

Harris, R.B. (2012). Sympathetic denervation of one white fat depot changes norepinephrine content and turnover in intact white and brown fat depots. Obesity (Silver Spring, Md.) *20*, 1355-1364.

Haynes, C.M., Yang, Y., Blais, S.P., Neubert, T.A., and Ron, D. (2010). The matrix peptide exporter HAF-1 signals a mitochondrial UPR by activating the transcription factor ZC376.7 in C. elegans. Molecular cell *37*, 529-540.

Houtkooper, R.H., Mouchiroud, L., Ryu, D., Moullan, N., Katsyuba, E., Knott, G., Williams, R.W., and Auwerx, J. (2013). Mitonuclear protein imbalance as a

conserved longevity mechanism. Nature *497*, 451-457.

Ikeda, K., Maretich, P., and Kajimura, S. (2018). The Common and Distinct Features of Brown and Beige Adipocytes. Trends in endocrinology and metabolism: TEM *29*, 191-200.

Kang, S.G., Yi, H.S., Choi, M.J., Ryu, M.J., Jung, S., Chung, H.K., Chang, J.Y., Kim, Y.K., Lee, S.E., Kim, H.W., et al. (2017). ANGPTL6 expression is coupled with mitochondrial OXPHOS function to regulate adipose FGF21. The Journal of endocrinology *233*, 105-118.

Kim, K.H., Jeong, Y.T., Oh, H., Kim, S.H., Cho, J.M., Kim, Y.N., Kim, S.S., Kim, D.H., Hur, K.Y., Kim, H.K., et al. (2013). Autophagy deficiency leads to protection from obesity and insulin resistance by inducing Fgf21 as a mitokine. Nature medicine *19*, 83-92.

Kim, K.H., Son, J.M., Benayoun, B.A., and Lee, C. (2018). The Mitochondrial-Encoded Peptide MOTS-c Translocates to the Nucleus to Regulate Nuclear Gene Expression in Response to Metabolic Stress. Cell metabolism *28*, 516-524.e517.

Kim, M.S., Pak, Y.K., Jang, P.G., Namkoong, C., Choi, Y.S., Won, J.C., Kim, K.S., Kim, S.W., Kim, H.S., Park, J.Y., et al. (2006). Role of hypothalamic Foxo1 in the regulation of food intake and energy homeostasis. Nature neuroscience *9*, 901-906.

Kim, S.J., Kwon, M.C., Ryu, M.J., Chung, H.K., Tadi, S., Kim, Y.K., Kim, J.M., Lee, S.H., Park, J.H., Kweon, G.R., et al. (2012). CRIF1 is essential for the synthesis and insertion of oxidative phosphorylation polypeptides in the mammalian mitochondrial membrane. Cell metabolism *16*, 274-283.

Kim, S.J., Xiao, J., Wan, J., Cohen, P., and Yen, K. (2017). Mitochondrially derived peptides as novel regulators of metabolism. The Journal of physiology *595*, 6613-

6621.

Koch, M., Varela, L., Kim, J.G., Kim, J.D., Hernandez-Nuno, F., Simonds, S.E., Castorena, C.M., Vianna, C.R., Elmquist, J.K., Morozov, Y.M., et al. (2015). Hypothalamic POMC neurons promote cannabinoid-induced feeding. Nature *519*, 45-50.

Kwon, M.C., Koo, B.K., Moon, J.S., Kim, Y.Y., Park, K.C., Kim, N.S., Kwon, M.Y., Kong, M.P., Yoon, K.J., Im, S.K., et al. (2008). Crif1 is a novel transcriptional coactivator of STAT3. The EMBO journal *27*, 642-653.

Lan, J., Rollins, J.A., Zang, X., Wu, D., Zou, L., Wang, Z., Ye, C., Wu, Z., Kapahi, P., Rogers, A.N., et al. (2019). Translational Regulation of Non-autonomous Mitochondrial Stress Response Promotes Longevity. Cell reports *28*, 1050-1062.e1056.

Lee, C., Kim, K.H., and Cohen, P. (2016). MOTS-c: A novel mitochondrial-derived peptide regulating muscle and fat metabolism. Free radical biology & medicine *100*, 182-187.

Lee, C., Zeng, J., Drew, B.G., Sallam, T., Martin-Montalvo, A., Wan, J., Kim, S.J., Mehta, H., Hevener, A.L., de Cabo, R., et al. (2015). The mitochondrial-derived peptide MOTS-c promotes metabolic homeostasis and reduces obesity and insulin resistance. Cell metabolism *21*, 443-454.

Lu, H., Tang, S., Xue, C., Liu, Y., Wang, J., Zhang, W., Luo, W., and Chen, J. (2019a). Mitochondrial-Derived Peptide MOTS-c Increases Adipose Thermogenic Activation to Promote Cold Adaptation. International journal of molecular sciences *20*.

Lu, H., Wei, M., Zhai, Y., Li, Q., Ye, Z., Wang, L., Luo, W., Chen, J., and Lu, Z.

(2019b). MOTS-c peptide regulates adipose homeostasis to prevent ovariectomy-induced metabolic dysfunction. Journal of molecular medicine (Berlin, Germany) *97*, 473-485.

Lv, Y., Zhang, S.Y., Liang, X., Zhang, H., Xu, Z., Liu, B., Xu, M.J., Jiang, C., Shang, J., and Wang, X. (2016). Adrenomedullin 2 Enhances Beiging in White Adipose Tissue Directly in an Adipocyte-autonomous Manner and Indirectly through Activation of M2 Macrophages. The Journal of biological chemistry *291*, 23390-23402.

Mishra, P., Carelli, V., Manfredi, G., and Chan, D.C. (2014). Proteolytic cleavage of Opa1 stimulates mitochondrial inner membrane fusion and couples fusion to oxidative phosphorylation. Cell metabolism *19*, 630-641.

Mok, B.Y., de Moraes, M.H., Zeng, J., Bosch, D.E., Kotrys, A.V., Raguram, A., Hsu, F., Radey, M.C., Peterson, S.B., Mootha, V.K., et al. (2020). A bacterial cytidine deaminase toxin enables CRISPR-free mitochondrial base editing. Nature *583*, 631-637.

Mottis, A., Herzig, S., and Auwerx, J. (2019). Mitocellular communication: Shaping health and disease. Science (New York, N.Y.) *366*, 827-832.

Munzberg, H., Huo, L., Nillni, E.A., Hollenberg, A.N., and Bjorbaek, C. (2003). Role of signal transducer and activator of transcription 3 in regulation of hypothalamic proopiomelanocortin gene expression by leptin. Endocrinology *144*, 2121-2131.

Murphy MP. (2009). How mitochondria produce reactive oxygen species. Biochemical Journal *417*, 1–13.

Nisoli, E., Clementi, E., Carruba, M.O., Moncada, S. (2007). Defective

mitochondrial biogenesis: a hallmark of the high cardiovascular risk in the metabolic syndrome? Circulation Research *100*, 795-806.

Nunn, A.V., Guy, G.W., Brodie, J.S., Bell, J.D. (2010). Inflammatory modulation of exercise salience: using hormesis to return to a healthy lifestyle. Nutrition Metabolism, 7

Padilla, S.L., Carmody, J.S., and Zeltser, L.M. (2010). Pomc-expressing progenitors give rise to antagonistic neuronal populations in hypothalamic feeding circuits. Nature medicine *16*, 403.

Pedersen, B.K., Steensberg, A., and Schjerling, P. (2001). Exercise and interleukin-6. Current opinion in hematology *8*, 137-141.

Quiros, P.M., Mottis, A., and Auwerx, J. (2016). Mitonuclear communication in homeostasis and stress. Nature reviews. Molecular cell biology *17*, 213-226.

Ramanjaneya, M., Bettahi, I., Jerobin, J., Chandra, P., Abi Khalil, C., Skarulis, M., Atkin, S.L., and Abou-Samra, A.B. (2019). Mitochondrial-Derived Peptides Are Down Regulated in Diabetes Subjects. Frontiers in endocrinology *10*, 331.

Ramirez, S., Gomez-Valades, A.G., Schneeberger, M., Varela, L., Haddad-Tovolli, R., Altirriba, J., Noguera, E., Drougard, A., Flores-Martinez, A., Imbernon, M., et al. (2017). Mitochondrial Dynamics Mediated by Mitofusin 1 Is Required for POMC Neuron Glucose-Sensing and Insulin Release Control. Cell metabolism *25*, 1390-1399.e1396.

Reynolds, J., Lai, R.W., Woodhead, J.S.T., Joly, J.H., Mitchell, C.J., Cameron-Smith, D., Lu, R., Cohen, P., Graham, N.A., Benayoun, B.A., et al. (2019). MOTS-c is an Exercise-Induced Mitochondrial-Encoded Regulator of Age-Dependent Physical Decline and Muscle Homeostasis. bioRxiv, 2019.2012.2022.886432.

Reynolds, J.C., Bwiza, C.P., and Lee, C. (2020). Mitonuclear genomics and aging. Human genetics *139*, 381-399.

Ristow, M., and Zarse, K. (2010). How increased oxidative stress promotes longevity and metabolic health: The concept of mitochondrial hormesis (mitohormesis). Experimental gerontology *45*, 410-418.

Roh, E., Song, D.K., and Kim, M.S. (2016). Emerging role of the brain in the homeostatic regulation of energy and glucose metabolism. Experimental & molecular medicine *48*, e216.

Santoro, A., Campolo, M., Liu, C., Sesaki, H., Meli, R., Liu, Z.W., Kim, J.D., and Diano, S. (2017). DRP1 Suppresses Leptin and Glucose Sensing of POMC Neurons. Cell metabolism *25*, 647-660.

Sanz, E., Yang, L., Su, T., Morris, D.R., McKnight, G.S., and Amieux, P.S. (2009). Cell-type-specific isolation of ribosome-associated mRNA from complex tissues. Proceedings of the National Academy of Sciences of the United States of America *106*, 13939-13944.

Schulz, T.J., Zarse, K., Voigt, A., Urban, N., Birringer, M., and Ristow, M. (2007). Glucose Restriction Extends Caenorhabditis elegans Life Span by Inducing Mitochondrial Respiration and Increasing Oxidative Stress. Cell metabolism *6*, 280-293.

Shao, L.W., Niu, R., and Liu, Y. (2016). Neuropeptide signals cell non-autonomous mitochondrial unfolded protein response. Cell research *26*, 1182-1196.

Sharma, M.R., Koc, E.C., Datta, P.P., Booth, T.M., Spremulli, L.L., and Agrawal, R.K. (2003). Structure of the mammalian mitochondrial ribosome reveals an expanded functional role for its component proteins. Cell *115*, 97-108.

Shpilka, T., and Haynes, C.M. (2018). The mitochondrial UPR: mechanisms, physiological functions and implications in ageing. Nature reviews. Molecular cell biology *19*, 109-120.

Suhm, T., Kaimal, J.M., Dawitz, H., Peselj, C., Masser, A.E., Hanzén, S., Ambrožič, M., Smialowska, A., Björck, M.L., Brzezinski, P., et al. (2018). Mitochondrial Translation Efficiency Controls Cytoplasmic Protein Homeostasis. Cell metabolism *27*, 1309-1322.e1306.

Tan, J.X., and Finkel, T. (2020). Mitochondria as intracellular signaling platforms in health and disease. The Journal of cell biology *219*.

Taylor, R.C., Berendzen, K.M., and Dillin, A. (2014). Systemic stress signalling: understanding the cell non-autonomous control of proteostasis. Nature reviews. Molecular cell biology *15*, 211-217.

Toda, C., Kim, J.D., Impellizzeri, D., Cuzzocrea, S., Liu, Z.W., and Diano, S. (2016). UCP2 Regulates Mitochondrial Fission and Ventromedial Nucleus Control of Glucose Responsiveness. Cell *164*, 872-883.

Vargovic, P., Ukropec, J., Laukova, M., Cleary, S., Manz, B., Pacak, K., and Kvetnansky, R. (2011). Adipocytes as a new source of catecholamine production. FEBS letters *585*, 2279-2284.

Wallace, D.C. (2008). Mitochondria as chi. Genetics *179*, 727-35

Wallingford, N., Perroud, B., Gao, Q., Coppola, A., Gyengesi, E., Liu, Z.-W., Gao, X.-B., Diament, A., Haus, K.A., Shariat-Madar, Z., et al. (2009). Prolylcarboxypeptidase regulates food intake by inactivating alpha-MSH in rodents. The Journal of clinical investigation *119*, 2291-2303.

Waterson, M.J., and Horvath, T.L. (2015). Neuronal Regulation of Energy

Homeostasis: Beyond the Hypothalamus and Feeding. Cell metabolism *22*, 962-970.

Weimer, S., Priebs, J., Kuhlow, D., Groth, M., Priebe, S., Mansfeld, J., Merry, T.L., Dubuis, S., Laube, B., Pfeiffer, A.F., et al. (2014). D-Glucosamine supplementation extends life span of nematodes and of ageing mice. Nature Communications *5*, 3563.

Wrighting, D.M., and Andrews, N.C. (2006). Interleukin-6 induces hepcidin expression through STAT3. Blood *108*, 3204-3209.

Yang, X., and Ruan, H.B. (2015). Neuronal Control of Adaptive Thermogenesis. Frontiers in endocrinology *6*, 149.

Yun, J., and Finkel, T. (2014). Mitohormesis. Cell metabolism *19*, 757-766.

Zarse, K., and Ristow, M. (2015). A mitochondrially encoded hormone ameliorates obesity and insulin resistance. Cell metabolism *21*, 355-356.

Zhang, Q., Wu, X., Chen, P., Liu, L., Xin, N., Tian, Y., and Dillin, A. (2018). The Mitochondrial Unfolded Protein Response Is Mediated Cell-Non-autonomously by Retromer-Dependent Wnt Signaling. Cell *174*, 870-883.e817.

국문초록

시상하부 POMC 뉴론-지방조직 간 미토콘드리아 호르메시스 반응에 의한 에너지 대사 조절 연구

민세희

서울대학교 대학원 의학과 중개의학 전공

약한 정도의 미토콘드리아 스트레스는 오히려 건강에 도움이 되고 수명을 연장시키는 현상을 미토호르메시스라고 한다. 본 연구는, 시상하부에서 체중 조절에 가장 중요한 신경세포로 알려진 POMC 뉴론의 미토콘드리아 리보솜에 높은 수준 또는 낮은 수준의 스트레스를 주는 것이 전신적 대사에 서로 상반된 효과를 가져온다는 사실을 확인하였다. 시상하부 POMC 뉴론 특이적으로, 미토콘드리아 리보솜 복합체를 구성하면서 OXPHOS를 미토콘드리아 내막으로 운반해주는데 중요한 역할을 담당하는 Crif1 이라는 단백질을 homo-knockout 시킴으로써 POMC 뉴론에 강한 미토콘드리아 스트레스를 주면 POMC 신경세포가 사멸되면서 심한 비만증이 발생하였다. 이에 반해, POMC 뉴론에 Crif1 단백을 hetero-knockout 시킴으로써 약한 정도의 스트레스를 주면 에너지 소모량이 증가하여 식이 섭취량이 많아짐에도 불구하고 비만증이 발생하지 않는 high-turnover metabolism 대사표현형을 보였다. Crif1 heterodeficiency 마우스에서는 서혜부 백색 피하지방조직의 갈색화가 관찰되었고, 갈색지방조직의 지방방울 크기가 작아졌으며, 이러한 현상은 지방조직에서의 열발생 및 미토콘드리아 미접힘반응과 관련된 유전자

발현의 증가를 동반하였다. Crif1 heterodeficiency 마우스의 시상하부 POMC 뉴론에서는 베타-엔도르핀 및 미토콘드리아 유래펩티드의 하나인 MOTS-c의 발현이 증가하였다. 또한 마우스의 제 3 뇌실을 통하여 MOTS-c 또는 베타-엔도르핀을 주입하였을 때 Crif1 heterodeficiency 마우스의 말초 지방조직에서 관찰된 갈색지방화와 같은 표현형이 재현됨을 관찰함으로써, 이들 물질이 상기 현상을 매개하는 인자임을 확인하였다. 마지막으로 마우스를 중등도 강도로 트레드밀에서 달리기 운동을 2주 동안 일정하게 시키면, 시상하부 POMC 세포에서 MOTS-c 및 베타-엔도르핀 발현이 증가하고 말초 지방조직의 열발생, 미토콘드리아 미접힘반응, 그리고 갈색지방화가 관찰하였다. 따라서 지속적인 운동을 하였을 때 열발생을 통하여 에너지를 소모함으로써 비만 발생이 억제되는 현상이 뇌 시상하부 POMC 뉴론의 미토콘드리아 호르메시스를 통하여 일어남을 증명하였다.

주요어 : 미토콘드리아 리보솜 스트레스, 시상하부, 열발생, 운동, POMC 뉴론, 비만, MOTS-c, 미토호르메시스

학번 : 2016-30009